

Investigations of the substantia nigra pars reticulata function and their implications for the disinhibition model of basal ganglia output

Giulio Spagnol

Thesis submitted for the degree of Doctor of Philosophy (D.Phil.)

February 2022

Magdalen College

MRC Brain Network Dynamics Unit

Nuffield Department of Clinical Neurosciences

University of Oxford

Abstract

The substantia nigra pars reticulata (SNr) is an output nucleus of the basal ganglia, a group of neuronal circuits important for movement. According to a widely recognised model of the functional organisation of basal ganglia circuits, GABAergic SNr neurons contribute to action selection and execution through decreasing their firing rates and thus, disinhibiting their targets in the thalamus, midbrain and/or brainstem. Nonetheless, significant increases in SNr neuron firing rates have been reported during different motor behaviours in non-human primates and songbirds. Furthermore, it has been suggested that SNr neurons might not only encode for and control movement execution, but also movement preparation. Despite recent advances, relatively little is known about how SNr neurons function in rodents to control movement.

To elucidate the functional role of SNr in motor behaviours, I first developed a novel delayed-Go task for head-fixed mice that incorporates aspects of both movement preparation and execution. I then used combinations of optogenetics and electrophysiology to manipulate and/or monitor the activity of GABAergic SNr neurons during different moments of the task.

In the delayed-Go task, mice were first exposed to an auditory Delay Cue, and after a variable period (Delay Window) in which mice had to refrain from licking, they had to respond to a visual Action Cue by licking a spout to collect a water reward. Trial outcomes included ‘Hit’ (licked in good time in response to the Action Cue), ‘Premature Hit’ (inappropriately licked during the Delay Window) and ‘Miss’ (failed

to lick in response to Action Cue). Mice learned to perform the delayed-Go task to satisfactory levels of success (i.e., acceptable rates of Hit trials) in about two weeks of non-consecutive daily sessions. Optogenetically-driving SNr neurons during the Action Cues of Hit trials delayed the reaction time to move (first licks). However, reaction times were shortened in Premature Hit and Hit trials when SNr neurons were optogenetically-driven during specific phases of movement preparation (Delay Cue and Delay Window, respectively). Overall, optogenetic manipulations showed that SNr neuron activity has a causal impact on movement preparation and execution. Electrophysiological recordings revealed that, in Hit trials, many SNr neurons engage in firing-rate modulations around the time of Action Cue and movement onset. Critically, these modulations mainly consisted of increased firing rates. Examination of SNr neuron activity in Premature Hit and Miss trials helped disambiguate the encoding of movement vs. cues. Irrespective of trial type, SNr neurons did not show the 'ramping up' activity that is typical of neurons encoding motor preparation. Overall, electrophysiological recordings suggest that most SNr neurons encode the execution of, but not preparation for, licking movements by increasing their firing rates.

In conclusion, my investigations do not support classical models that posit appropriately-timed decreases in the activity of many SNr neurons as the fundamental mechanism that allows movement execution to occur. Furthermore, my studies do not provide evidence of SNr neurons encoding motor preparation with changes in firing rates. Finally, my research suggests that the causal impact of SNr neuron activity on

movement depends on context, that is, whether an animal is preparing to move or is executing movement.

Acknowledgements

I want to thank my supervisor, Professor Peter Magill, for the constant support he has shown during the entirety of my doctoral fellowship. I am deeply grateful to my second supervisor Dr. Kouichi Nakamura – the better craftsman, as someone said. Without his work and supervision, this report would have been unfeasible. Thanks to Dr. Riccardo Avvisati for assisting me in the initial phase of this project, to Robert Toth and Mooad Benjaber for the technical support, to all the members of the BNDU for their friendship and support. On a personal note: Antonio, Eva, Daniel, Tenri and Mike: thanks, no but seriously.

Table of Contents

Abstract 2
Acknowledgments 5
Table of Contents 6
List of Figures 9
List of Abbreviations 11
1. Introduction 14
1.1 Direct and indirect pathways of basal ganglia 15
1.2 SNr circuit anatomy and physiology 17
1.2.1 Projections 17
1.2.2 Electrophysiological properties 20
1.2.3 Topographical organization 22
1.2.4 Discussion 23
1.3 Disinhibition models of the basal ganglia 24
1.3.1 Hikosaka's disinhibition hypothesis 24
1.3.2 Chevalier and Deniau's disinhibition model 26
1.3.3 Mink's disinhibition model 27
1.3.4 Challenges to the disinhibition models 28
1.4 Neural mechanisms of movement planning 31
1.5 Aims of research 36
2. Materials and Methods 37
2.1Animals 37
2.2 Overview of surgical procedures carried out on mice 37
2.3 Procedures for head plate implantation and viral vector injections 38
2.3.1 Preparatory steps for cranial surgery 38
2.3.2 Head plate implantation 39
2.3.3 Intracranial viral vector injections 40
2.4 Behavioural training 41
2.4.1 Housing and controlled access to fluids 41

2.4.2 Behavioural box environment 42
2.4.3 Operant delayed–Go task training 43
2.5 Procedures for electrophysiological and optogenetic experiment 45
2.5.1 Preparation for electrophysiological recordings 45
2.5.2 Optic fiber implant procedure 46
2.6 *In vivo* optical stimulation via chronically implanted optic fibers 46
2.7 *In vivo* electrophysiological recordings and optogenetic stimulation 48
2.8 Histological verification 50
2.9 Signal quantification and statistical analyses 50
3. Designing a novel delayed-Go task to engage SNr in movement preparation and execution 53
3.1 Introduction 53
3.2 Building an operant chamber for the delayed-Go task 55
3.3 Design of the delayed-Go task 58
3.4 Learning the delayed-Go task: an example 61
3.5 Mice learned the delayed-Go task in about 2 weeks of training over non-consecutive daily sessions 64
3.6 Discussion 72
4. Optogenetic driving of SNr neurons during the delayed-Go task ... 76
4.1 Introduction 76
4.2 Optogenetic driving of SNr neurons during Action Cue delays lick reaction time in Hit trials 81
4.3 Optogenetic driving of SNr neurons during Delay Window shortens lick reaction time in Hit trials 86
4.4 Optogenetic driving of SNr neurons during Delay Window does not change lick reaction time in Hit trials 88
4.5 Optogenetic driving of SNr neurons during Delay Cue does not change lick reaction time in Hit trials 91
4.6 Optogenetic driving of SNr neurons during Delay Cue accelerates lick reaction time in Premature Hit trials 94
4.7 Optogenetic driving of SNr neurons altered the amount of Hit, Premature Hit, and Miss trials in ChR2 and control groups 98
4.8 Discussion 101

5. Encoding of the delayed-Go task by SNr neurons 107
5.1 Introduction 107
5.2 Materials and Methods 107
5.3 Most SNr neurons increase their firing rate at movement onset in Hit trials 111
5.4 Some SNr neurons increase their firing rates in Premature Hit trials 117
5.5 SNr neurons can encode Cues but not movement in Miss trials 120
5.6 Summary of SNr neurons activity patterns during the delayed-Go task 123
5.7 Optogenetic activation of SNr neurons during Action Cue and Delay Window 126
5.8 Discussion 138
6. General discussion 144
6.1 Introduction 144
6.2 Summary of key findings 147
6.3 Implications and further directions 149
6.4 Concluding remarks 154
7. References 156

List of Figures and boxes

Figure 1.1 Simplified concept of direct and indirect pathways in the basal ganglia network 16
Figure 1.2 Schematic summary of SNr output pathways 19
Figure 1.3 Control of saccadic eye movement by the basal ganglia 25
Figure 1.4 Movement preparation in the mouse brain 35
Figure 3.1 Apparatus for integration of neuronal function in head-fixed mice performing for the delayed-Go task 59
Figure 3.2 Schematic time course of a delayed-Go task 62
Figure 3.3 Performance of a mouse on day 1 and day 15 of the delayed-Go task 65
Figure 3.4 Mice learn the delayed-Go task in about 2 weeks of training over non-consecutive daily sessions 71
Figure 3.5 Mice learn the Action Cue faster than Delay Cue 73
Figure 4.1 Schematic design of patterns of laser stimulation during different moments of the delayed-Go task 80
Figure 4.2 Experimental design using optogenetics to target SNr neuronal population 82
Figure 4.3 Reaction time in Hit trials is delayed when SNr neurons are optogenetically driven during the Action Cue 85
Figure 4.4 Optogenetic modulation doesn't accelerates reaction time in Hit trials ... 87
Figure 4.5 Reaction time in Hit trials is faster when SNr neurons are optogenetically driven during the Delay Window 89
Figure 4.6 Reaction time in Premature Hit is not affected when SNr neurons are optogenetically driven during the Delay Window 92
Figure 4.7 Reaction time in Hit trials is not affected when SNr neurons are optogenetically driven during the Delay Cue 95
Figure 4.8 Reaction time in Premature Hit trials is accelerated when SNr neurons are optogenetically driven during the Delay Cue 97
Figure 4.9 First licks of Hit trials and Premature Hit trials after laser offset 99
Figure 4.10 Rate changes in the delayed-Go task from optogenetic driving of SNr neurons 102
Figure 5.1 Experimental design for the electrophysiological recordings and optical manipulation of SNr neuronal population in mice 114
Figure 5.2 Distribution of the peak normalized firing rate of neurons in Hit trials sorted by the peak activity 119

Figure 5.3 Distribution of the peak normalized firing rate of neurons in Premature Hit trials sorted by the peak activity 123
Figure 5.4 Distribution of the peak normalized firing rate of neurons in Miss trials sorted by the peak activity 126
Figure 5.5 Comparison of spike PETH curves of SNr Clusters during the delayed-Go task 129
Figure 5.6 Firing rates histograms of SNr neurons during the delayed-Go task 130
Figure 5.7 Optogenetic modulation of SNr neurons during Action Cue 134
Figure 5.8 Reaction time in Hit trials is delayed when SNr neurons are optogenetically driven during the Action Cue 136
Figure 5.9 Optogenetic modulation of SNr neurons during Delay Window 140
Figure 5.10 Reaction time in Hit trials is faster when SNr neurons are optogenetically driven during the Delay Window 142

Box1 Schematic design of patterns and outcomes of laser stimulation during different moments of the delayed-Go taks 110

List of Abbreviations

A

AC	Action Cue
AAV	Adeno-Associated Virus
ALM	Anterior lateral motor cortex
ANOVA	Analysis of variance
ArchT	Archaerhodopsin from Halorubrum strain

B

BG	Basal ganglia

C

ChR2	Channelrhodopsin 2
CD	Caudate nucleus
CL	Centro-lateral nucleus of the thalamus
CM	Centro-medial nucleus of the thalamus
Cre	Cre recombinase enzyme
CSC	Central superior colliculus

D

DA	Dopamine receptors
DAPI	4′,6-diamidino-2-phenylindole
DC	Delay Cue
DiD	1,1’-dioctadecyl-3,3,3',3’-tetramethylindocarbocyanine perchlorate
DW	Delay Window
dMSNS	Direct pathway striatal medium spiny neurons

E

EYFP	Enhanced yellow fluorescent protein
FEF	Frontal eye field

G

GABA	Gamma-aminobutyric acid
GPe	Globus pallidus pars interna
GPi	Globus pallidus pars externa

I

IC	Inferior colliculus
iMSNs	Indirect pathway striatal medium spiny neurons
IPSPs	Inhibitory postsynaptic potentials
ITI	Inter-trial-interval

L

LSC	Lateral superior colliculus
LTS	Low threshold spike
L5	Lateral trigeminal area

M

Med	Medullary reticular formation
MidRF	Midbrain reticular formation
MD	Mediodorsal nucleus of the thalamus
MSC	Medial superior colliculus
MSNs	Medium-sized spiny neurons
MWUT	Mann–Whitney U test

N

NA	Numerical aperture

P

PBS	phosphate-buffered saline
Pf	Parafascicular nucleus
PNo	Pontine reticular formation
PPN	Pedunculopontine nucleus
PETH	Peri-event-time-histogram
PT	Pyramidal tract neurons
PV-Cre	Parvalbumin-Cre
P5	Peritrigeminal nucleus

S

SC	Superior colliculus
SD	Standard deviation
SEM	Standard error of mean
SNr / SNpr	Substantia nigra pars reticulata
SNc / SNpc	Substantia nigra pars compacta
STN	Subthalamic nucleus
Su5	Supratrigeminal area

T

TRN	Thalamic reticular nucleus of the thalamus
T-type Ca2+	T-type calcium channels

V

VA	Ventral anterior thalamic nucleus
VGAT	Vesicular GABA transporter

	VGAT-IRES Vesicular GABA transporter- internal ribosome entry site-Cre expressing recombinase
VL	Ventral lateral nucleus of the thalamus
VM	Ventral medial nucleus of the thalamus

Z

ZI	Zona incerta

1. Introduction

The basal ganglia (BG) are subcortical structures distributed in the forebrain, diencephalon, and midbrain, consisting of many interlinked nuclei that are responsible for, amongst other functions, action selection (Donahue and Kreitzer 2015; Mink 1996), control of movement strength (Turner and Desmurget 2010), learning of motor skills (Graybiel 2008), and timing of movement initiation (Buhusi and Meck 2005). One basal ganglia functional organisation model has influenced research over the last decades (Albin, Young, and Penney 1989; DeLong 1990). According to this model, the basal ganglia's output nuclei accomplish nearly opposing behavioural effects by receiving direct or indirect projections from the striatum. The direct pathway projections are thought to disinhibit thalamocortical and brainstem circuitry by inhibiting the tonic firing of GABAergic basal ganglia output nuclei, such as substantia nigra pars reticulata (SNr) and globus pallidus pars interna (GPi), thereby promoting movement. In contrast, activation of the indirect pathway is hypothesized to increase SNr firing via subthalamic nucleus (STN)-mediated excitation, thus inhibiting the downstream circuitry and suppressing movement (Calabresi et al. 2014). Despite the model's significant conceptual advancements, numerous basic assumptions about the basal ganglia output nuclei have yet to be validated in behaving animals. Several competing explanations on the functional organization and operational principles of the BG output nuclei have been proposed over the years. However, the role of the substantia nigra pars reticulata and the globus pallidus pars interna in movement has yet to be determined.

1.1 Direct and indirect pathways of basal ganglia

Although the intrinsic circuitry of the basal ganglia (BG) is complex, Albin (1989) and DeLong (1990) proposed a model that hypothesized a dual organization of the striatal outputs and the dual organization of BG outputs. This model proposes that two circuits, the so-called direct and indirect pathways, arise from discrete populations of striatal medium-sized spiny neurons (MSNs) that project to distinct target structures (Figure1.1). In the direct or striatonigral pathway, cortical stimulation causes glutamate release, activating MSNs that monosynaptically project to the substantia nigra pars reticulata and the globus pallidus pars interna. Because MSNs are GABAergic cells, they have an inhibitory effect on SNr neurons that are also GABAergic. This disinhibition from the SNr GABAergic neurons supposedly allows the thalamic glutamatergic neurons, which receive SNr input and project to the cortex, to become more active. The behavioural outcome of this increased target activity is predicted to be locomotor activation/ initiation of movement. In contrast, in the indirect or striatopallidal pathway, cortical activation of a distinct population of MSNs which project indirectly to the SNr via the globus pallidus pars externa (GPe) and the subthalamic nucleus (STN), inhibits the GABAergic neurons of the GPe, leading to a disinhibition of the glutamatergic neurons of the STN. The enhanced firing of excitatory STN neurons then activates SNr GABAergic neurons that project to the thalamus and other BG targets. As a result, locomotor activity and movement are predicted to be reduced. MSNs of the direct and indirect pathway can also be distinguished by their characteristic expression of dopamine (DA) receptors. MSNs in

the direct pathway express D1 DA receptors, whereas MSNs in the indirect pathway express D2 receptors. This neurochemical segregation is thought to add to the evidence for a dichotomous effect of direct and indirect route activation (Gerfen et al. 1990; Gerfen and Surmeier 2011). Although individual structures of the basal ganglia have been studied extensively, the organization and circuit mechanism of the BG output nuclei remains unclear. In the following sections, I will focus on the SNr, the volumetrically most prominent output nucleus of the rodent basal ganglia and discuss the circuit organization and different theories on its impact on the broader motor system and movement.

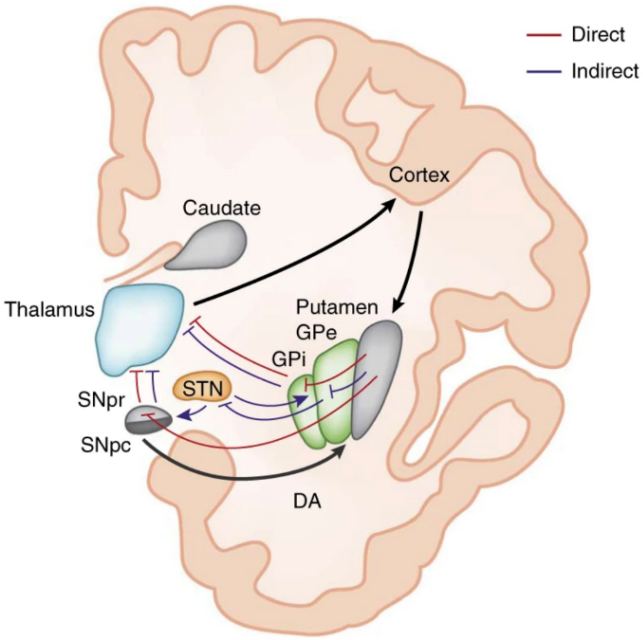


Figure 1.1 Simplified concept of direct and indirect pathways in the basal ganglia network. The direct pathway (red) conveys cortical information through D1-MSNs in the striatum directly to basal ganglia output nuclei GPi and SNpr. The indirect pathway (blue) conveys cortical information through D2-MSNs in the striatum via GPe and STN to basal ganglia output nuclei. The caudate nucleus, the putamen, and the accumbens nucleus are all considered input nuclei and receiving mainly cortical, thalamic and nigral information. The output nuclei GPi and SNr project to the thalamus,

which sends efferents that in turn close the cortico-basal ganglia-thalamo-cortical loop. The network is modulated by dopamine (DA) from SNpc dopamine neurons. SNpr, substantia nigra pars reticulata; GPe, globus pallidus pars externa; STN, subthalamic nucleus; CN, caudate nucleus; Put, putamen; Acb, accumbens nucleus. Image adapted from (Calabresi et al. 2014).

1.2 SNr circuit anatomy and physiology

In rodents, the substantia nigra pars reticulata is the biggest output nucleus of the basal ganglia in terms of volume and sends out projections to the superior colliculus (SC), motor and intralaminar thalamic nuclei, and the pedunculopontine nucleus (PPN) (Mena-Segovia, Bolam, and Magill 2004; Alexander and Crutcher 1990a; Hikosaka 2007; McElvain et al. 2021). In mice, the prevalent population of neurons in the SNr is parvalbumin-positive GABAergic neurons (~ 85 %). Although the SNr predominantly contains GABAergic neurons, a small population of dopaminergic neurons is also present (± 5% of neurons in the SNr express tyrosine hydroxylase). Evidence suggests that a small percentage of putatively dopaminergic neurons in the SNr project to the thalamus and PPN (McElvain et al. 2021; González-Hernández and Rodríguez 2000; Prensa and Parent 2001; Cebrián, Parent, and Prensa 2005).

1.2.1 Projections

The lack of a systematic anatomical mapping has prevented a complete identification of SNr projections thus far. Furthermore, it is still unclear whether SNr projections throughout the diencephalon and brain stem arise from the same or segregated neurons

(Anderson and Yoshida 1977; Deniau and Thierry 1997; Parent and De Bellefeuille 1983; Wright and Arbuthnott 1981). Only recently, a study by McElvain et al. (2021) systematically mapped the SNr axonal projections and synaptic terminals across the brain combining viral tracing and genetically restricted parvalbumin-Cre (PV-Cre) mouse line. This study confirmed that 1) the predominant population in SNr is the parvalbumin-positive GABAergic neurons, as previously demonstrated by González-Hernández and Rodríguez (2000); 2) in the diencephalon SNr targets include major motor thalamic nuclei such as ventromedial (VM), ventroanterior (VA), as well as intralaminar/midline, mediodorsal (MD), centro-lateral/medial (CL/CM), and parafascicular (Pf) thalamic nuclei, thalamic reticular nucleus (TRN) as seen in other species (Cebrián, Parent, and Prensa 2005; Graybiel and Ragsdale 1979; Utter and Basso 2008). In the brainstem, McElvain observed a greater number of projections beyond the well-established ones to the superior colliculus and PPN (Hikosaka 2007). Extensive SNr projections target large domains of the midbrain reticular formation (MidRF), pontine reticular formation (PNo), and medullary reticular formation (Med). Downstream projections target brainstem nuclei such as 1) Superior colliculus, implicated in oculomotor and head orientation (Fukushima 1987; May et al. 2019); 2) medial nucleus (Med), supratrigeminal area (Su5), peritrigeminal (P5), and lateral trigeminal (L5), implicated in orofacial sensorimotor systems; and the PNo, implicated in hindlimb control (Brownstone and Chopek 2018). The presence of collateral projections to the thalamus, SC, and PPN has been assayed previously with dual chemical tracer injection and antidromic stimulation, yet with conflicting results

(Anderson and Yoshida 1977; Beckstead and Frankfurter 1982; Deniau et al. 1977; Parent and De Bellefeuille 1983). McElvain data indicate that SNr neurons emit a broad but selective pattern of axonal collateralization, with diencephalic regions receiving broader collateral input than brain stem regions (Figure1.2).

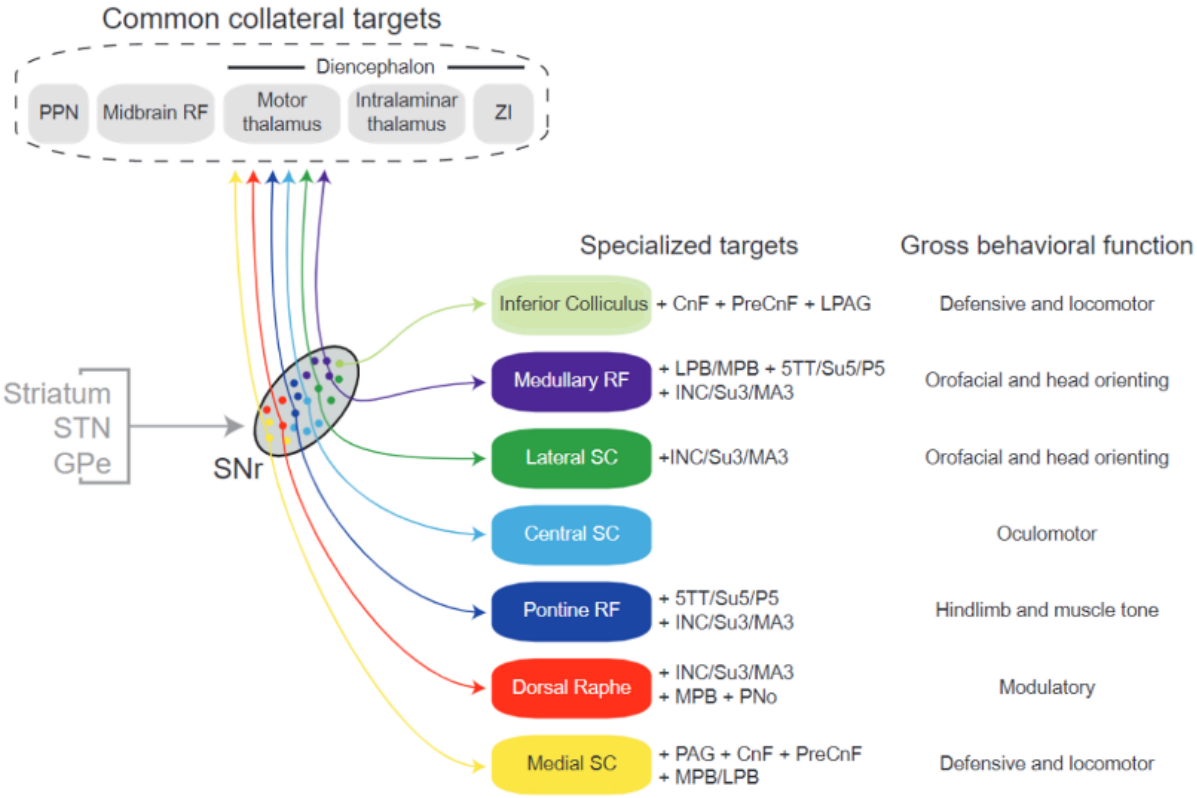


Figure 1.2 Schematic summary of SNr output pathways. Mouse SNr is divided into subpopulations based on genetics and axonal outputs. Each population projects to functionally distinct brain stem regions. Collateral projections span to small brain stem nuclei and a set of common target regions. All populations show a distinct one-to-many projection pattern. Adapted from (McElvain et al. 2021).

Quantitative analysis also showed that the majority of targets of SNr are the VA and VM motor thalamus, PPN, and superior colliculus (McElvain et al. 2021). However, what emerged is that the total SNr outputs cover areas outside of these targets, with the majority of overall output focused on several large brainstem regions and the zona incerta (ZI) and motor thalamus to a lesser extent.

1.2.2 Electrophysiological properties

GABAergic neurons in SNr show distinct electrophysiological characteristics. They show spontaneous repeated firing that may reach 40–80 Hz *in vivo* and the capacity (ex vivo), to produce high–frequency discharges with limited spike adaptation (Atherton and Bevan 2005; Deniau et al. 1978; Guyenet and Aghajanian 1978; Juraska, Wilson, and Groves 1977; Nakanishi, Kita, and Kitai 1987). The delayed rectification and the short action potential are presumably caused by a significant voltage-dependent K+ conductance (Deniau et al. 2007). Even when the neuron is highly depolarized, this membrane conductance contributes to the prolonged high–frequency spike discharge of SNr cells because it prevents the membrane potential from reaching the Na+ inactivation threshold. (Nakanishi, Kita, and Kitai 1987). During behaviour, SNr neurons increase or decrease their spike rate across broad ranges and variable durations of time (Gulley et al. 1999; Hikosaka and Wurtz 1983a; Jin and Costa 2010). Whether this variability could be originating from different synaptic inputs, network interactions, or a range of electrophysiological properties intrinsic to SNr neurons, is

still unclear. New evidence collected in mice (McElvain et al. 2021) found a remarkable intrinsic electrophysiological difference in SNr neurons. SNr firing responses to depolarizing inputs are highly linear. In contrast, responses to hyperpolarizing inputs are highly non-linear, and the capacity for post inhibitory rebound firing varies significantly across the population. Furthermore, the continuum found for each electrophysiological property (e.g., firing rates ranges, gain and rebound kinetics) can differentially tune the firing capabilities of individual neurons in the SNr. Also, SNr neurons with distinct electrophysiological specializations project to different large brainstem regions. Neurons that project to collicular nuclei such as the lateral superior colliculus (LSC) and the central superior colliculus (CSC) have a rapid rise and fall of their action potential and high spontaneous and maximum firing ranges. In contrast, projections to the medial superior colliculus (MSC) and the inferior colliculus (IC) arise from pools of neurons with relatively slower rates. Thus, projections to large brain stem areas likely arise from subpopulations of SNr neurons whose properties are tuned differentially. The intrinsic electrophysiological parameters of each of these projection populations span over a very restricted range. According to McElvain, this suggests that different projection populations have specific functional properties (McElvain et al. 2021).

1.2.3 Topographical organization

SNr-brain stem projection neurons have also been found to cluster spatially in the SNr (McElvain et al. 2021). Projection neurons with slower active and passive properties are more concentrated in the nucleus's medial portion, overlapping with terminal fields from associative striatal regions. In contrast, rapidly responding projection neurons occupy the lateral half of the SNr, where sensorimotor striatal afferents terminate (Deniau, Menetrey, and Charpier 1996). SNr neurons projecting to the VA, MD, or Pf thalamus displayed the full diversity of firing properties observed across SNr neurons. Similarly, SNr neurons projecting to the PPN were tuned broadly with heterogeneous properties and lacked statistically significant differences from randomly selected SNr neurons. In addition to a lack of specialized intrinsic properties, SNr-thalamus and SNr-PPN projection neurons were distributed throughout the SNr. Thus, projections to the thalamus and PPN arise from broadly tuned projection pools in the SNr, in contrast to the specialized features of SNr projections to most large brain stem areas. The organization of striatonigral projections has been studied extensively (Desban et al. 1995; Faull and Mehler 1978; Gerfen 1992; Deniau, Menetrey, and Charpier 1996). However, the precise representation of all striatal inputs remains unclear; there is good evidence that multiple components of the "striatal mosaic" are mapped in the SNr as longitudinal laminae, which form an "onion-like" structure (Deniau, Menetrey, and Charpier 1996) . Within the nigral longitudinal laminae, individual projections occupy a well-defined position. In the most ventral nigral lamina the projections of the auditory striatal region are followed by the visual and associated visuomotor region and the

visuocingulate region. The lamellae of the striatal sensorimotor region occupy a more dorsal position within the lateral part of the SNr. Projections of the striatal regions related to the prefrontal cortical areas (i.e., perirhinal, orbital, insular and prelimbic areas) envelop the SNr more medially and dorsally (Deniau, Menetrey, and Charpier 1996; Deniau et al. 2007).

1.2.4 Discussion

Taken together, this new evidence shows that SNr looks more like a circuit containing distinct projection neuronal populations that are electrophysiologically specialised and topographically organised rather than a single monolithic output. Collateralization towards the thalamus also indicates that the SNr targets the diencephalon in a relatively diffuse manner compared with brain stem nuclei. The view that SNr projections disinhibit some major motor centers like the superior colliculus via firing rate decrease (Hikosaka 2007) and that the SNr contributes to action selection through disinhibition of downstream motor targets has been established for years (Hikosaka and Wurtz 1983a). Nonetheless, significant increases in SNr firing rates, driven by an unknown circuit mechanism, are often reported during different behaviours (Gulley et al. 1999; Jin and Costa 2010; Mink and Thach 1991; Turner and Anderson 1997). The wide range of intrinsic electrophysiological features of SNr neurons and their topographical segregation raises the question of whether common disinhibition processes apply to all SNr outputs, which work over a wide range of firing rates, or whether signalling

mechanisms alter depending on the circuit demands of downstream and diencephalic structures. There is no clear answer to that question; competing evidences and hypotheses will be discussed in the next section.

1.3 Disinhibition models of the basal ganglia

1.3.1 Hikosaka's disinhibition hypothesis

The relationship between SNr neuronal activity and movement initiation was initially observed in cat and monkey recordings by Hikosaka and Wurtz (Hikosaka and Wurtz 1983c; Hikosaka and Wurtz 1983d; Hikosaka and Wurtz 1983b; Hikosaka and Wurtz 1983a). Hikosaka's work indicated that SNr neurons provide tonic inhibition to the superior colliculus during saccades, which, when released, allow collicular output neurons to send command signals to the saccade generating nuclei in the brainstem (Figure 1.3).

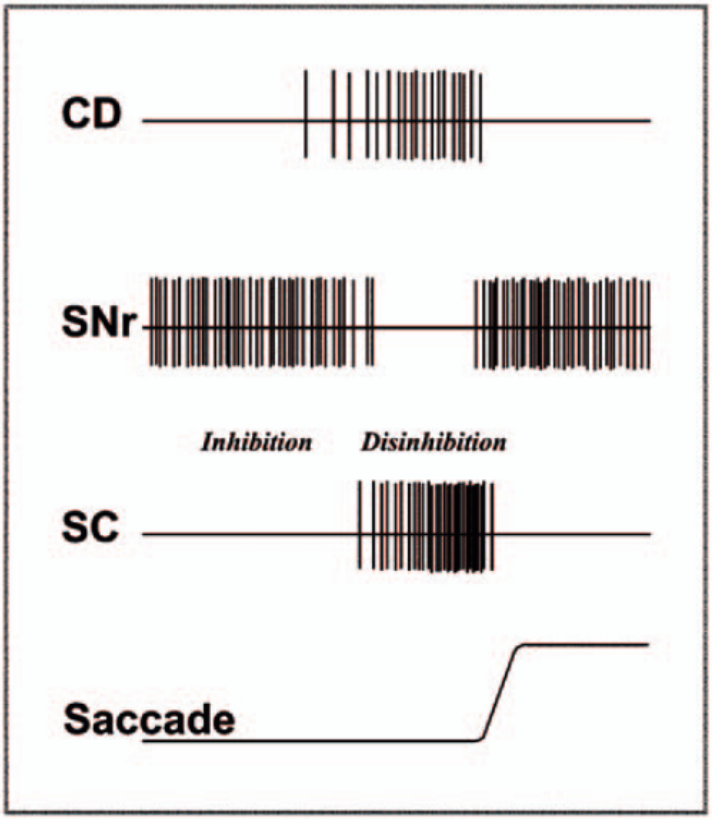


Figure 1.3 Control of saccadic eye movement by the basal ganglia. Tonic firing of GABAergic neurons in the SNr inhibits the SC. SNr tonic inhibition can be disrupted by GABAergic inputs from the caudate nucleus (CD). SNr disinhibition, together with excitatory inputs from cortical areas, allows SC neurons to fire in burst, which starts a saccade to a contralateral location. Image adapted from (Hikosaka and Wurtz 1983a).

This mechanism has since been known as the "disinhibition model" of the basal ganglia. It suggests that pauses in BG-output activity "gate" the task-related activation of its downstream motor targets via disinhibition. Several observations have supported this model. Electrical stimulation of SNr evokes inhibitory postsynaptic potentials (IPSPs) in collicular output neurons (Karabelas and Moschovakis 1985). Injecting bicuculline, a GABA antagonist, into the colliculus of non-human primates causes

irrepressible saccadic eye movements (Hikosaka and Wurtz 1985a). Likewise, injecting muscimol, a GABAergic agonist, into the nigra of non-human primates produces uncontrollable saccades in monkeys (Hikosaka and Wurtz 1985). Additional behavioural evidence for this model can be found in a recent paper by Freeze (Freeze et al., 2013). Using cell-type-specific targeting of channelrhodopsin-2 (ChR2), the author could optically activate either direct or indirect pathway striatal medium spiny neurons (dMSNs or iMSNs, respectively) while recording SNr activity and monitoring behaviour in the open field. He found that stimulating dMSNs and iMSNs produced diverse SNr firing rate responses, yet only the inhibited SNr neurons predicted locomotor activation during direct pathway activation. These findings confirmed SNr inhibitory influence on saccades, and hence a role for the nigro-collicular pathway in the start of saccadic eye movements and movements initiation in general (Basso and Sommer 2011).

1.3.2 Chevalier and Deniau's disinhibition model

Over the years, studies further built on Hikosaka's hypothesis extending the disinhibition model beyond the nigrocollicular projection/pathway and generalizing it as a mechanism that basal ganglia use to control upstream motor targets (e.g., thalamus) and other movements (e.g., limbs). Combining simultaneous unit recordings in SNr, superior colliculus, and thalamus with pharmacological stimulation of striatum, (Chevalier and Deniau 1990) have shown that striatal activity readily induces a phasic

silencing of the tonically active nigral neurons, accompanied by a robust firing in colliculus and thalamus. According to the authors, "when the striatum is silent, the motor structures are kept under an inhibitory constriction and are shielded from disturbing noise, when the striatum is active, it enables motor structures to work" (Chevalier and Deniau 1990).

1.3.3 Mink's disinhibition model

A theoretical proposal by Mink (Mink 1996) further extended this hypothesis, stating that the output nuclei of the basal ganglia do not use disinhibition uniformly but in a disjunct manner. According to Mink, when a voluntary movement is initiated, motor regions in the cerebral cortex send a corollary signal to the subthalamic nucleus (through the projections of the so-called "hyperdirect pathway" by Nambu et al. (2002), causing extensive activation of GPi and SNr and subsequent suppression of competing motor patterns. Simultaneously, signals from the cerebral cortex motor and other areas are sent to the striatum, which filters and alters them in a context-dependent manner and then focally inhibits GPi and SNr to remove tonic inhibition from motor pattern generators implicated in the desired movement. As a result, the output of the basal ganglia focally selects and activates preferred motor mechanisms while broadly inhibits competing motor programs, allowing movement to occur without interference. Mink's model of focused selection and inhibition of competing motor programs by the basal ganglia partially contradicts Hikosaka's model because it predicts simultaneous

excitation and inhibition of the SNr and GPi. Many studies over the years have supported Mink's hypothesis (Jin and Costa 2010; da Silva et al. 2018; Jin, Tecuapetla, and Costa 2014). In particular, a work by Tecuapetla et al. (2014) has causally tested Mink's model with optogenetics (Deisseroth 2011). Using photometry through optic fibers to measure GCaMP6s activation, the author observed that striatonigral and striatopallidal neurons are concomitantly active during spontaneous contraversive movements, and optogenetic unilateral inhibition of either striatal projection pathway impaired contralateral movements without affecting ipsilateral movements. Furthermore, optogenetic inhibition of both pathways cancelled contralateral turns and further biased ipsilateral turns. These findings support Mink's view that activity in both projection pathways is required to achieve a particular movement. For example, activated direct pathway neurons could select the desired motor programs. In contrast, simultaneously active indirect pathway neurons inhibit competing motor programs.

In line with other models (Albin, Young, and Penney 1989; Hikosaka 2007), Mink’s model explains how basal ganglia function to control movement initiation and selection. However, many studies have shown that a reduction in vigour of voluntary movement represents one of the most severe effects when basal ganglia activity is disrupted and, more specifically, when dopamine signalling is lost (Palmiter 2008; Salamone and Correa 2012). Moreover, severe lesions or inactivation of the basal ganglia output nuclei can alter the velocity and fluidity of movements without necessarily altering their selection or initiation (Turner and Desmurget 2010; Horak and Anderson 1984). A recent study by Panigrahi et al. (2015) has corroborated these

findings by combining *in vivo* electrophysiological recordings and optical manipulation of the dorsal striatum with an effort-based operant task that required mice to adjust the vigour of a reaching movement to obtain reward. The study demonstrated that inhibition of striatal activity led to slower and less vigorous movements. It also demonstrated that the repletion of dopamine in a mouse model of Parkinson's disease is sufficient to restore striatal activity and invigorate movement. Finally, Cui et al. (2013) and Isomura et al. (2013) have shown how recruiting both direct and indirect pathways is crucial for lever pressing. As proposed by Mink, these studies show that basal ganglia play an important role in regulating motor programs. However, they suggest that a balanced activity of both direct and indirect pathway neurons could be more determinant for the invigoration of specific movements and preventing concomitant invigoration of competing motor behaviours than movement initiation or selection.

1.3.4 Challenges to the disinhibition models

Over the years, several studies have suggested that the influence of BG output might be more subtle than the previously discussed models suggested and might primarily consist of modulation of thalamic activity. This idea arose initially from the observation that inactivation of the output nucleus of the BG did not abolish task-related activity in the BG-recipient thalamus (Anderson and Turner 1991; Inase, Buford, and Anderson 1996).That result was reinforced recently by Goldberg and Fee

(Goldberg and Fee 2012) using the songbird as a model. Goldberg and Fee (Goldberg & Fee 2012) also verified two insights suggested previously from between-studies comparisons (Nambu, Tokuno, and Takada 2002; Turner and Desmurget 2010). First, task-related increases in firing are far more prevalent than decreases in BG-output neurons (Mink and Thach 1991; Turner and Anderson 1997) and in BG-recipient thalamus (Anderson and Turner 1991). Second, that the latencies of task-related activity in BG-output neurons do not lead those of the BG-recipient thalamus but may lag behind them. Schwab et al. (2020) confirmed this in monkeys showing that the motor thalamus activity precedes basal ganglia activity at movement onset. By showing coactivation of BG output and thalamus with movement, these two studies strongly argue against the idea that task-related changes in neuronal activity in BG-recipient regions of the thalamus are permitted or caused by the temporal pattern of input from the BG as disinhibition models predict (Mink 1996; Chevalier and Deniau 1990). According to the authors, basal ganglia and thalamic discharge may be driven by layer 5 projections from the motor cortex (Inase, Buford, and Anderson 1996; Goldberg and Fee 2012), but this hypothesis has not been tested yet.

According to McElvain et al. (2021), the PPN and the MidRF are brainstem hubs receiving converging collateral input from all the projections pools in SNr. Whether these projections mediate specific functions such as locomotion remains to be determined. It is worth noticing, though, that the PPN is a component of the mesencephalic motor region (MLR) which has been demonstrated to be involved in muscle tone and arousal (Pienaar, Vernon, and Winn 2017) and to mediate striatal

effects on locomotion (Roseberry et al. 2016; Takakusaki 2013). Moreover, SNr projections to orofacial regions in the Med collateralize to brainstem nuclei are involved in orofacial sensorimotor signalling (Su5, P5, L5) and head orientation (InC) (Fukushima 1987; Kolta et al. 2010). The studies and the findings from McElvain that SNr-thalamus projections comprise aggregate collaterals of SNr- brain stem projections neurons suggest that SNr neurons affect simultaneously cortical and brain stem regions. Branching ascending-descending collateral projections might regulate behaviour and indicate that movement could be controlled directly through the SNr projections to brainstem nuclei without necessarily being modulated by higher motor structures, e.g., (motor thalamus or motor cortex).

Despite recent advancements (Freeze et al. 2013; Tecuapetla et al. 2014; Catanese and Jaeger 2021; Catanese and Jaeger 2020; Morrissette et al. 2019), relatively little information is available on SNr function in rodents during behaviour. Most evidence has been collected in monkeys performing fixation tasks (Hikosaka and Wurtz 1983a) and supported by experiments in anesthetized rats (Chevalier and Deniau 1990). Alternative hypotheses also have been collected in songbirds (Goldberg and Fee 2012) or non-human primates (Schwab et al. 2020). However, it ultimately remains unclear how, in behaving mice, SNr contributes to the selection and initiation of movement. Optogenetic tools have now been widely used to investigate specific causal relationships between genetically defined populations of neurons and behaviour (Deisseroth 2011; Stamatakis and Stuber 2012). Manipulation of GABAergic neuronal

population in SNr time-locked to movement initiation could clarify how, in rodents, basal ganglia output nuclei regulate motor functions.

SNr is part of the cortico-basal ganglia-thalamocortical loop that regulates motor functions. SNr neurons are known to project to the motor thalamus, which in turn projects to the cortex. The parafascicular nucleus (Pf) of the thalamus, another target of SNr, projects back to the striatum (Alexander and Crutcher 1990a). The new study of McElvain et al. (2021) revealed how all the downstream-projecting SNr neurons also have a thalamic axonal branch, signifying that upstream projections to the thalamic branches carry updated information about the commands distributed to the different motor strucutres in the midbrain and brainstem in a subpopulation-distinct manner (Grillner and Thompson 2021). This type of information can be described as an efference copy. The efference copy information forwarded to the cortex and striatum is crucial for the planning of upcoming movements (motor planning) and for reinforcement learning, rather than the actual movement being executed at that particular moment (Fee and Goldberg 2011; Redgrave and Gurney 2006; Frank 2005; Fee 2012). In the next section, I will introduce the concept of movement preparation and describe how it emerges from a multi-regional cortico-basal ganglia thalamocortical loop. I will also show how SNr role in this circuit is still poorly understood and how clarifying it might be crucial to understand better how basal ganglia regulate motor functions.

1.4 Neural mechanisms of movement planning

Movement planning (also known as "movement preparation") is considered to take place in those regions of the brain where the initial correlations between neural activity and future actions arise. Movement planning has been widely studied using delayed response tasks, in which a sensory stimulus instructs a future action. During the delay, neurons in the frontal and parietal cortex and connected structures show persistent and ramping activity related to specific movements long before movement onset (Svoboda and Li 2018; Guo, Li, et al. 2014). This neural activity is referred to as preparatory activity and is a crucial feature of movement planning and thus for future movement.

Neural activity has to meet distinct criteria to be classified as preparatory activity. These criteria have been identified by Riehle and Requin (1993) and are 1) changes in neural spike rate must occur before movement initiation; 2) neural activity must selectively encode for specific movements, such as saccade location, or movement direction of the limbs or the tongue; 3) neural activity predicts certain features of the following movement execution, such as reaction time.

Neural activity correlated with movement planning was recorded for the first time in non-human primates by Evarts (1968). In this study, monkeys were instructed to hold a handle from 2 to 5 s and wait for a visual cue (delayed-go cue) that told them whether to push or pull the handle. A consistent subset of neurons in the primary motor cortex increased their activity seconds before the delayed go cue. However, since the

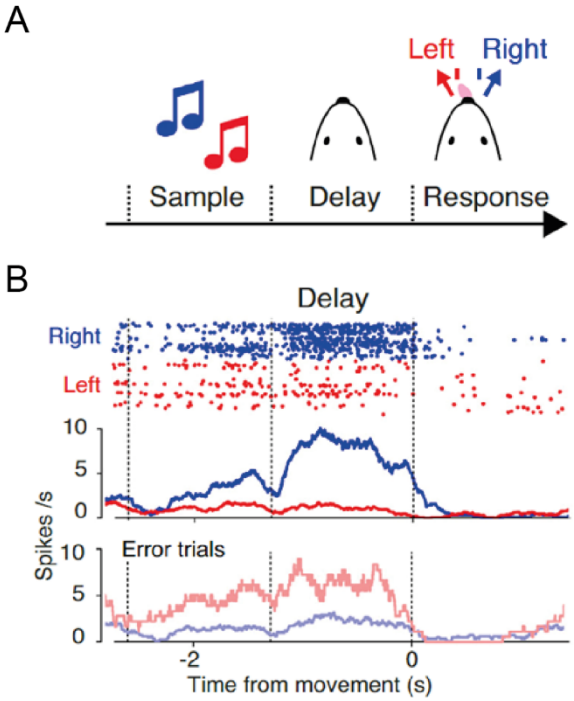
activity on error trials still encoded the future movement rather than the instruction, Evarts concluded that this activity was selective for preparing the movement. Since then, tasks involving arm movements and eye movements in non-human primates have been widely used to study movement planning.

The primary motor cortex (Riehle and Requin 1989; Tanji and Evarts 1976; Crutcher and Alexander 1990), premotor and supplemental motor cortex (Riehle and Requin 1989; Crutcher and Alexander 1990), frontal eye field (FEF) (Cisek and Kalaska 2005; Bruce and Goldberg 1985), parietal cortex (Maimon and Assad 2006), striatum (Alexander and Crutcher 1990b), superior colliculus (Wurtz and Goldberg 1972), motor thalamus (Tanaka 2007), and cerebellum (Ohmae, Kunimatsu, and Tanaka 2017) have all been found to encode preparatory activity, revealing it as a distributed neural phenomenon across interconnected multi-regional networks.

Similar experiments have been recently performed on rodents. Rodent motor behaviours can offer a comprehensive and precise analysis of neural activity and a wider range of experimental (cell-type-selective) manipulations. In two studies by (Guo, Li, et al. 2014; Chen et al. 2017; Li et al. 2016), head-restrained mice performed a task in which they reported a decision by directional licking after a delay period. Combining electrophysiology and calcium imaging, the authors found that preparatory activity for licking direction occurred first in the anterior lateral motor cortex (ALM) and remained confined to ALM until movement onset (Figure 4). Using optogenetic perturbation methods (Deisseroth 2011), Guo et al. (2014), and Li et al. (2016) further delineate the role of ALM as a critical hub in the network that supports the preparatory

activity. In mice, transient unilateral optogenetic inactivation in ALM during movement planning perturbed preparatory activity and caused an ipsiversive bias in future licking direction. Additionally, transient bilateral inactivation of ALM also perturbed preparatory activity and randomized licking direction. However, the same inactivation patterns in surrounding cortical regions did not perturb preparatory activity.

Figure 1.4 Movement preparation in the mouse brain. A: Example of a delay response task. **B:** Example of a single neuron recorded in the ALM encoding movement preparation. Top, raster plot,



correct trials. Single dots correspond to an action potential. Bottom, average spike rates for different trial types, error trials are included. In error trials the activity still predicts movement direction. Image adapted from (Svoboda and Li 2018).

Two studies in non-human primates (Tanaka 2007; Tanaka 2006) showed that the thalamus encodes preparatory activity and that the suppression of thalamic nuclei

projecting to the parietal cortex and the frontal eye field (FEF) delays memory-guided saccades. These results suggested that 1) preparatory activity could not be maintained by cortex in isolation but could be part of other multi-regional interactions, and 2) thalamocortical loops might help maintain preparatory activity for memory-guided movements.

These results were confirmed in mice by Guo et al. (2017). Combining recordings and optogenetics in a delay directional lick task, Guo investigated ALM and thalamic ventromedial and ventral anterior-lateral nuclei that are connected in a bidirectional manner. What emerged from this work is that, similar to ALM, thalamic neurons exhibit preparatory activity, and unilateral inactivation of the thalamus during the delay epoch caused an ipsiversive bias of lick direction. Also, optogenetic inactivation of the thalamus caused a near-total collapse of ALM activity and inactivation of ALM diminished activity in the thalamus. This study confirms that thalamocortical loops are a hub of movement preparation and that movement preparation requires reciprocal excitation across multiple brain areas. A very recent paper by Wang et al. (2021) further elucidated this by demonstrating that in rodents movement preparation is supported by a cortico-basal ganglia-thalamo-cortical circuit. The study also demonstrated how optogenetic perturbation of the SNr-to-thalamus projections affected short-term memory biasing future licking choices but did not affect movement execution.

So far, preparatory activity has been observed prominently in the motor cortex, thalamocortical loops, and in identified pyramidal tract neurons (PT) that project directly to the spinal cord and brainstem motor centers (Guo, Li, et al. 2014; Tanji and Evarts 1976; Guo et al. 2017; Sommer and Wurtz 1998). However, preparatory activity does not trigger movements. Furthermore, how preparatory activity is converted to goal-directed movements remains unknown.

A study by (Kaufman et al. 2016) analysed the primate motor cortex during the transition from planning to movement showed a 'timing' signal that likely originates outside the motor cortex. This suggests that movement initiation likely involves coordinating multiple brain systems, including the basal ganglia, midbrain, and brainstem motor centers. As discussed in previous sections, how SNr control saccades became a prototypical example of voluntary movement initiation. SNr projects to and inhibits lateral regions of the superior colliculus, which regulates rhythmic licking (Rossi et al. 2016) and projects to the ALM-projecting motor thalamus. The lateral superior colliculus also receives prominent input from ALM. Considering SNr relevant role in the cortico-basal ganglia thalamocortical loop, its collateral projections to the motor thalamus (McElvain et al. 2021), and the role of efference copies in movement planning (Fee 2012), it seems plausible to imagine its involvement in movement preparation. What remains to be elucidated is 1) whether SNr encodes movement preparation (so far, only Wang et al. 2021 reported preparatory activity in SNr did not seem to affect movement); 2) if optogenetic perturbation of SNr during movement

preparation will have disruptive behavioural effects like those reported in other thalamocortical structures encoding preparatory activity.

1.5 Aims of research

This thesis aim is to answer the following questions:

1) Do SNr neurons encode movement preparation like the other structures of the cortico-basal ganglia thalamocortical loop, e.g., VM and ALM?

2) Does SNr activity have a causal impact on movement, and does this impact change with respect to movement preparation or movement initiation?

3) How do SNr neurons change their activity to movement? More specifically, I addressed whether SNr neurons show a uniform decrease in firing rates as Hikosaka's disinhibition model predicts or whether they show opposing activity changes, as predicted by Mink.

For aim 1, I designed a novel delayed-Go behavioural task to engage SNr in movement preparation and execution. For aim 2, I selectively drove SNr GABAergic neurons with ChR2 in distinct moments of the task. For aim 3, I performed *in vivo* electrophysiological recordings in distinct moments of the task.

2. Materials and Methods

2.1 Animals

All experiments using animals were carried out following the Animals (Scientific Procedures) Act of 1986 (United Kingdom). For most experiments, heterozygous VGAT-IRES-Cre male mice (*Slc32a1*$^{tm2(cre)Lowl/}$J, obtained from the Jackson Laboratory; Stock No: 016962; maintained in Oxford on a C57BL/6J background) were used. These mice express Cre recombinase under the control of the promoter of the *Slc32a1* gene encoding the protein vesicular GABA transporter (VGAT, also known as vesicular inhibitory amino acid transporter); when these mice are used in combination with Cre-dependent tools (e.g., viral vectors) they allow for selective experimental access to GABAergic neurons, including those in the SNr (e.g., for optogenetic manipulations). For some control experiments, C57BL/6J male mice were used (obtained from Charles River Laboratories). Both lines of mice were aged 3–5 months at the start of experiments.

2.2 Overview of surgical procedures carried out on mice

All behavioural, optogenetic and electrophysiological experiments (including related controls) were performed in awake head-fixed mice. All mice underwent a first surgical session for implantation of a head plate on the skull (see Sections 2.3.1 and 2.3.2) that allowed for subsequent head fixation (see Section 2.4.2). In some cases, Cre-dependent

viral vectors were intracranially injected during the same surgical session before implantation of the head plate (see Section 2.3.3). Most mice then (after behavioural training) underwent a second surgical session to gain access to the brain for electrophysiological recordings (Section 2.5.1 or to implant indwelling optic fibers (Section 2.5.2).

2.3 Procedures for head plate implantation and viral vector injection

2.3.1 Preparatory steps for cranial surgery

All surgeries were conducted under aseptic conditions. Mice were anesthetised with Isoflurane (IsoFlo ®; induction at 4% v/v, maintenance at 1-2% v/v; Abbott Laboratories, USA) in oxygen-enriched air (Novo Lite Mark 5, Intermedical, UK) and mounted in a stereotaxic apparatus (1430 series, Kopf Instruments, USA). Mice were placed on a homeothermic blanket (50-7220-F, Harvard Apparatus, Canada) to maintain their body temperature (~37°C), and their eyes were covered with a thin layer of protective lubricant (Optixcare, VETUK, UK). Before incising the scalp, it was shaved, cleaned with 70% v/v ethanol and betadine (Betadine ®, Avrio Health, USA) and infiltrated with local anaesthetic (0.25% w/v bupivacaine [Marcaine] solution, Hospira, USA). The skin overlying the skull was cut and removed. The underlying periosteum was then removed, and the bone cleaned with swabs soaked in sterile saline before being allowed to dry. Mice then progressed to head plate implantation (Section

2.3.2) or to intracranial viral vector injections (Section 2.3.3) before head plate implantation.

2.3.2 Head plate implantation

A burr hole (suitable for housing a small screw) was drilled above the cerebellum. The exposed skull with covered by a thin layer of precision cyanoacrylic glue (Bostick, 30813350, UK) onto which a custom-made titanium head plate (CJ2005485, 31 mm width x 12mm length x 1 mm depth, ~0.50g, Get It Made Ltd, UK) was directly positioned under stereotaxic control. Once the head plate was stable, a small stainless-steel screw (2 x 1 mm, M2, DIN84, RS, UK) was passed through the rear hole in the head plate and then screwed into the bone. This screw acted an anchor point. For those mice progressing to electrophysiological experiments (see Section 2.7), a second screw was implanted in the bone overlying the frontal cortex and attached to a grounding wire. Once the glue was set, silicone (Body Double "Fast Set", 498-494, Smooth-On, USA) was applied within the centre well of the head plate to cover the midline and Bregma (as well as any future craniotomy sites). After the silicone had set, dental cement (C&B Metabond® Quick Adhesive Cement System, Parkell Inc., USA) was added to cover any exposed areas of the skull, the cerebellar screw, and the horizontal bar of the head plate. At the end of the surgery, the skin edges were glued down using VetBond (VetBond, 3M, USA). Once the cement was set, the mouse was removed from ear bars. After surgery (see below), animals received analgesia (buprenorphine;

s.c.; 0.1 mg/kg/8 h; (Buprenex), 3421278, Reckitt, UK) and were allowed to recover fully.

2.3.3 Intracranial viral vector injections

For some experiments using VGAT-IRES-Cre mice, an adeno-associated virus (AAV) vector expressing, in a Cre-dependent manner, an opsin (Channelrhodopsin-2; ChR2) fused to a reporter (enhanced yellow fluorescent protein; EYFP) was unilaterally injected into the SNr region to allow for subsequent later optogenetic manipulation of transduced neurons. For control purposes, some VGAT-IRES-Cre mice were instead injected with an AAV harbouring only EYFP. The following viral vectors were used to selectively target opsins and/or reporter molecules to GABAergic neurons: AAV2-EF1a-DIO-hChR2(E123T/T159C)-EYFP, (#AV4868B, UNC Vector core, $6.2x10^{12}$ vg/ml) and AAV2-EF1a-DIO-EYFP (#AV4842F, UNC Vector Core, 4.5 x 10^{12} vg/ml). After drilling a small hole in the skull directly above the right SNr, a glass micropipette (internal tip diameter of 15-20 μm; pulled from graduated capillary tubes [Sigma, BlauBrand 708707]) containing the viral vector in undiluted manufacturer's solution was manually lowered under stereotaxic control into the SNr region, using the following stereotaxic coordinates: 3.0 mm posterior of Bregma, 1.5 mm lateral of Bregma, and 4.0 mm ventral to the brain surface (Paxinos and Watson 2006). Approximately 120 nl of the vector solution was then slowly injected (~30 nl/minute) using positive air pressure under manual control. To minimize reflux after injection, the micropipette was left in place for at least 8 minutes after the injection. After slow

withdrawal of the micropipette from the brain, surgery continued for the implantation of the head plate (see Section 2.3.2 above).

2.4 Behavioural training

2.4.1 Housing and controlled access to fluids

As a means of motivating the head-fixed mice to engage with the behavioural task, their access to fluids was controlled (hereafter termed 'water restriction') before training. The protocol for water restriction started after mice had fully recovered from cranial surgery (at least 3 or 4 days). All mice were single housed after head plate implantation in a 12 h light/dark cycle, and all experiments were performed during the light cycle. Dry food was continuously available (Rodent diet 5053, Scott Pharma, USA). After trialling several protocols for controlling access to fluids (data not shown), it was determined that satisfactory levels of task engagement were best achieved by restricting the daily water intake to the licenced minimum of 1.0 ml per 30g weight per 24 hours. The minimum volume of water was thus made available in a bowl in each individual cage at consistent times of the day. Mice typically consumed this water within a few minutes. This corresponds to approximately 35% of ad libitum water consumption for C57BL/6J mice (Mouse Phenome Database from the Jackson Laboratory: http://www.jax.org/phenome). All mice undergoing water restriction were monitored and weighed daily for welfare purposes. Water restriction was typically accompanied by a moderate loss of weight (5-10% of 'pre-restriction' weight). If mice dropped below 85% of their pre-restriction weight, or if mice showed overt signs of

dehydration (weight loss, sunken or recessed eyes, fuzzy facial fur) water restriction was immediately suspended. Mice never displayed overt signs of dehydration. After stabilization of body weight, typically after 3–4 days of water restriction, the training procedure began. Trained and motivated mice (see Section 2.4.3 below) often received all the available water allocation (e.g., 1 ml) within a daily task session. After behavioural sessions in which mice consumed less than the minimum intake of water, a water supplement (0.2–0.5 ml) was provided to achieve the minimum consumption rate. It was noted that consistent water restriction and training were very important, including on weekends, because even one day of ad libitum access to water could cause significant weight gain and consequential loss of motivation for several days thereafter.

2.4.2 Behavioural box environment

For task training and optogenetic/electrophysiological experiments in awake head-fixed mice, a custom-made behavioural box was built (see Chapter 3). Once a mouse was head-fixed, and the body placed in a plastic tube (free to move limbs), the mouse and head-fixation apparatus were placed in the dark behavioural box (0.05 lx) isolated from ambient light, sounds, and electrical noise. Tone and light stimuli were delivered using a custom stimulus box positioned ~5 cm anterior to the centre of the mouse head. The stimulus box was equipped with two LEDs (2439, green, 520 nm, ~2.1 lm; blue, 455 nm, ~0.03 lm, Adafruit, USA) and speakers (1784, sound pressure level, ~70 dB; frequencies, ~1, 4, 5 or 15 kHz, Adafruit, USA). Light wavelengths and tone frequencies were chosen to lie within the visible and audible range of C57BL/6J mice

(Bowen, Winkowski, and Kanold 2020; Huberman and Niell 2011). Rewards (water drops of ~0.01 ml each) were delivered using a metal spout attached to a syringe whose plunger was powered by a stepper motor. The stimulus box and reward delivery system were manipulated and monitored through custom programmed microcontrollers (Arduino Mega 2560, Arduino, Italy).

2.4.3 Operant delayed–Go task training

A schematic layout of the delayed–Go task is presented in Chapter 3. Each trial begins with a randomized inter-trial interval (ITI) of 4.3–10.0 s, during which the mice were allowed to lick the reward spout but did not receive any reward (ITI was pseudorandomized using Arduino programming language utilizing the "*random ()*" function). The mice were informed of the initiation of a trial by a Delay Cue consisting of a single high-pitch tone (15 kHz) lasting 300 ms. After the Delay Cue offset, a Delay Window begins and randomly lasts for 0.3–1.3 s, during which the mice had to withhold from licking the reward spout. If the mice licked the reward spout during the Delay Window, the trial was aborted, classified as a "Premature Hit" and the ITI started again. When mice successfully withheld from licking during the Delay Window, the mice were then presented with an Action Cue consisting of a 300 ms flash of the green LED. An Action Window began at Action Cue onset and lasted for 1s, during which time the mice had to lick to collect the water reward (single drop of ~0.01 ml). If the mice licked during the Action window, the trial was classified as a "Hit," and considered successful. If the mice failed to lick during the Action Window, the trial

was classified as a "Miss" and the ITI started again. Both Premature Hit and Miss trials were considered unsuccessful. A single task session has a maximum of 200 trials; after the last trial, the session automatically ended. Licks were detected using a piezoelectric sensor (RS Pro Vibration sensor, RS, UK) that was attached to the metal spout delivering the water reward. Analog readout from the sensor reporting the deflection of the spout was processed by Processing software (version 3, https://processing.org/) operated by an Arduino board (Arduino Mega 2560, Arduino, Italy) and sampled at a sampling rate of 100 Hz and saved as a comma-separated value (CSV) file. An arbitrary threshold was set to detect individual lick events online and the detected licks were immediately used to determine the outcome of the trial, e.g., providing water reward or aborting the trial and entering next ITI.

We divided the training into three different and sequential stages. The first stage involved habituation; after the mice had recovered from cranial surgery, they were habituated to the head-fixation apparatus for at least 3 days for increasing periods (e.g., 10, 20, and 30 min on Day 1, 2, and 3, respectively) until they were comfortable for at least one hour of fixation with intermittent water rewards. The second stage involved initial task training and lasted 7–10 days; in this stage, mice were trained in daily sessions (~30 minutes each). To facilitate the learning process, we initially rewarded the mice at Action Cue offset in a non-operant manner and progressively decreased this "free reward" in stages. Once mice reached 35–50% of Hit responses, we advanced to the third stage which lasted for 15–30 days. During this stage, mice underwent daily behavioural sessions (typically 20 minutes each) of the delayed-Go task, often

combined with electrophysiological recordings and/or optogenetic stimulation (see Section 2.6 and 2.7 below).

2.5 Procedures for electrophysiological and optogenetic experiments

2.5.1 Preparation for electrophysiological recordings

After recovering from head plate implantation surgery and viral injection, mice were habituated to the head-fixation apparatus as mentioned above. After satisfactory habituation, mice underwent behavioural training on the delayed-Go task. Some mice that had satisfactorily completed the behavioural training were taken forward for electrophysiological experiments. Twenty-four hours before acute electrophysiological data acquisition, a second cranial surgery was performed on these mice under isoflurane anaesthesia (see Section 2.3.1). In this surgery, a small unilateral craniotomy was made above SNr (craniotomy centred at 3 mm posterior and 1.5 mm lateral of Bregma), and the exposed brain protected with removable elastomer (Body Double "Fast Set", Smooth On, USA) to allow for electrode access in future experiments. After the elastomer had set, the mice received analgesia (buprenorphine; s.c.; 0.1 mg/kg/8 h; (Buprenex), 3421278, Reckitt, UK) and were allowed to recover fully.

2.5.2 Optic fiber implant procedure

After recovering from head plate surgery and viral injection, between 5 and 7 days before optogenetic stimulation, a second cranial surgery was performed on the mice that completed the behavioural training. In this surgery, existing burr holes from previous virus injection surgery were re-drilled in the skull above SNr (3 mm posterior and 1.5 mm lateral of Bregma). With the anchoring screws in place, the optic fiber implant (CFML22U-20, uncleaved fiber optic cannula, ⌀1.25 mm stainless ferrule, ⌀200 μm Core, Thorlabs, USA) was then lowered to the appropriate depth for SNr (4.5 mm below brain surface). Dental cement (C&B Metabond Quick Adhesive Cement System, Parkell, USA) was added to cover any exposed areas of the skull, anchoring screws, and the base of the fiber optic connector screw in several stages. When the cement had hardened, the mouse received analgesia (buprenorphine; s.c.; 0.1 mg/kg/8 h; (Buprenex), 3421278, Reckitt, UK) and were allowed to recover fully.

2.6 *In vivo* optical stimulation via chronically implanted optic fibers

For optical stimulation of ChR2-expressing neurons, laser light of 473 nm (06-MLD, Cobolt, Solna Sweden) was applied as driven by transistor-transistor logic (TTL) pulses from an Arduino board (Arduino Mega 2560, Arduino, ITA). In those mice used in experiments entailing optogenetics without electrophysiology, an optic fiber patch cord (MF1.25, 200 μm diameter; numerical aperture, 0.22 NA; Doric Lenses, Canada) was directly attached to the top optic fiber implant with a ceramic sleeve. Light

radiation was adjusted pre-implantation with an integrating-sphere optical power meter (PM100USB and S140C, Thorlabs, USA) to reach 6–12mW at the end of the implanted optic fiber. All optogenetic experiments took place inside the behavioural box (see Section 2.4.2). To prevent light 'leaking' both from the skull and the junction between the patch chord and the optic fiber ferrules, the entire optic fiber implant was wrapped with tinfoil.

Light delivered to the brain might reach the retinas of the mice (Danskin et al. 2015). To test for the possibility that laser light delivery affected the visual perception and behaviour of the mice (expressing ChR2), we implanted C57BL/6J mice with an optic fiber lowered into the SNr (as above for VGAT-IRES-Cre mice; Section 2.5.2). Light intensity was adjusted pre-implantation with an integrating-sphere optical power meter (PM100USB and S140C, Thorlabs, USA) to reach ~10 mW at the end of the implanted optic fiber.

The use of strong light power during optogenetic experiments has lately gained attention. The use of high light powers might cause nonspecific thermal effects on neural activity and in particular, to cause neuronal silencing, possibly via an impact on inward rectifier potassium channels expressed by neurons and glia (Cardozo Pinto and Lammel 2019; Wiegert et al. 2017). To better assess the effects of light-driven activation of ChR2, control experiments were performed on VGAT-IRES-Cre mice that had received intracerebral injections of AAVs harbouring EYFP but not ChR2 (see Section 2.3.3).

2.7 *In vivo* electrophysiological recordings and optogenetic stimulation

Mice were head-fixed and an "optrode" (i.e., a multi-channel electrode with integrated optic fiber) was inserted unilaterally into the SNr. Once-daily recordings (<1 h head fixation per session) were performed over 3–5 days per mouse. *In vivo* electrophysiological recordings were obtained by acute insertion of a customized silicon probe with spatially defined recording contacts (CJ2004981, NeuroNexus, USA). The probe had four shanks separated by 200 μm, each of which had sixteen recording contacts arranged in four tetrodes (contact area, 121 μm; contact interval, 25 μm) and with the tetrodes separated by 250 μm on each shank. Each contact had an impedance of 0.4–2.0 MΩ (measured at 1,000 Hz). 50-μm diameter optic fibers (B280-2335-10, MFC_200/230-0.37_10mm_ZF1.25(G)_FLT, Doric Lenses, Canada) were mounted 200 μm above the most dorsal recording contact on the 1st and 3rd shanks. The probe was manually advanced into the brain using a zero-drift micromanipulator (1760-61, Kopf, USA) under stereotaxic control. To mark the recording sites on the last day of electrophysiological recordings, the back of the silicon probe was evenly coated before use with the red fluorescent dye 1,1'-dioctadecyl-3,3,3',3'-tetramethylindocarbocyanine perchlorate (DiD; D3911, Invitrogen, USA) by application of a 100 mg/ml DiD solution in acetone (Magill et al. 2006). The same probe was cleaned after each experiment in a proteolytic enzyme solution (Magill et al., 2006) and used through a series of experiments. This was sufficient to ensure that contact impedances and recording performance were not altered by probe use and reuse. Neurons were recorded in and around the SNr (3.0 mm posterior and 1.5 mm

lateral of Bregma; DV: 4 − 4.7 mm). Recordings were started 10–20 minutes after probe insertion to allow the electrode/brain interface to stabilize. Skull screws above the frontal cortex were used as ground and external reference. The extracellular signals registered on the 64 recording contacts were buffered directly above the head of the animal through two A32-Omnetics32 adapters (Adpt-A32-OM32, Neuronexus ,USA) connected to two headstages (RHD2132, Intan Technologies, USA) serving as analog to digital converters and amplifiers and connected to Open Ephys acquisition box. Filtered data was saved to a computer at a 30 kHz sampling rate (DSP cut-off 1Hz, bandpass filter 1.85 Hz – 7600 Hz). All recordings took place inside a Faraday cage. For optical stimulation of ChR2, laser light of 473 nm (06-MLD Cobolt, Solna Sweden) was applied as driven by TTL pulses from an Arduino board (Arduino Mega 2560). An optic fiber patch cord (B280-2335-10, MFC_200/230-0.37_10mm_ZF1.25(G)_FLT, Doric Lenses, Canada) was directly attached to the optrode with a ceramic sleeve. Light intensity was adjusted pre-implantation with an integrating-sphere optical power meter (PM100USB and S140C, Thorlabs, USA) to reach 6 –12 mW at the end of the implanted optrode. All recordings took place inside a Faraday cage within the behavioural box (see Section 2.4.2).

2.8 Histological verification

After completion of experiments, mice were deeply anaesthetized with pentobarbital (OAK, USA) and transcardially perfused with ~25 ml of 0.05M phosphate-buffered saline (PBS, pH 7.4) followed by ~25 ml fixative (4% w/v paraformaldehyde dissolved in 0.1 M phosphate buffer, pH 7.4). Brains were post-fixed in fixative and cut into 50-µm thick sections in the parasagittal plane on a vibrating microtome (VT1000S; Leica Microsystems, Germany). Sections were mounted on glass slides, coverslipped with a glycerol-based aqueous mountant (VECTASHILED, Vector Laboratories, UK), and imaged with an epifluorescence microscope (Zeiss Axioscan, Zeiss, with objective lenses Plan-APOCHROMAT, magnification 0.45 or 0.8, Germany). Placement of the optical fibers and optrodes was assessed on the basis of DiD staining (painted on the back of the probe). Tissues were stained with 4′,6-Diamidino-2-phenylindole dihydrochloride (DAPI).

2.9 Signal quantification and statistical analyses

For the analyses of electrophysiological recordings during electrophysiological and behavioural sessions with optogenetic control of SNr neurons, the CSV data containing lick readout and trial progression acquired at 100 Hz with Processing and the Open Ephys recording data sampled at 30 kHz storing unit recordings and/or laser pulse time stamps needed to be synchronized. This was done *post hoc* by way of TTL pulses sent from Arduino and recorded with Open Ephys. Each Open Ephys recording was started before and ended after the recording of accompanying CSV data. Immediately before

the onset of each trial, a 100 ms TTL pulse was sent to one of the ADC channels of an Open Ephys acquisition board (Open Ephys Acquisition Board, Open Ephys, USA). After recording, the falls of the 100 ms-long TTL pulses saved in Open Ephys data were aligned with the onsets of trials in Processing CSV data by estimating the precise sampling rate (tended slightly lower than 100 Hz, e.g., 99.966 Hz) and the initial offset of Processing CSV data to minimize the temporal mismatch at those alignment points between the two-time series. All the data points in Processing CSV data were then assigned with the timestamps at 30 kHz resolution. We used two of the four headstage ports available in the Open Ephys acquisition board, each of which was interfaced with one Intan chip for 32 channels, i.e., half of the recording contacts of the probe. Data acquisition was driven by an Opal Kelly XEM-6310 FPGA module, running a modified version of Intan's Rhythm FPGA firmware (https://github.com/open-ephys/rhythm). The FPGA ensured that data acquisition is synchronized between all Intan chips and serializes the data for transmission via a USB 3.0 port. Spike sorting was performed with a MATLAB tool IronClust (https://github.com/flatironinstitute/ironclust). Clusters of spike waveforms with more than 1.5% of their ISIs shorter than 1.5 ms were considered multi-units lacking a refractory period and excluded from single-unit activity analyses. In the creation of peri-event time histograms (PETHs) for licks and spikes, a bin size of 40 ms was used. The histogram curves were smoothed by applying a moving average of 5 data points with MATLAB "smooth" function. When analysing the trials, each session's last consecutive Miss trials were excluded because we cannot distinguish whether the animals lost their vigour or failed to respond to the cues. Many

sessions were terminated after consecutive Miss trials (~15). Also, for the analyses of spike PETHs, clusters with baseline firing rates of 2 Hz or lower were excluded because they are unlikely to be SNr neurons, whose baseline firing rates are typically ranging 40–80 Hz in awake mice (Lobb and Jaeger 2015). The baseline firing rates were measured by counting the number of spikes at 1 s windows 0.1 s before the onset of each trial and dividing the sum of spike counts by the sum of the duration of those windows. Z-scores (z) of firing rates were obtained using the mean (μ) and standard deviation (σ) across these 1 s windows, unless otherwise mentioned, as: $z = \frac{x - \mu}{\sigma}$, where x is the firing rate. Box plots provide a visual representation of summary statistics for a data sample. Given numeric data, the corresponding box plot displays the following information: the median, the lower and upper quartiles, and any outliers (computed using the interquartile range). The line inside of each box is the sample median. The top and bottom edges of each box are the upper and lower quartiles, respectively. The distance between the top and bottom edges is the interquartile range (IQR). The upper quartile corresponds to the 0.75 quantile and the lower quartile corresponds to the 0.25 quantile. Outliers are values that are more than 1.5 · IQR away from the top or bottom of the box. Each outlier using an 'o' symbol. The whiskers are lines that extend above and below each box. One whisker connects the upper quartile to the nonoutlier maximum (the maximum value that is not an outlier), and the other connects the lower quartile to the nonoutlier minimum (the minimum value that is not an outlier). Further analysis was performed using custom MATLAB functions and scripts (written by Dr. Kouichi C. Nakamura).

3. Designing a novel delayed–Go task to engage SNr in movement preparation and execution

3.1 Introduction

One of the long-standing aims of neuroscience research is to connect the dynamics of brain circuits to behaviour, explaining one on the basis of the other (O'Connor, Huber, and Svoboda 2009). Cell-type-specific monitoring and manipulation are required to decode the principles of neuronal circuits (Luo, Callaway, and Svoboda 2008). Due to the widespread availability of transgenic mice that allow cell-type-specific targeting, the mouse has become a well-established system for dissecting the functions of mammalian neural circuits (Dymecki and Kim 2007).

Over the last decade, increasingly sophisticated procedures for quantitative behaviours have been developed for head-fixed mice, somewhat inspired by investigations in behaving non-human primates that are head fixed (Schwarz et al. 2010). Head-fixed mice have been trained in choice-based activities using operant conditioning to discriminate odours (Komiyama et al. 2010; Abraham et al. 2012), auditory stimuli (Sanders and Kepecs 2012), visual stimuli (Andermann, Kerlin, and Reid 2010), and tactile cues (Pammer et al. 2013). In addition, the recent development of 'delayed response tasks' for head-fixed rodents has allowed for detailed mechanistic studies of motor preparation (Guo et al. 2017; Guo et al. 2014; Li et al. 2015; Guo et

al. 2014). Specifically, in one study by (Guo et al. 2017), head-fixed mice performed a task in which they reported a decision by directional licking after a delay period. To achieve my thesis aims, I had to develop a task that would likely engage SNr neurons both in movement preparation and execution. In recent years several studies have investigated SNr encoding of cued movements (licking) in operant tasks as well as the preparation of such movements (Catanese and Jaeger 2021; Morrissette et al. 2019; Guo et al. 2017). An adaptation of a delayed–licking operant behaviour could be particularly suitable for my purposes because the inclusion of a delay period between instructive cues would in theory allow for interrogation of neuronal circuit functions related to the preparation, initiation, and termination of a well-defined movement. I, therefore, decided to establish a novel delayed–Go behavioural task in which head-fixed mice were exposed first to an auditory cue ('get ready'), and after a variable delay period, they had to rapidly respond ('Go') to a visual cue by licking a spout to collect a water reward (see Section 3.3). Since I was not interested in studying the lateralization of licking and wanted to facilitate the task learning process, I decided to remove the directional licking component from the original task (Guo et al. 2017).

3.2 Building an operant chamber for the delayed–Go task

While licking is itself an innate behaviour, licking as part of delayed–Go task demands learning that is dependent on timely delivery of cues and rewards. Unfortunately, commercially available devices are often costly and less flexible to meet ever-changing

research needs. Therefore, I designed and built a bespoke behavioural testing apparatus ('rig') suitable for intracranial optogenetic manipulations and electrophysiological recordings in head-fixed mice performing the delayed-Go task (Figure 3.1). The same rig was also used for initial task training of the mice. The rig was built around stereotaxic equipment that facilitated for high-precision targeting of brain structures. I thus placed two anterior-posterior, custom-made titanium stereotaxic bars (CJ2005485 Get It Made Ltd, UK), based on those in a standard stereotaxic frame (Model 1430; Kopf, USA) in a custom-made dark behavioural box that attenuated ambient light, sounds, and electrical noise. Mice where head fixed onto the frame through a custom-made titanium head bar holder mounted on standard optomechanical components (Thorlabs). For electrophysiological recordings, a 3-axis stereotaxic manipulator (Model 1760-61-SB; Kopf) was fixed to one bar, and then a single-axis stepper motor (IVM-1000; Scientifica) was fixed to the manipulator. I optimized the stimulus box and reward delivery system for sending out the timing and duration of behavioural events through variable-length TTL pulses. Tone and light stimuli are delivered via a custom-made stimulus box positioned at 5 cm anterior to the centre of the mouse head. The stimulus box was equipped with two LEDs (2439, green, 520 nm, ~2.1 lm; blue, 455 nm, ~0.03 lm, Adafruit, USA) and speakers (1784, sound pressure level, ~70 dB; frequencies, ~1, 4, 5 or 15 kHz, Adafruit, USA). Light wavelengths and tone frequencies were chosen to lie within the visible and audible range of C57BL/6J mice (Bowen, Winkowski, and Kanold 2020; Huberman and Niell 2011). Rewards (water drops of ~0.01 ml each) were delivered using a metal spout attached to a syringe whose

plunger was powered by a stepper motor. Licks were detected using a piezoelectric sensor (RS Pro Vibration sensor, RS, UK) that was attached to the metal spout delivering the water reward. The stimulus box and reward delivery system were manipulated and monitored through custom programmed microcontrollers (Arduino Mega 2560, Arduino, Italy). A camera was used to detect mice licks in real-time (Microsoft LifeCam Studio, 2 MP, 1920 x 1080 pixels, 30 fps, 1080p, 1920 x 1080 pixels, 5 M). Data are recorded in real-time, and distinct TTL signals are used to trigger lasers or other equipment (see Materials and Methods, sections 2.4.2 and 2.4.3).

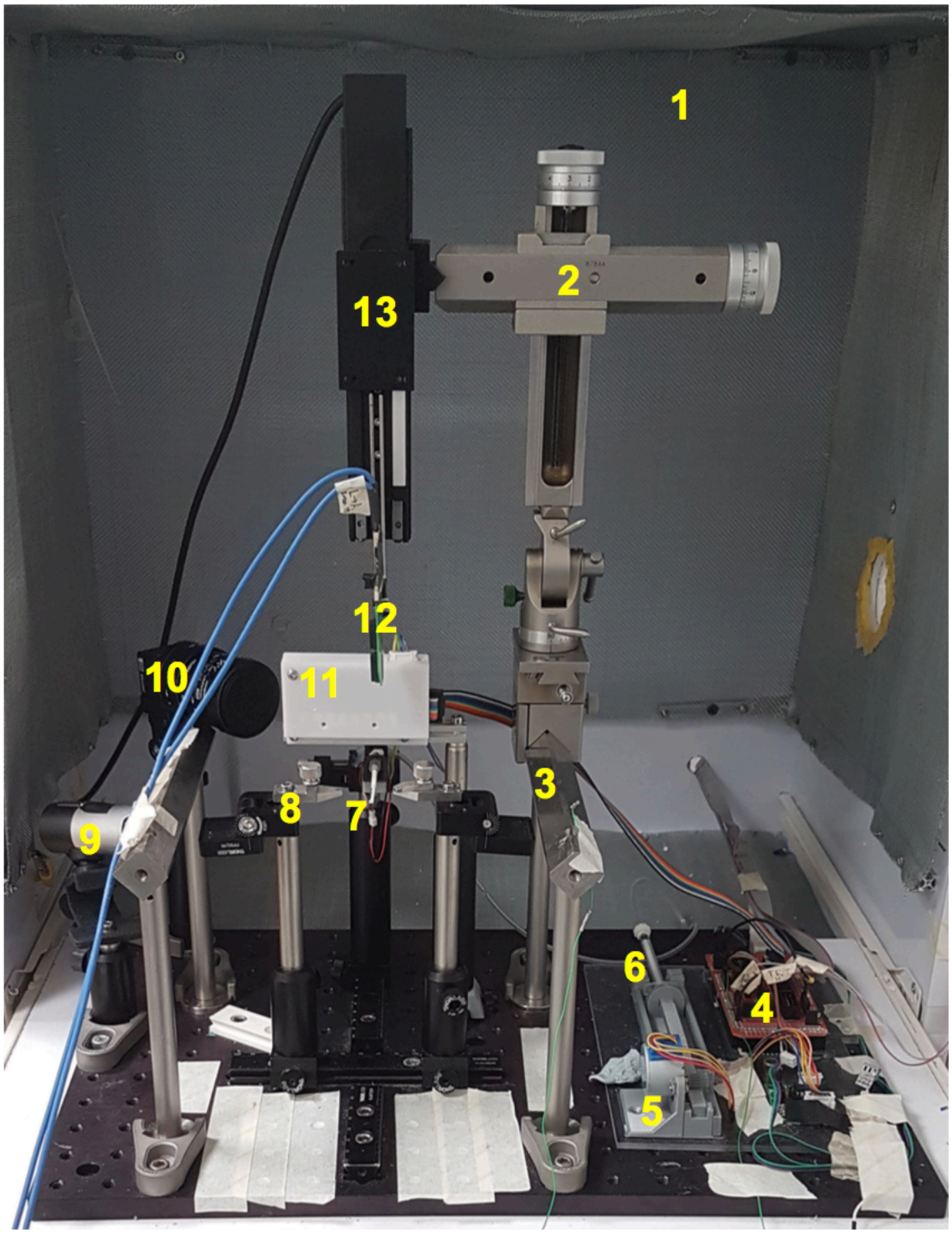


Figure 3.1 Apparatus for interrogation of neuronal function in head-fixed mice performing for the delayed–Go behavioural task. (1) Sound attenuating chamber, housing an operant rig and a Faraday cage. **(2)** Stereotaxic manipulator. **(3)** Stainless steel stereotaxic frame (anterior–posterior bar). **(4)** Arduino circuit board. **(5)** Motor that operated the syringe pump for dispensing liquid (water) rewards. **(6)** 3-D printed support for syringe pump. **(7)** Custom-made spout for water delivery and

licking detection. **(8)** Optical posts and custom-designed holders for head fixation. **(9,10)** Webcams. **(11)** Custom-designed stimulus box for light and sound delivery and data acquisition. **(12)** 2×32 channels Intan head stage for electrophysiological recordings; connectable to a silicon probe and an Open Ephys acquisition box. **(13)** Single axis stepper motor for advancing electrodes into the brain. Note that mice were placed in an elevated plastic tube for testing (not shown).

3.3 Design of the delayed–Go task

A schematic layout of the delayed–Go task and its three key trial outcomes is shown in Figure 3.2. Each trial of the delayed–Go task begins with a randomized inter-trial interval (ITI) of 4.3–10.0 s, during which the mice are allowed to lick the reward spout but cannot receive any reward. The mice are informed of the initiation of a trial by a Delay Cue consisting of a single high pitch tone (15 kHz) lasting for 300 ms. After the Delay Cue offset, a Delay Window begins and randomly lasts for 0.3–1.3 s, during which the mice have to withhold from licking the reward spout. Mice are not allowed to lick in the Delay Window, so movement preparation is not confounded with movement execution. The Delay Window duration was designed to best adapt to mice attention span and impulsivity (Mar et al. 2013), a jittered (variable) Delay Window was introduced to prevent the mice from solving the task by counting. After successfully holding back from licking during the Delay Window, the mice are presented with a 300 ms-long flash of a green LED (an Action Cue). An Action Window begins at Action Cue onset and lasts for 1s, i.e., outlasting Action Cue; during an Action Window, mice have to lick the spout to collect the liquid reward (0.01 ml water). If the mice lick during an Action window, the trial is classified as "Hit" and

considered successful, followed by an ITI (Figure 3.2A). If the mice lick the reward spout during the Delay Window, the trial is aborted, classified as a "Premature Hit" (one form of failure), and an ITI starts again (Figure 3.2B). If the mice withhold from licking throughout the trial, the trial is classified as a "Miss" (another form of failure), and an ITI starts again (Figure 3.2C). A single session has a maximum of 200 trials; after the last trial, the session automatically ends. When mice achieve 100 Hits, the session ends earlier. In order to facilitate the learning process, I initially partly rewarded the mice at Action Cue offset in a non-operant manner and progressively decreased the free reward in stages (Figure 3.3). For further details, see Materials and Methods, section 2.4.3.

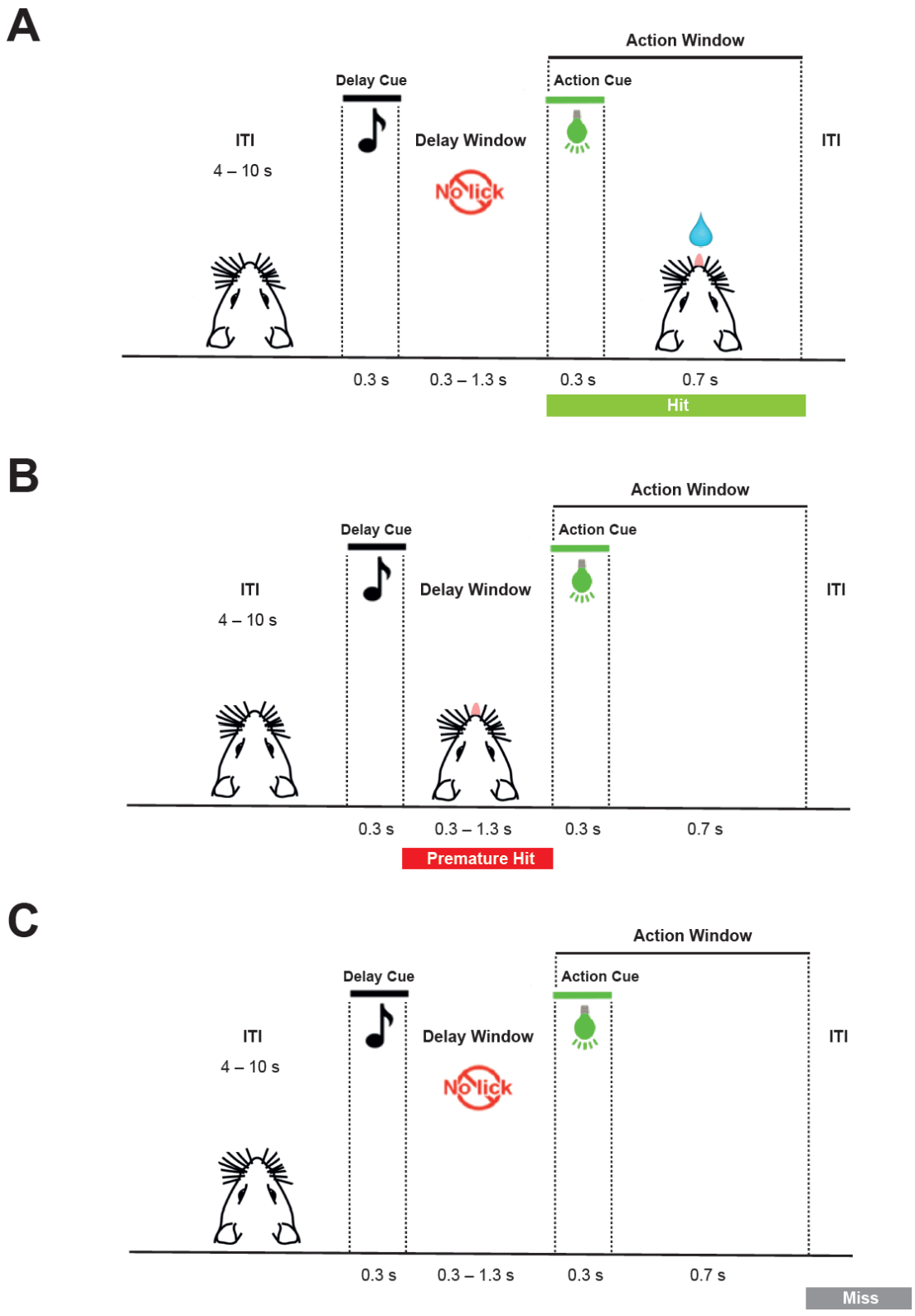

A
Action Window
Delay Cue
Action Cue
ITI
4 – 10 s
Delay Window
No lick
ITI
0.3 s
0.3 – 1.3 s
0.3 s
0.7 s
Hit
B
Action Window
Delay Cue
Action Cue
ITI
4 – 10 s
Delay Window
ITI
0.3 s
0.3 – 1.3 s
0.3 s
0.7 s
Premature Hit
C
Action Window
Delay Cue
Action Cue
ITI
4 – 10 s
Delay Window
No lick
ITI
0.3 s
0.3 – 1.3 s
0.3 s
0.7 s
Miss

Figure 3.2 Schematic time course of a delayed–Go task trial. **A:** Hit trial. After an initial randomized inter-trial interval (ITI), a mouse is presented with a Delay Cue (300 ms-long high pitch tone), which is followed by a Delay window (0.3–1.3 s). If the mouse successfully withholds from licking, the mouse is presented with an Action cue (300 ms-long flash of a green LED), and an Action Window (1 s) begins at Action Cue onset. If the mouse licks during the Action Window, he collects water reward, and the trial is classified as "Hit," and an ITI starts again. **B:** Premature Hit trial. If the mouse licks the reward spout during the Delay Window, the trial is aborted, classified as a "Premature Hit" (one form of failure), and an ITI starts again. **C:** Miss trial. If the mouse withholds from licking throughout the trial, the trial is classified as a "Miss" (another form of failure), and an ITI starts again.

3.4 Learning the delayed–Go task: an example

Before the behavioural training of mice, their access to fluids was controlled (see section 2.4.1) and they were habituated to head fixation (see section 2.4.3). To show how mice progressed in the behavioural training, I first present an example of two sessions recorded from one mouse (gms064) on day 1 and 15of training on the delayed–Go task. On day 1 of the training session (> 100 trials), the mouse struggled to solve the delayed–Go task. The peri-event time histogram (PETH) curve of licking shows that responses peaked after the Action Window (Figure 3.3A and Figure 3.4B). The high amount of Miss trials (38.3%) and the low number of Hit trials (4.7%) indicate that the mouse failed to associate the Action Cue with the correct behavioural response (i.e., lick within brief Action Window to collect water reward) (Figure 3.3C). The mouse extensively collected non-operant rewards (Free Reward, 37.5% of trials) (Figure 3.3C). On day 15, the licks peaked within the Action Window (Figure 3.3D

and Figure 3.4E). The mouse achieved a high number of Hit trials (54.3%) without the help of free reward trials and a low number of Miss trials (9.8%) (Figure 3.3F). The increase in Hit trials and drop in Miss trials from day 1 suggests that the mouse successfully learned to associate the Action Cue with the appropriate behavioural response. The increase in the proportion of Premature Hit trials from day 1 to day 15 could be accounted for by the notion that this mouse learned the Action Cue faster than the Delay Cue, although other mice showed decreased incidences of Premature Hits over training (see Figure 3.4D).

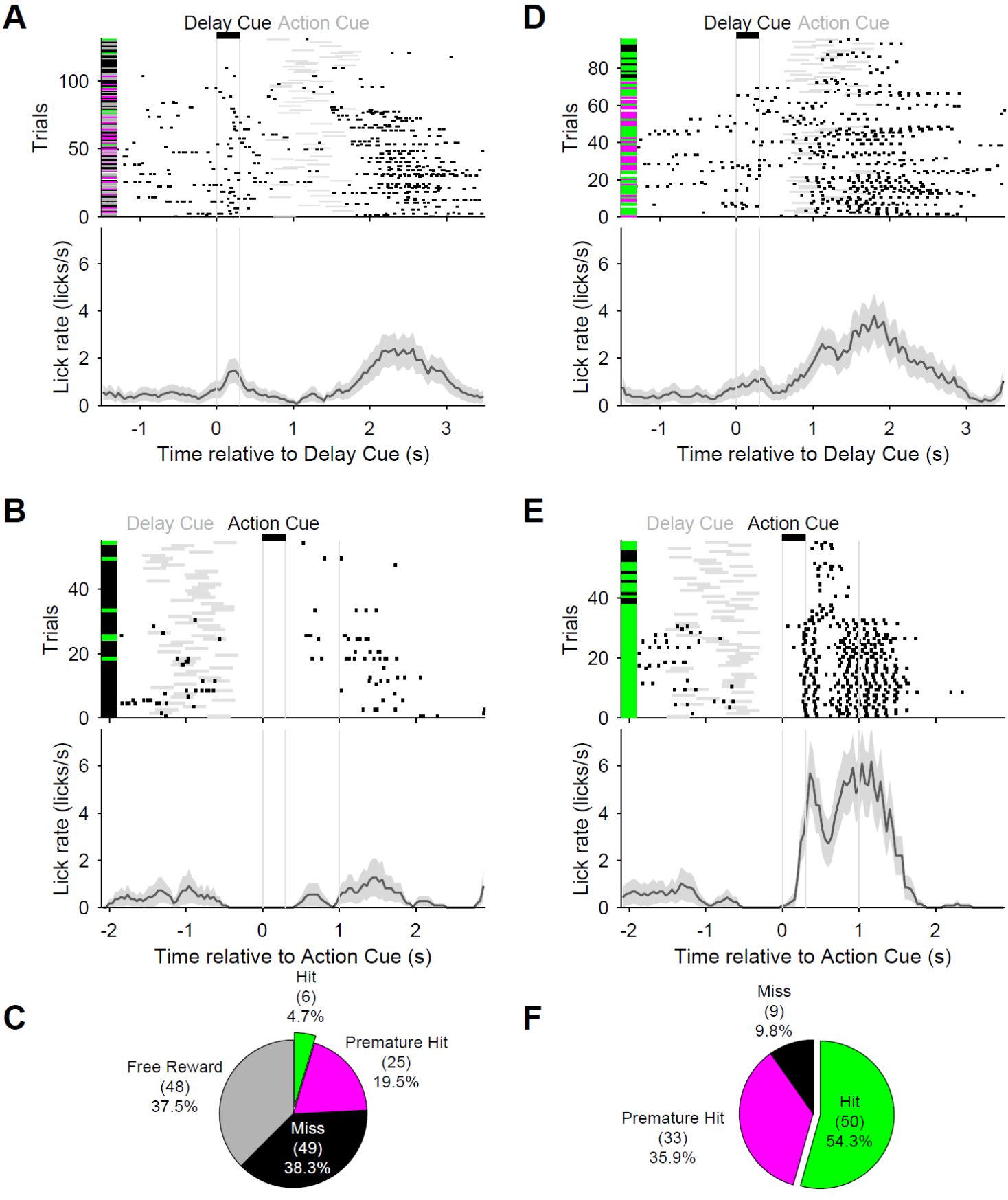

A
Delay Cue Action Cue
Trials
100
50
0
Lick rate (licks/s)
6
4
2
0
-1
0
1
2
3
Time relative to Delay Cue (s)
D
Delay Cue Action Cue
Trials
80
60
40
20
0
Lick rate (licks/s)
6
4
2
0
-1
0
1
2
3
Time relative to Delay Cue (s)
B
Delay Cue Action Cue
Trials
40
20
0
Lick rate (licks/s)
6
4
2
0
-2
-1
0
1
2
Time relative to Action Cue (s)
E
Delay Cue Action Cue
Trials
40
20
0
Lick rate (licks/s)
6
4
2
0
-2
-1
0
1
2
Time relative to Action Cue (s)
C
Hit
(6)
4.7%
Premature Hit
(25)
19.5%
Free Reward
(48)
37.5%
Miss
(49)
38.3%
F
Miss
(9)
9.8%
Premature Hit
(33)
35.9%
Hit
(50)
54.3%

Figure 3.3 Performance of a mouse on day 1 and day 15 of the delayed–Go task. A: Top, the raster plot of licks during the task on day 1, aligned to onset of the 0.3 s Delay Cue (t = 0). Each black tick indicates a single lick. The horizontal grey bars in the middle correspond to the 0.3 s Action Cue (presented after a randomized duration of Delay Window, 0.3–1.3 s, in Hit and Miss trials). The colour bars on the left hand indicate trial outcomes in order of occurrence in session: Hit (green), Premature Hit (magenta), Miss (black), and Free Reward (grey). Bottom, PETH of mice licks for all trials. **B:** Similar to A, but with licks aligned to onset of the 0.3 s Action Cue (t = 0). Only Hit and Miss trials are shown. **C:** Pie chart of trial outcomes on day1. **D:** Similar to A, but for day 15 of training. **E:** Similar to B, but for day 15 of training. **F**: Pie chart of trial outcomes on day 15. Note that the session did not have free reward trials anymore.

3.5 Mice learned the delayed–Go task in about 2 weeks of training over non-consecutive daily sessions

After confirming with pilot studies that mice could successfully learn the delayed–Go task, I proceeded with injecting more mice with Cre-dependent viral vectors for optogenetic experiments (see Materials and methods section 2.3.3) and trained them on the delayed–Go task. Twelve mice (n = 8 injected with ChR2; n = 4 used as control injected with EYFP only) were trained and their behavioural performance monitored for 3–7 weeks, with daily sessions lasting for an average of 20 ± 10 minutes each (sessions n = 420). The following analysis of behavioural data did not consider transitions between different stages of experiments (e.g., the start of optogenetic or electrophysiology experiments). To assess learning progress without the effects of laser, laser-on trials during optogenetic experiments were omitted. Also, because Miss trials towards the end of each session might arise from the loss of engagement (e.g.,

satiation after receiving numerous water rewards) and/or failure in processing the instructive cues, the last consecutive Miss trials at the end of each session were removed from the analysis.

To solve the delayed–Go task, mice have to withhold from licking when presented with the Delay Cue and lick (within a brief time window) when presented with the Action Cue. If mice successfully perform both actions within the same trial, they score a "Hit" and collect a water reward. I, therefore, measured the evolution of the Hit rate over sessions and used it as an indicator of task learning by the mice. On average, both ChR2 and control groups increased their Hit rates, i.e., the proportion of Hit trials compared to the sum of Hit, Premature Hit, and Miss trials, while individually progressing at various rates (ChR2 group, 6.27 ± 2.04 % Hit rate for day 1, 39.30 ± 7.05 % for day 15; Control group, 9.02 ± 1.59 % Hit rate for day 1, 66.77 ± 2.81 % for day 15; mean ± SEM) (Figure 3.4A). The Hit rates significantly increased from day 1 to day 15 for both ChR2 and control groups (ChR2, $p = 1.5540\text{x}10^{-04}$; Control, $p = 0.0286$) (Figure 3.4F). This significant increase in Hit trials between day 1 and day 15 is a good indicator that mice successfully learned to associate both cues to the appropriate behavioural response and therefore learned the delayed–Go task. It is worth noting that, unlike in alternative choice tasks (e.g., Go-No Go task), 50% of correct responses (50% Hit rate) do not mean

that the mouse is randomly performing. The low (~10%) Hit rates of Day 1 of training (Figure 3.4F–J, left boxplots) exemplify the near-random behaviour of naïve mice.

With this task, mice could learn the Delay Cue and the Action Cue separately. One strategy that mice could enact to solve the task is to ignore the Delay Cue, wait until the Action Cue is presented to them, and then perform a "Hit" and collect the liquid reward. This strategy would in turn confound the examination of whether SNr neurons encode or are important for motor preparation. To control whether mice adopted this unwelcome strategy, I performed separate analyses for Delay Cue and Action Cue to determine whether mice learned to associate them with the proper behavioural responses to Action Cue alone or both cues.

To check the learning of the Action Cue, I measured the ratio of Hit trials to the sum of Hit and Miss trials over sessions (Hit / (Hit + Miss) rate). If mice had learned to associate the Action Cue to lick, I would expect a progressive increase in Hit trials and a decrease in Miss trials. I saw a consistent increase of Hit / (Hit + Miss) rate over sessions (ChR2 group, 12.46 ± 5.31 % for day 1, 83.46 ± 7.51 % for day 15; Control group, 16.76 ± 2.80 % for day 1, 92.95 ± 4.64 % for day 15; mean ± SEM) (Figure 3.4B). The Hit / (Hit + Miss) rate significantly increased from day 1 to day 15 for both ChR2 and control groups (ChR2 $p = 1.5540\text{x}10^{-04}$, Control $p = 0.0286$ (Figure 3.4G), indicating that the mice successfully learned the Action Cue.

To check the progression of the mice in learning the Delay Cue, I measured the ratio of Hit trials to the sum of Hit and Premature Hit trials over sessions (Hit / (Hit + Premature Hit) rate). If mice had learned to correctly associate the Delay Cue to withhold from licking and at the same time to lick when presented with the Action Cue, I would expect a progressive decrease of Premature Hit trials and an increase in Hit trials. I observed a steady increase of Hit / (Hit + Premature Hit) over sessions (ChR2 group, 15.48 ± 2.76 % for day 1, 43.98 ± 7.70 % for day 15; Control group, 17.14 ± 3.12 % for day 1, 72.00 ± 6.73 % for day 15; mean ± SEM) (Figure 3.4C). Hit / (Hit + Premature Hit) rate significantly increased from day 1 to day 15 for both ChR2 and control groups (ChR2 p = 1.5540x10^{-04}, Control p = 0.0286) (Figure 3.4H), thus suggesting that the mice successfully learned the Delay Cue to some extent (though imperfectly). The significant increase of both Hit / (Hit + Miss) rate and Hit / (Hit + Premature Hit) rate after 15 days of training shows that mice did learn to associate both Action Cue and Delay Cue, rather than ignoring the Delay Cue altogether.

Unlike Miss trials, Premature Hit trials took longer to decrease (ChR2 group, 29.41 ± 7.79 % for day 1, 51.05 ± 8.01 % for day 15; Control group, 45.17 ± 5.77 % for day 1, 15 27.17 ± 6.95 % for day 15) (Figure 3.4D). The mean values of Premature Hit trials significantly increased from day 1 to day 15 for the ChR2 and significantly decreased for Control group (ChR2, p = 6.2160x10^{-04}; Control, p = 0.0286;) (Figure 3.4I).

Further evidence of mice learning the Action Cue is given by the decrease in the proportion of Miss Trials over sessions (ChR2 group, 64.30 ± 9.63 % for day 1, 9.63 ± 4.29 % for day 15; Control group 45.08 ± 5.7 % for day 1,15 6.05 ± 4.47 % for day 15; mean ± SEM) (Figure 3.4E). The Miss rate significantly decreased from day 1 to day 15 for both ChR2 and control groups (ChR2 p = 0.0019, Control p = 0.0286) (Figure 3.4J).

The marginal decrease in Premature Hit trials led me to hypothesize that the mice learned the Action Cue faster than the Delay Cue. An analysis of the speed at which mice increased Hit / (Hit + Miss) rate and Hit / (Hit + Premature Hit) rate, which I consider indicated learning of Action Cue and Delay Cue, respectively, confirmed this (Figure 3.5). On average, it took mice 4.9 days to show an increase of 30% in learning the Action cue (Hit/ Hit + Miss, n = 10 mice, ChR2 and control mice were mixed). This was significantly faster ($p = 1.94\times10^{-4}$) than the time spent (15.5 days) to show the same increase in the Delay Cue (Hit/ Hit + Premature Hit; n = 11 mice). In other words, ChR2 group took longer than 15 days to decrease the number of Premature Hit Rates.

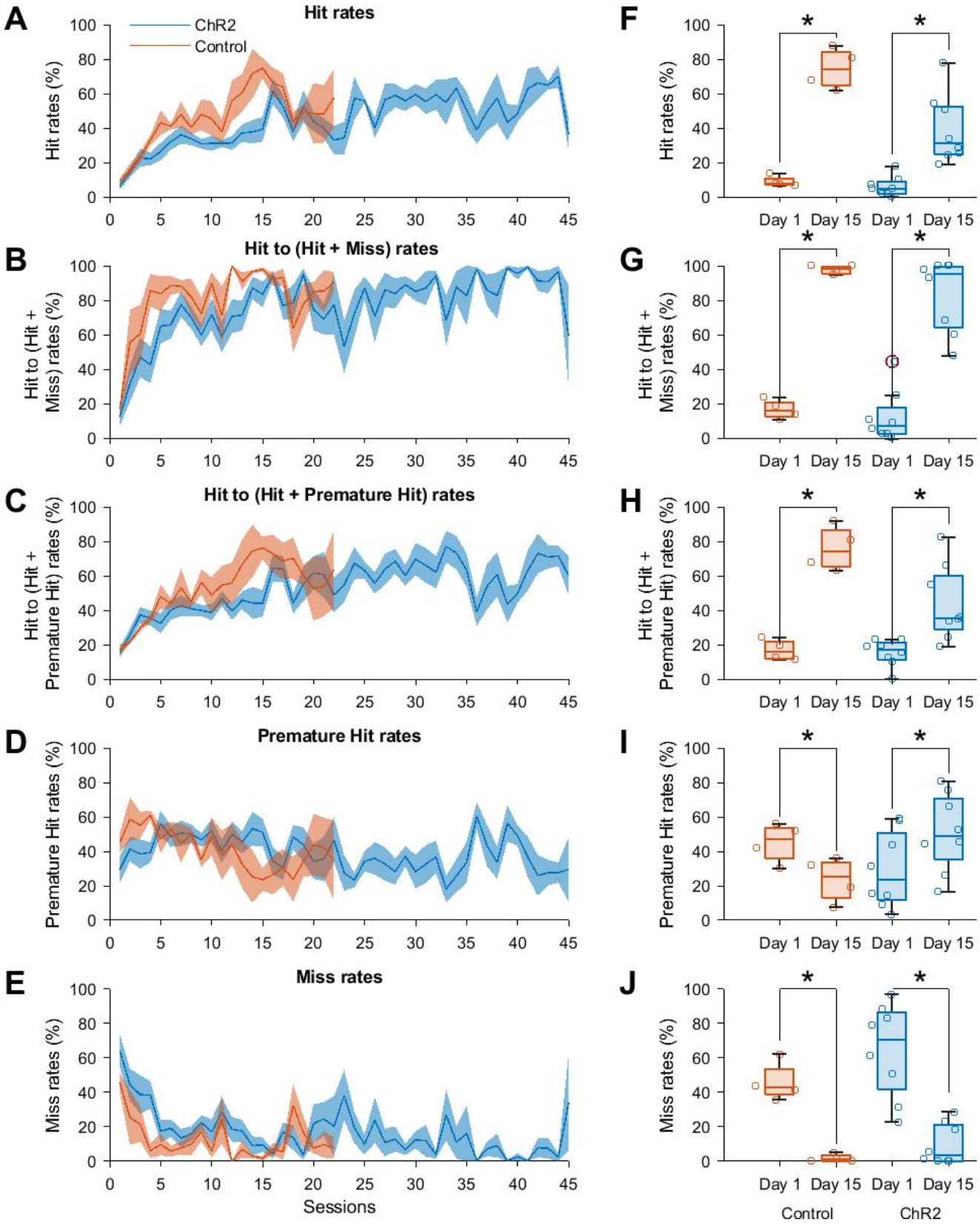

A
Hit rates
ChR2
Control
Hit rates (%)
B
Hit to (Hit + Miss) rates
Hit to (Hit + Miss) rates (%)
C
Hit to (Hit + Premature Hit) rates
Hit to (Hit + Premature Hit) rates (%)
D
Premature Hit rates
Premature Hit rates (%)
E
Miss rates
Miss rates (%)
Sessions
F
G
H
I
J
Day 1
Day 15
Control
ChR2

Figure 3.4 Mice learn the delayed–Go task in about 2 weeks of training over non-consecutive daily sessions. Mice's learning of the delayed–Go task (blue, ChR2 group; red, control group). Solid lines represent mean values; shaded areas represent standard error of mean (SEM). **A**: Hit rates over days of training. **B:** Hit/ (Hit + Miss) rates over days of training. **C:** Hit/ (Hit + Premature Hit) rates over days of training. **D:** Premature Hit rates over days of training. **E:** Miss rates over days of training. **F–J:** Comparison of Hit rates (F), Hit/ (Hit + Miss) rates (G), Hit/ (Hit + Premature Hit) rates (H), Premature Hit rates (I), and Miss rates (J) on day 1 and day 15. Box plots denote the minimum and maximum values that are not outliers (whiskers), interquartile range, and medians (see Materials and methods section 2.9). * $p < 0.05$, MWUT.

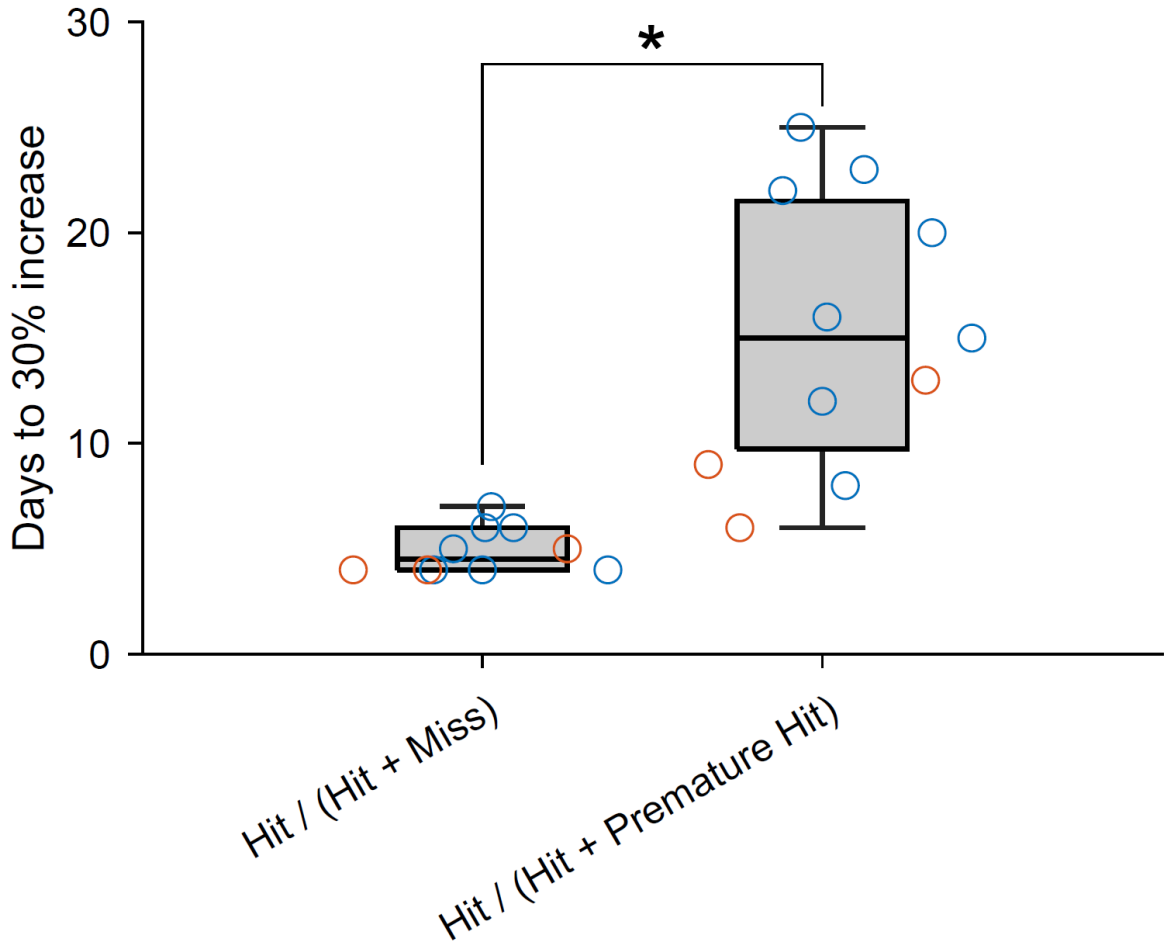


Figure 3.5 Mice learn the Action Cue faster than the Delay Cue. Learning speed for the Action Cue, as quantified by time taken to achieve a 30% increase in Hit/ (Hit + Miss) rates, and that of the Delay Cue, as indicated by time to a 30% rise in Hit/ (Hit + Premature Hit) rates. Box plots denote the minimum and maximum values that are not outliers (whiskers), interquartile range, and medians (see Materials and methods section 2.9). * $p < 0.05$, MWUT.

3.6 Discussion

In this chapter, I presented the results of training head-fixed mice to perform a novel delayed–Go behavioural task. In each trial, mice were exposed first to an auditory cue, and after a variable delay period in which mice had to refrain from licking, they had to respond to a visual cue by licking a spout to collect a water reward. Mice had limited access to water and were thus motivated by thirst. Mice performed up to 200 behavioural trials per daily session for water rewards.

All 12 mice were successfully trained and used for analysis. Mice were typically trained in batches of 3–4 animals; they were not trained simultaneously and were occasionally given a rest day from training. Non–overlapping resting days account for the three missing sessions in Figure 3.5.1. Unlike the ChR2 group that kept on performing the behaviour up to 7 weeks while undergoing optogenetic and electrophysiology experiments, mice in the control group stopped the training after 3 weeks (after they had reached a satisfactory performance level and did not require further experiments).

Mice learned to perform the delayed–Go task to satisfactory levels of success in about two weeks of non-consecutive daily sessions. Furthermore, mice learned to associate both cues with an appropriate response (i.e., withhold from licking after the auditory "Delay Cue" and lick soon after the visual "Action Cue"). Overall, Premature Hit rates in both ChR2 and control mice decreased less over training than I expected (in ChR2 mice, they significantly decreased only at day 33 of training). This could

suggest that mice were impulsive and struggled to withhold from licking throughout the variable Delay Window. One potential way to minimise Premature Hits and accelerate the animals' learning of the Delay Cue would have been to introduce a form of punishment (e.g., a brief air puff or a lengthy timeout delivered when the mouse licks during the Delay Window). It has been demonstrated that punishment appears to alter decision-making by influencing both expectation and validation of decision outcomes (Neville et al. 2020). One reason that prevented me from adopting an air-puff punishment was that the body movements of the mouse in response to the air-puff would have compromised the stability of electrophysiological recordings. Another way to tackle this problem could have been to reduce the duration of the Delay Window to test whether a shorter interval would have made the mouse less impulsive (Mar et al., 2013). However, significantly shortening the Delay Window might comprise the clear-cut detection of slowly evolving preparatory activity (e.g., "ramping" up or down) (Wang et al. 2021) in electrophysiological recordings (see Chapter 5). Some first licks in Hit trials had very short latencies (< 50 ms) that do not seem physiologically possible considering the synaptic delays between retina and tongue. This suggests that mice were "counting" the time during the Delay Window on small numbers of trials. Evidence for mice adopting "counting strategies" in behavioural tasks has been presented by Light et al. (2019). To mitigate counting strategies, I introduced the variable Delay Window (0.3 — 1.3 s). To better prevent counting strategies, further developments of the delayed-Go task could experiment with different Delay Window durations and greater or reduced variability. There are advantages to not taking further steps to improve behavioural performance;

an imperfect performance with failed trials (Premature Hits and Misses) is conceptually interesting to explore considering my research aims. One of my thesis aims is to investigate the role of SNr neuronal population in movement preparation and execution; to drastically reduce the number of failed trials would prevent me from comprehensively analysing the activity of SNr neurons when movement is not correctly planned (Premature Hits) or executed (Miss Trials).

Nevertheless, a high number of Premature Hits and differences in performance between ChR2 and control groups are suboptimal for experimental purposes. They could be explained by mice using individual strategies to solve the task. For future studies, several adjustments could be adopted to standardize mice performances between groups and generally improve performance and learning rate, among others: 1) increase the maximum number of trials allowed within a single session and/or reduce the volume of each liquid reward to avoid premature extinction of motivation; 2) increase the number of training sessions each day; 3) use negative reinforcement to discourage premature licking by applying air puffs or timeout punishments (Kaufman and Baron 1968).

Overall, my behavioural data results align with the time, and learning dynamics observed in mice learning similar tasks (Guo et al. 2017; Guo et al. 2014; Li et al. 2015; Guo et al. 2014; Catanese and Jaeger 2021). In all the above-cited studies, mice were trained to perform similar or more complex versions of the delayed–Go task and reached satisfactory performance levels within a few weeks of training (3 – 6 weeks). Furthermore, in all the above-cited studies, mice were head-fixed, had limited access

to water, and were trained in daily sessions performing hundred of trials. I believe that the novel delayed–Go task I have designed and implemented for my research could be used as a foundation for developing more complex behavioural tests in the future, e.g., lick/no-lick (go/no-go) or a lick-left/lick-right object location discrimination task. The lick/no-lick task has been successfully used to study neuronal correlates of perception, sensorimotor integration, and learning (O'Connor et al. 2010; O'Connor et al. 2013; Huber et al. 2012). Lick-left/lick-right paradigm has been successfully used to study preferential ipsilateral or contralateral encoding of movement by the basal ganglia, thalamus, and cortex (Catanese and Jaeger 2021; Guo et al. 2017).

In conclusion, establishing a robust delayed–Go paradigm was crucial to maximise the likely engagement of SNr neurons during movement preparation and execution, thence allowing the functional roles of these neurons to be investigated through optogenetic manipulation and electrophysiological recordings (see Chapters 4 and 5).

4. Optogenetic driving of SNr neurons during the delayed–Go task

4.1 Introduction

One of the aims of this thesis research is to assess whether SNr activity has a causal impact on movement preparation and execution. According to the influential disinhibition model, pauses in SNr output activity "gate" the task-related activation of its downstream targets (e.g., motor thalamus) via disinhibition (Hikosaka 2007). Furthermore, recent studies have demonstrated how optogenetic stimulation of BG output nuclei produces effects on thalamic firing-rate activity along with changes in licking behaviour (Catanese and Jaeger 2020) or muscle contractions (Kim et al. 2017).

The delayed-Go task that I developed for head-fixed mice (Chapter 3) was designed to help me disentangle the roles of SNr neurons in governing movement and allows for some distinct predictions to be made. For example, I reasoned that if SNr has a causal impact on movement via disinhibition, then increasing inhibition to its downstream targets during movement initiation by optically driving SNr GABAergic neurons at the Action Cue onset would impair the ability of mice to lick at the correct time (i.e., during the Action Window). This impairment would conceivably manifest as a slower reaction time (of first lick) following the Action cue and/or a diminished rate of Hit trials. (Figure 4.1A).

To determine the role of SNr output activity in movement preparation, I optically drove SNr GABAergic neurons during the Delay Window or the Delay Cue. I predicted

that increasing inhibition to SNr downstream targets at the delay stage of the task (Delay Window and Delay Cue) when targets are supposedly encoding motor preparation (Guo et al. 2017) would impair the mice's ability to lick. This impairment could manifest as reduced or delayed licks at movement execution (Hit trials following the Action Cue) (Figure 4.1B, D), or reduced or delayed licks at movement preparation (Premature Hit trials during the Delay Window (Figure 4.1C, E).

To test whether the predictions above held true, I trained 8 mice to perform the delayed-Go task (see section 2.4 and Chapter 3). Six of 8 mice were VGAT-IRES-Cre and received unilateral SNr injections of Cre-dependent viral vectors harbouring either ChR2-EYFP (n = 4 mice) or EYFP alone (n = 2 mice) before training (see section 2.3.3). Two of 8 mice were wildtype and did not receive injections of viral vectors. All 8 mice were unilaterally implanted with optic fibres in/above the SNr after behavioural training (see section 2.5.2) (Figure 4.2A). As the mice performed the delayed–Go task, a train of blue laser light pulses (10 ms pulses at 50 Hz, see section 2.6) was delivered to the SNr via the optic fibres on some trials (hereafter termed "laser-on"), with the duration of the train of pulses being varied according to whether it was delivered during the Action/Delay Cues (300 ms) or Delay Window (0.3—1.3 s). Laser-on trials were intermixed (with a proportion of 50:50) with trials without light delivery (“laser-off”). Within a single daily session of task performance, only one variant of laser timing was tested. The 2 VGAT-IRES-Cre mice receiving EYFP only virus and the 2 wildtype mice were together considered to be the control group. Transduction of SNr neurons

(in the case of VGAT-IRES-Cre mice only) and placement of optic fibres was assessed with posthoc histology (Figure 4.2B-D).

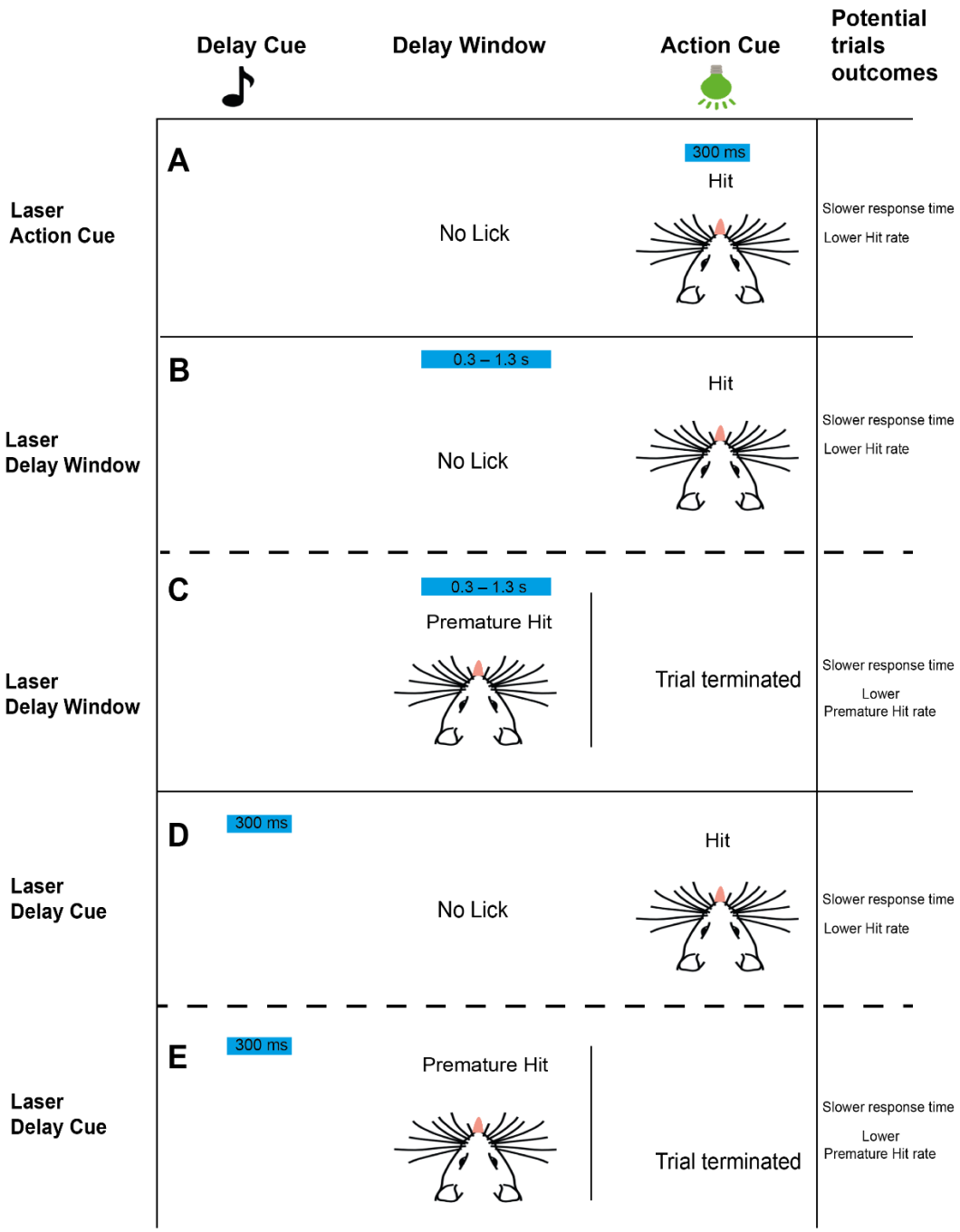
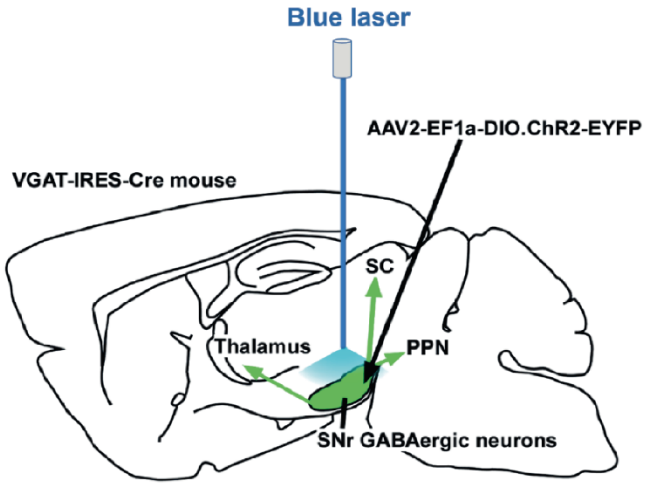
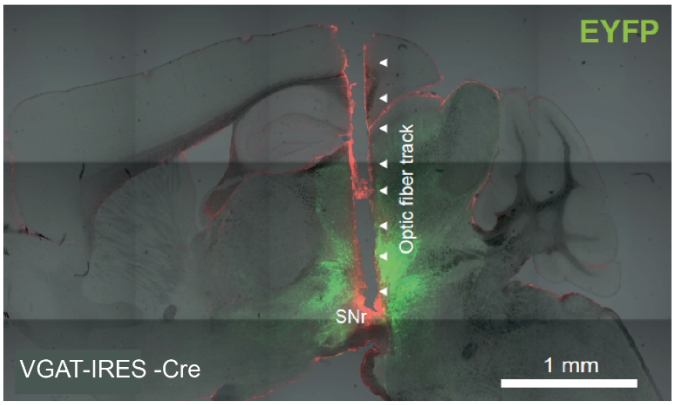


Figure 4.1 Schematic design of patterns of laser stimulation during different moments of the delayed–Go task. Blue laser is delivered **A:** at the Action Cue onset (300 ms); **B-C:** during the Delay Window (0.3 – 1.3 s); **D-E:** at the Delay Cue onset (300 ms).

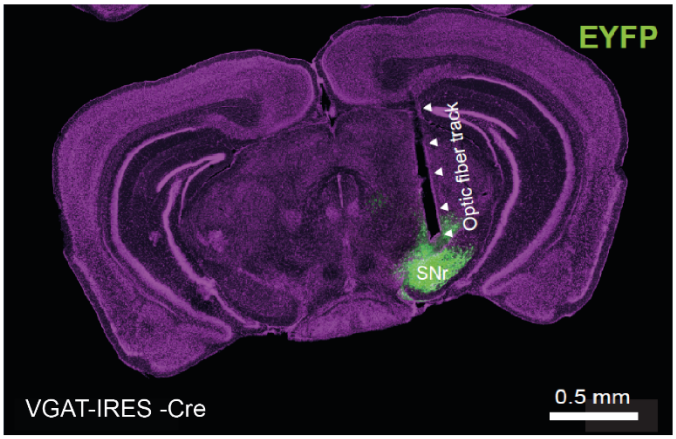
A


Blue laser
AAV2-EF1a-DIO.ChR2-EYFP
VGAT-IRES-Cre mouse
SC
Thalamus
PPN
SNr GABAergic neurons

B


EYFP
Optic fiber track
SNr
VGAT-IRES -Cre
1 mm

C


EYFP
Optic fiber track
SNr
VGAT-IRES -Cre
0.5 mm

D

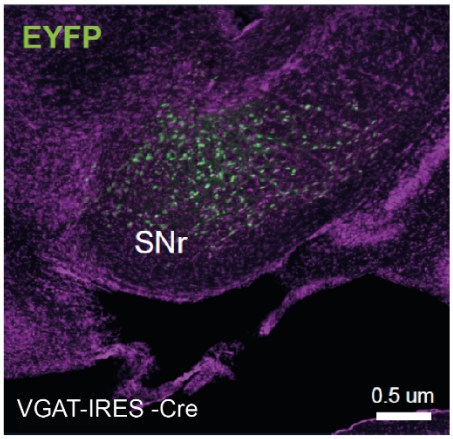

EYFP
SNr
VGAT-IRES -Cre
0.5 um

Figure 4.2 Experimental design using optogenetics to target SNr neuronal population. A: Schematic of the experimental paradigm. VGAT-IRES-Cre transgenic mice were injected with a Cre-dependent viral vector (AAV2-EF1a-DIO-ChR2-EYFP) in the SNr to express ChR2. SNr neurons were optogenetically activated by illumination with blue light through an optic fiber. **B**: Parasagittal view of the expression of the opsin-reporter fusion proteins (ChR2-EYFP; endogenous EYFP fluorescence) after AAV injections into the SNr of a VGAT-Cre mouse. Histology was performed to locate the position of the optic fiber (coated with red fluorescent dye) and injection sites. **C:** Coronal view of the expression of the reporter (EYFP) after AAV injections into the SNr of a VGAT-Cre mouse. Tissue was stained with DAPI, and histology was performed to locate the position of the optic fiber and injection sites. **D:** Higher magnification views of the SNr of the section in C (reduced brightness and contrast) showing EYFP-expressing SNr neurons.

4.2 Optogenetic driving of SNr neurons during Action Cue delays lick reaction time in Hit trials

To evaluate whether and how increased inhibition of SNr target structures would interfere with movement execution, I optogenetically activated SNr neurons during the Action Cue (0.3 s) during some Hit trials (laser-on) but not other Hit trials (laser-off). As an illustrative example, I computed the raster plots of the licks during laser-off (Figure 4.3A, top) and laser-on Hit trials (Figure 4.3B, top) of a single session for one mouse (gms064). The mouse frequently licked more than once in a single Hit trial, and the overall number of licks across all trials appeared similar between laser-on and laser-off trials. Reaction times, defined as the first licks (coloured blue or red) occurring after the Action Cue onset, appeared to vary between laser-on and laser-off trials. This result was confirmed by the peri-event time histograms (PETH) of first licks (Figure 4.3A,

B, bottom; blue and red traces). The times to first licks in laser-on trials appeared longer than the times to first licks in laser-off trials. Contrary to what I observed within a single session for this one mouse, in the ChR2 group, PETH curves of mean reaction time in laser-on trials peaked twice, before and after the curve in laser-off trials (Figure 4.3C). This double peak in reaction times did not emerge in the control group (Figure 4.3C). To compare the reaction time quantitively, I grouped the individual reaction times (n = 8 mice) across all the sessions (n = 57). In the control group (n = 4 mice), the times to first licks in laser-on trials (576 trials; 0.33 s ± 0.93 mean ± SEM) were not on average significantly different (p = 0.8) to times of first licks in laser-off trials (704 trials; 0.32 s ± 0.86 mean ± SEM). In contrast, in the ChR2 group (n = 4 mice), the times to first licks in laser-on trials (1358 trials; 0.35 ± 0.76 mean ± SEM) were on average significantly slower (p = 0.0018) than times to first licks in laser-off trials (1085 trials; 0.32 s ± 0.69 ; mean ± SEM) (Figure 4.3D).

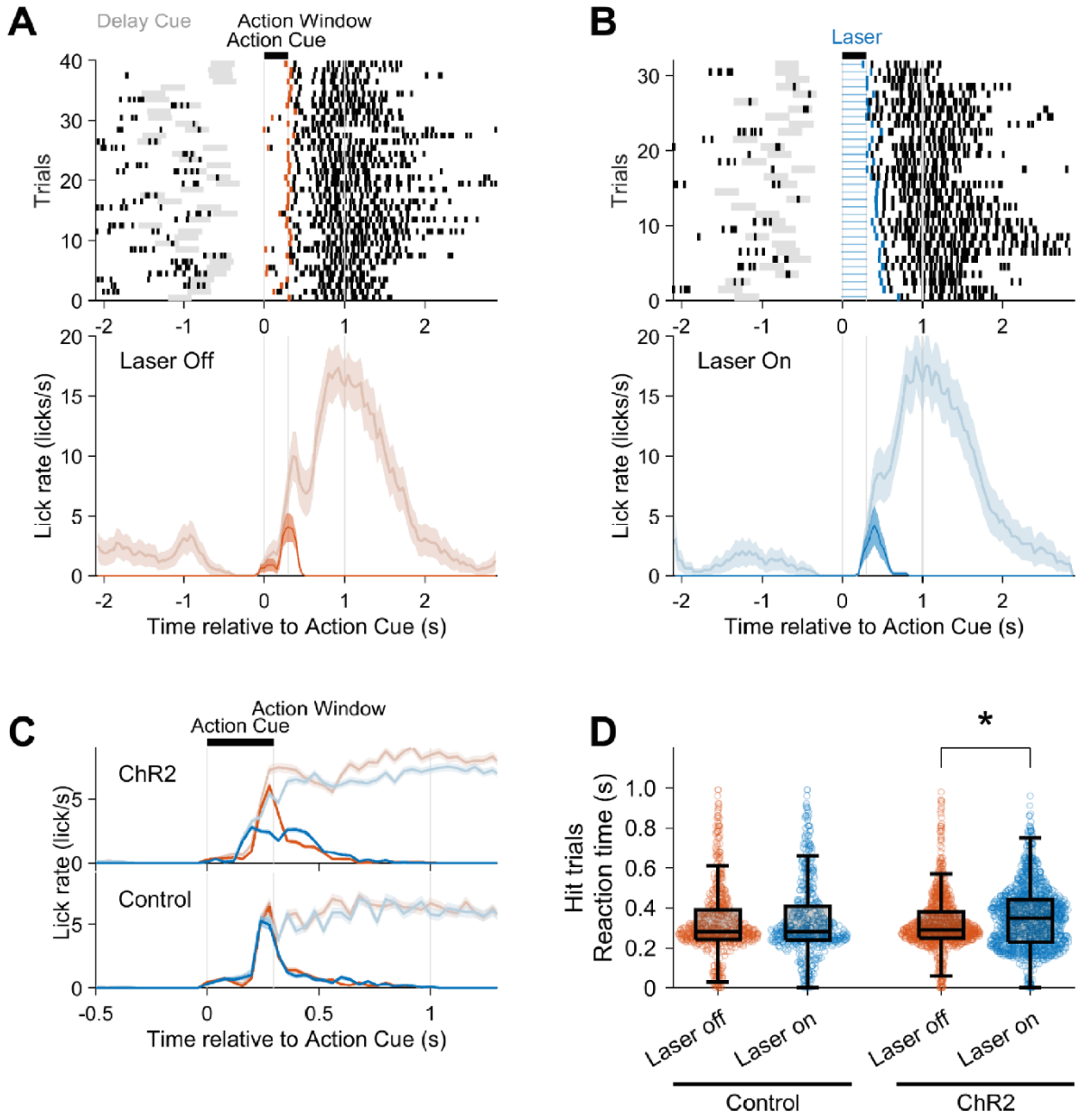


Figure 4.3 Reaction time in Hit trials is delayed when SNr neurons are optogenetically driven during the Action Cue. A, B: Raster plots (top) and PETH curves (bottom) of licks in Hit trials of a single session of a mouse (gms064) with ChR2 expression in SNr. The first licks in raster plots are color-coded in red for laser-off trials (A) and blue for laser-on trials (B). All licks are color-coded in pale red for laser off-trials (A) and pale blue for laser on-trials (B). The grey lines indicate timing of Delay Cues. The blue lines indicate timing of laser light delivered to SNr (i.e., during Action Cue). **C:** Group average PETH curves of the first licks (blue and red) and all the licks (pale blue and pale red) in laser-on (blue, pale blue) and laser-off (red, pale red) Hit trials. **D:** The group average comparison of reaction time (first licks) in Hit trials in laser-on (blue) and laser-off (red) trials. Box plots denote the minimum and maximum values that are not outliers (whiskers), interquartile range, and medians (see Materials and methods section 2.9). * $p < 0.05$, MWUT.

To further investigate the early peak, I computed the raster plots of the licks during laser-off (Figure 4.4A, top) and laser-on Hit trials (Figure 4.4B, top) of a single session for a second mouse (gms065). The times to first licks were shorter in laser-on trials than the times to first licks in laser-off trials. This result was confirmed by the peri-event time histograms (PETH) of first licks (Figure 4.4A, B, bottom; blue and red traces). To check whether early peak was induced by the laser or was due to individual mice differences I quantitively compared the individual reaction times of every mouse (n = 8 mice) across all the sessions (n = 57) (Figure 4.4C). The times to first licks in laser on-trials were faster than the times to first licks in laser-off trials in two mice in the ChR2 group (gms065; laser-on, 278 trials; 0.2736 s ± 0.0003; laser-off, 364 trials; 0.2739 s ± 0.007; mean ± SEM) (kms027; laser-on, 259 trials; 0.289 s ± 0.08; laser-off, 286 trials; 0.300 s ± 0.006; mean ± SEM). The differences were not significant (gms065 $p = 0.09$; kms027 $p = 0.3$).

Taken together, this data suggest that the optogenetic modulation delayed movement execution in Hit trials in two mice in the ChR2 group.

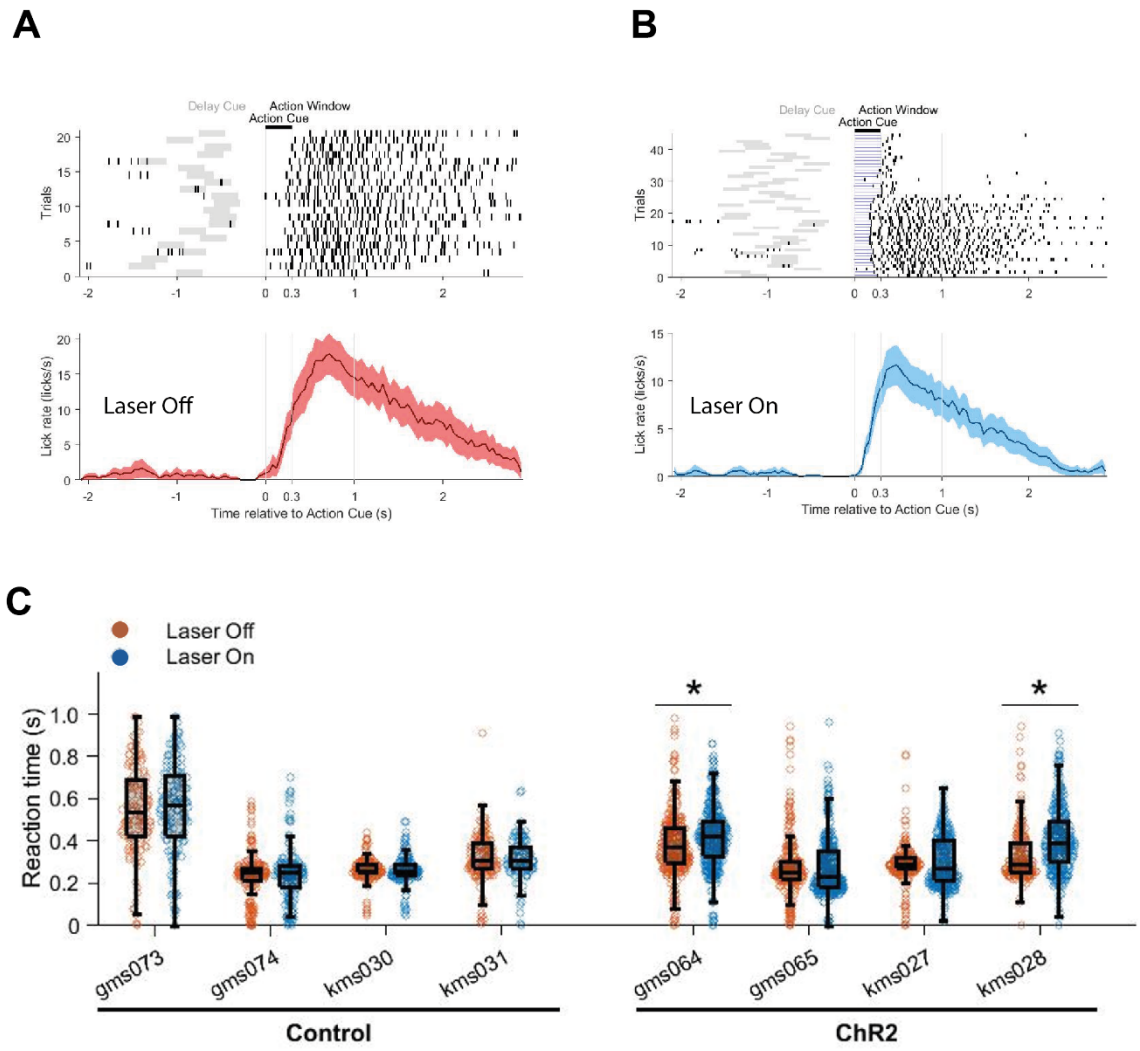


Figure 4.4 Optogenetic modulation doesn't accelerates reaction time in Hit trials. A, B: Raster plots (top) and PETH curves (bottom) of licks in Hit trials of a single session of a mouse (gms065) with ChR2 expression in SNr. The first licks in raster plots are color-coded in red for laser-off trials (A) and blue for laser-on trials (B). All licks are color-coded in pale red for laser off-trials (A) and pale blue for laser on-trials (B). The grey lines indicate timing of Delay Cues. The blue lines indicate timing of laser light delivered to SNr (i.e., during Action Cue). **C:** The group average comparison of reaction time (first licks) in Hit trials in laser-on (blue) and laser-off (red) trials for individual mice in the control group (left) and ChR2 group (right). Box plots denote the minimum and maximum values that are not outliers (whiskers), interquartile range, and medians (see Materials and methods section 2.9). * $p < 0.05$, MWUT.

4.3 Optogenetic driving of SNr neurons during Delay Window shortens lick reaction time in Hit trials

To assess whether and how inhibition of SNr target structures would interfere with motor preparation and therefore impair movement execution, I optogenetically activated SNr neurons during the Delay Window (0.3 – 1.3 s) during some trials (laser-on) but not other trials (laser-off). Initially, I focused analyses on effects of laser light on subsequent Hit trials. As an illustrative example, I computed the raster plots of the licks during laser-off Hit trials (Figure 4.5A, top) and laser-on Hit trials (Figure 4.5B, top) of a single session for one mouse (gms064). The overall number of licks appeared similar between laser-on and laser-off trials. In contrast to the effects of light delivered during the Action Cue (see Figure 4.3), the first licks appeared to happen earlier in laser-on trials than laser-off trials when light was delivered during the Delay Window. This result was confirmed by the first licks' peri-event time histograms (PETH) (Figure 4.5A, B, bottom; blue and red traces). First licks in laser-on trials peaked within the Action Cue, whereas those in laser-off trials peaked after the Action Cue. In the ChR2 group, the peak in the PETH curve of mean reaction time in laser-on trials preceded the peak in curves in laser-off trials (Figure 4.5C). This shift in reaction time was not observed in the control group (Figure 4.5C). To compare the reaction time quantitively, I grouped the individual reaction time of mice's first licks (n = 8) across all the sessions (n = 36). Boxplots show that in the control group (n = 4), first licks in laser-on trials (549 trials; 0.33 s ± 0.11; mean ± SEM) were not significantly faster ($p = 0.2$) than first

licks in laser of-trials (734 trials; 0.34 s ± 0.10; mean ± SEM). In contrast, in the ChR2 group (n = 4), first licks in laser-on trials (677 trials; 0.17 s ± 0.51; mean ± SEM) were significantly faster ($p = 1.165\times10^{-60}$) than first licks in laser-off trials (429 trials; 0.31 s ± 0.71; mean ± SEM) (Figure 4.5D).

Contrary to what observed in Figure 4.3, optogenetic modulation during movement preparation (Delay Window) shortened lick reaction time in Hit trials in the ChR2 group.

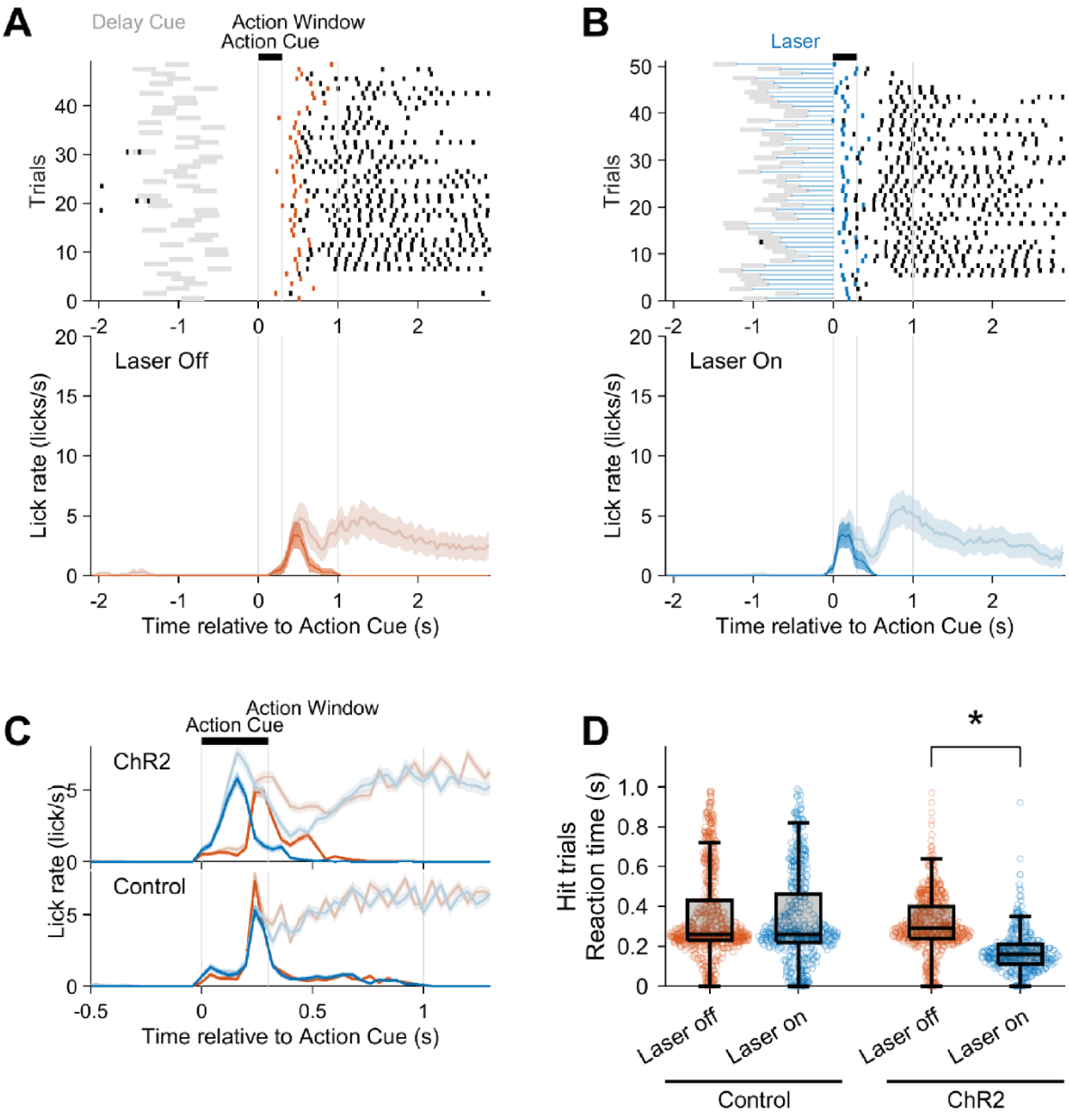


Figure 4.5 Reaction time in Hit trials is faster when SNr neurons are optogenetically driven during the Delay Window. A, B: Raster plots (top) and PETH curves (bottom) of licks in Hit trials of a single session of a mouse (gms064) with ChR2 expression in SNr. The first licks are color-coded in red for laser-off trials (A) and blue for laser-on trials (B). All licks are color-coded in pale red for laser off-trials (A) and pale blue for laser on-trials (B). Note that laser light delivery started at the end of the Delay Cue and was stopped at the end of the Delay Window (when the Action Cue then started). **C:** Group average PETH curves of the first licks (blue and red) and all the licks (pale blue and pale red) in laser-on (blue, pale blue) and laser-off (red, pale red) Hit trials. **D:** The group average comparison of reaction time in Hit trials in laser-on (blue) and laser-off (red) trials. Box plots denote the minimum and maximum values that are not outliers (whiskers), interquartile range, and medians (see Materials and methods section 2.9). * $p < 0.05$, MWUT.

4.4 Optogenetic driving of SNr neurons during Delay Window does not change lick reaction time in Premature Hit trials

Having assessed the effect of driving the SNr neurons during Delay Window on movement execution, I wanted to evaluate whether and how licking behaviour during movement preparation is altered by optogenetic activation of SNr during Delay Window. Therefore, I optogenetically activated SNr neurons during the Delay Window (0.3 – 1.3 s) during some trials (laser-on) but not other trials (laser-off). I focused analyses on effects of laser light on licking during Premature Hit trials. As an illustrative example, I computed the raster plots of the licks during laser-off (Figure 4.6A, top) and laser-on Premature Hit trials (Figure 4.6B, top) of a session for a mouse (gms064). After the Delay Cue, the first licks (coloured blue or red) did not seem to

change between laser-off trials and laser-on trials. This result was confirmed by the first licks' peri-event time histograms (PETH) (Figure 4.6A, B, bottom: blue and red traces). First licks in laser-off and laser-on trials did not show evident differences. In the control group, PETH curves of mean reaction time in laser-on trials peaked within the Delay Window, the mean reaction time in the ChR2 group is not affected by the laser (Figureure 4.6C). To compare the reaction time quantitively, I grouped the individual reaction time of mice's first licks (n = 8) across all the sessions (n = 36). Boxplots show that in the control group (n = 4), first licks in laser-on trials (412 trials; 0.43 s ± 0.10; mean ± SEM) were significantly faster ($p = 0.042$) then first licks in laser off-trials (580 trials; 0.47s ± 0.14; mean ± SEM). Oppositely, in the ChR2 group (n = 4), first licks in laser-on trials (694 trials; 0.50 s ± 0.11; mean ± SEM) were not significantly faster ($p = 0.145$) than first licks in laser-off trials (432 trials; 0.47 s ± 0.13; mean ± SEM) (Figure 4.6D).

When presented during motor preparation (Delay Window) optogenetic modulation accelerated lick rate in Premature Hit trials only in the control group.

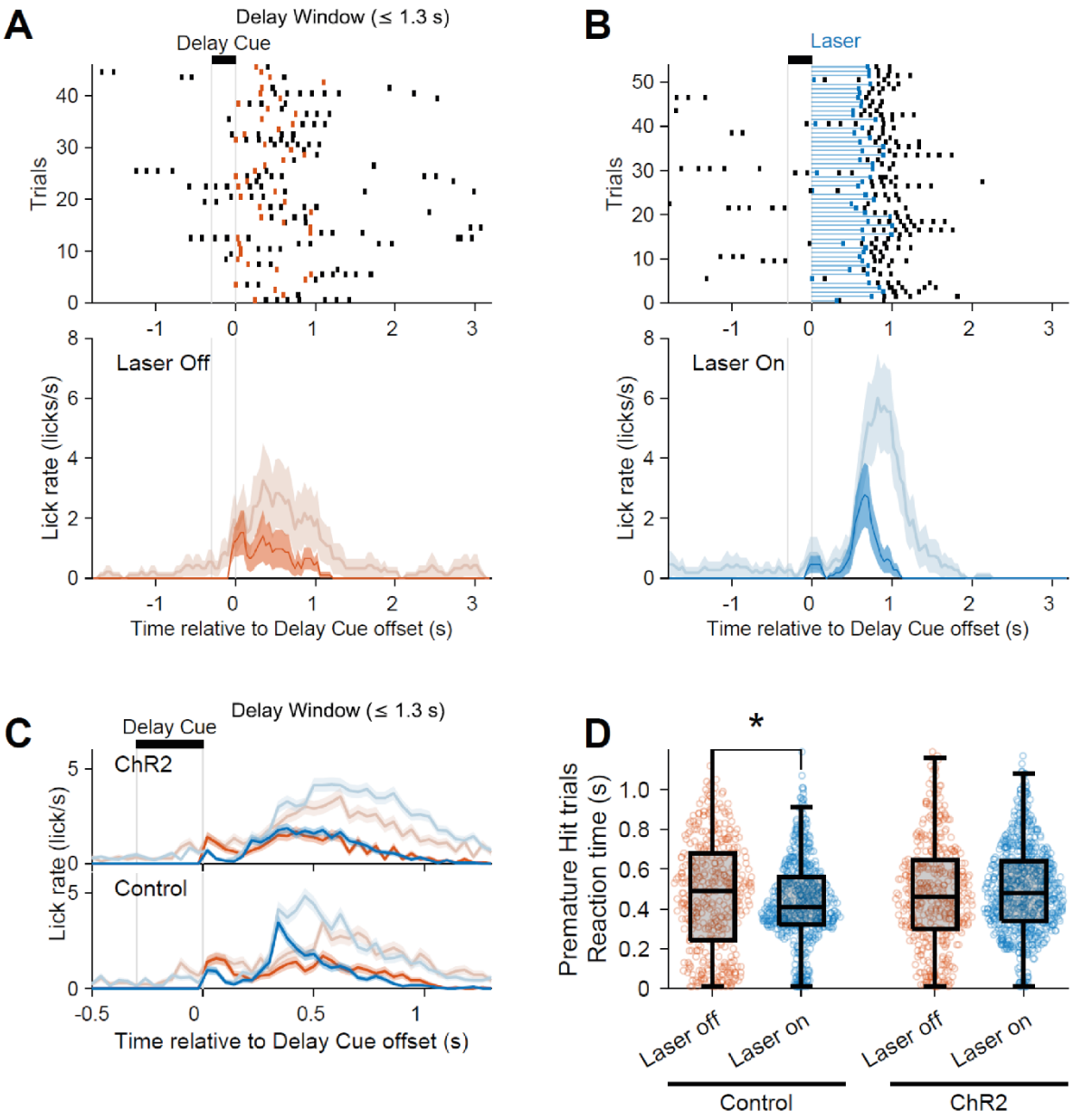


Figure 4.6 Reaction time in Premature Hit is not affected when SNr neurons are optogenetically driven during the Delay Window. A, B: Raster plots (top) and PETH curves (bottom) of licks in Premature Hit trials of a single session of a mouse (gms064) with ChR2 expression in SNr. The first licks are color-coded in red for laser-off trials (A) and blue for laser-on trials (B). All licks are color-coded in pale red for laser off-trials (A) and pale blue for laser on-trials (B). Note that laser light delivery started at the end of the Delay Cue and was stopped at the time of the first lick that occurred during the Delay Window. **C:** Group average PETH curves of the first licks (blue and red) and all the licks (pale blue and pale red) in laser-on (blue, pale blue) and laser-off (red, pale red) Premature Hit trials. **D:** The group average comparison of reaction time in Premature Hit trials in laser-on (blue)

and laser-off (red) trials. Box plots denote the minimum and maximum values that are not outliers (whiskers), interquartile range, and medians (see Materials and methods section 2.9). * $p < 0.05$, MWUT.

4.5 Optogenetic driving of SNr neurons during Delay Cue does not change lick reaction time in Hit trials

Having assessed the effect of driving the SNr neurons during Delay Window and Action Cue on movement execution and preparation, I wanted to evaluate whether and how licking behaviour during movement execution is impaired by optogenetic activation of SNr during Delay Cue. Therefore, I optogenetically activated SNr neurons during the Delay Cue (0.3 s) and computed the raster plots of the licks during laser-off (Figure 4.7A, top) and laser-on Hit trials (Figure 4.7B, top) of a session for a mouse (gms064). In response to the Action Cue onset, the overall number of licks and the first licks (coloured blue or red) appeared similar between laser-on and laser-off trials. This result was confirmed by the first licks' peri-event time histograms (PETH) (Figure 4.7A, B, bottom; blue and red traces). First licks in laser-on and laser-off trials seem to peak around the same time around the end of the Action Window. Similar to what I observed within a single session in both the ChR2 and the control group PETH curves of mean reaction time in laser-on and laser-off are peaking simultaneously during the Action Window (Figure 4.7C). To compare the reaction time quantitively, I grouped the individual reaction time of mice's first licks (n = 6) across all the sessions (n = 26). Boxplots show that in the control group (n = 2), first licks in laser-on trials (275 trials; 0.40 s ± 0.8; mean ± SEM) were not significantly faster ($p = 0.4$) than first licks in laser

off-trials (350 trials; 0.38 s ± 0.8; mean ± SEM). Also, in the ChR2 group (n = 4), first licks in laser-on trials (309 trials; 0.34 s ± 0.9; mean ± SEM) were not significantly faster (p = 0.4) than first licks in laser-off trials (667 trials; 0.35 s ± 0.7; mean ± SEM) (Figure 4.7D).

When presented during the Delay Cue, optogenetic modulation did not affect lick reaction time in Hit trials.

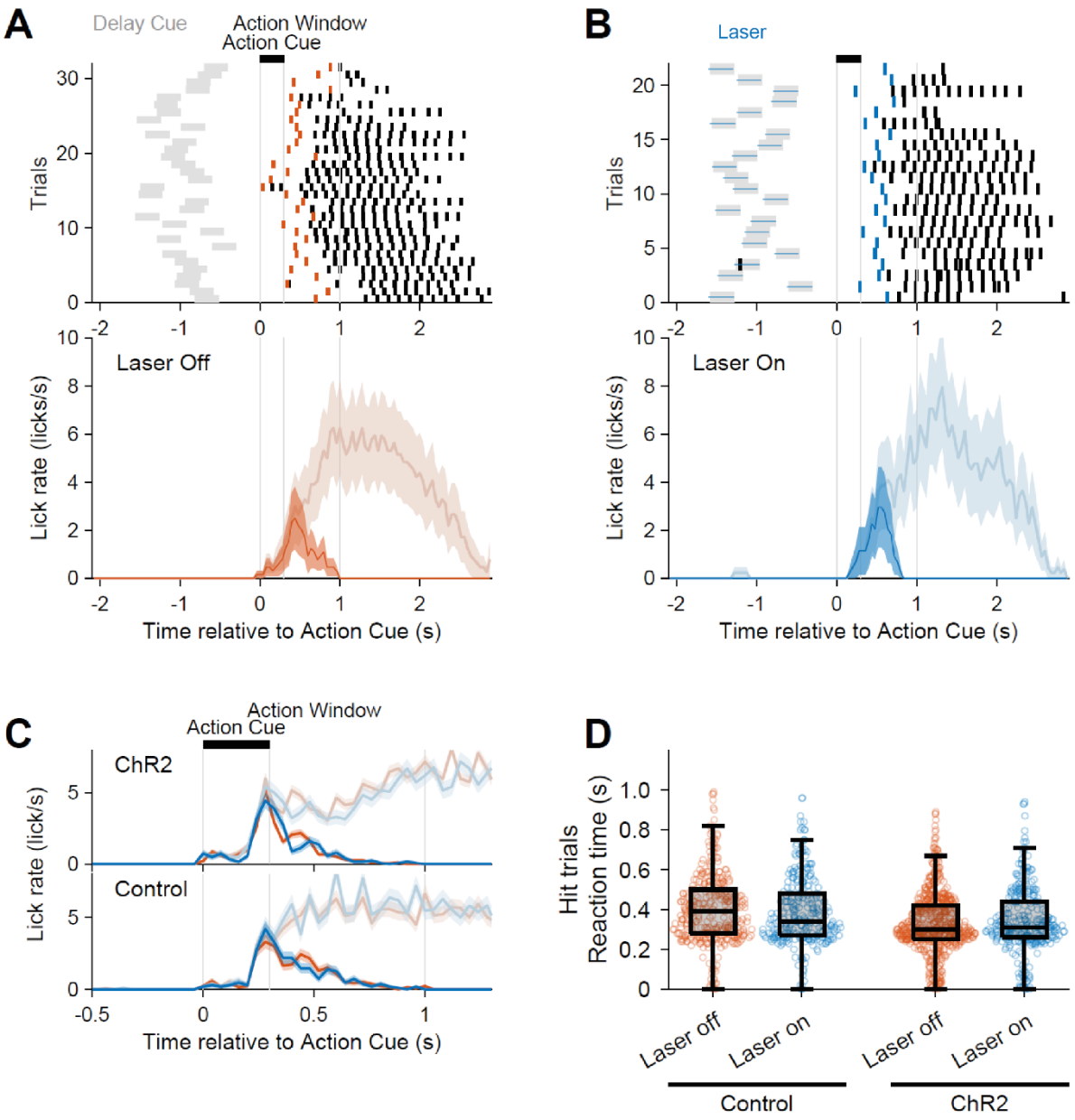


Figure 4.7 Reaction time in Hit trials is not affected when SNr neurons are optogenetically driven during the Delay Cue. A, B: Raster plots (top) and PETH curves (bottom) of licks in Hit trials of a single session of a mouse (gms064) with ChR2 expression in SNr. The first licks are color-coded in red for laser-off trials (A) and blue for laser-on trials (B). All licks are color-coded in pale red for laser off-trials (A) and pale blue for laser on-trials (B). **C:** Group average PETH curves of the first licks (blue and red) and all the licks (pale blue and pale red) in laser-on (blue, pale blue) and laser-off (red, pale red) Hit trials. **D:** The group average comparison of reaction time in Hit trials in laser-on (blue) and laser-off (red) trials. Box plots denote the minimum and maximum values that are not outliers (whiskers), interquartile range, and medians (see Materials and methods section 2.9).

4.6 Optogenetic driving of SNr neurons during Delay Cue accelerates lick reaction time in Premature Hit trials

Finally, to assess whether and how movement preparation is impaired by optogenetic activation of SNr during Delay Cue, I computed the raster plots of the licks during laser-off (Figure 4.8A, top) and laser-on Premature Hit trials (Figure 4.8B, top) of a session for a mouse (gms064). In response to the Delay Cue offset, the first licks (coloured blue or red) happened earlier in laser-on trials than laser-off trials and seemed synchronized over trials. This result was confirmed by the first licks' peri-event time histograms (PETH) (Figure 4.8A, B, bottom; blue and red traces). First licks in laser-on trials peaked sharply at ~200 ms after the Delay Cue offset, whereas those in laser-off trials did not clearly peak during the Delay Window. Similar to what I observed within a single session in the ChR2 group PETH curves of mean reaction time in laser-on trials sharply peaked after the Delay Cue offset (Figure 4.8C). To compare the reaction time quantitively, I grouped the individual reaction time of mice's first licks (n = 6) across all the sessions (n = 26). Boxplots show that in the control group (n = 2), first licks in laser-on trials (137 trials; 0.35 s ± 0.13; mean ± SEM) were not significantly faster (p = 0.8) than licks in laser of-trials (91 trials; 0.35s ± 0.14; mean ± SEM). Oppositely, in the ChR2 group (n = 4), first licks in laser-on trials (716 trials; 0.24 s ± 0.8; mean ± SEM) were significantly faster ($p = 3.574\times10^{-33}$) than first licks in laser-off trials (377 trials; 0.47 s ± 0.15; mean ± SEM) (Figure 4.8D).

Contrary to what observed in Figure 4.7, when presented during the Delay Cue optogenetic modulation accelerated lick reaction time in Premature Hit trials.

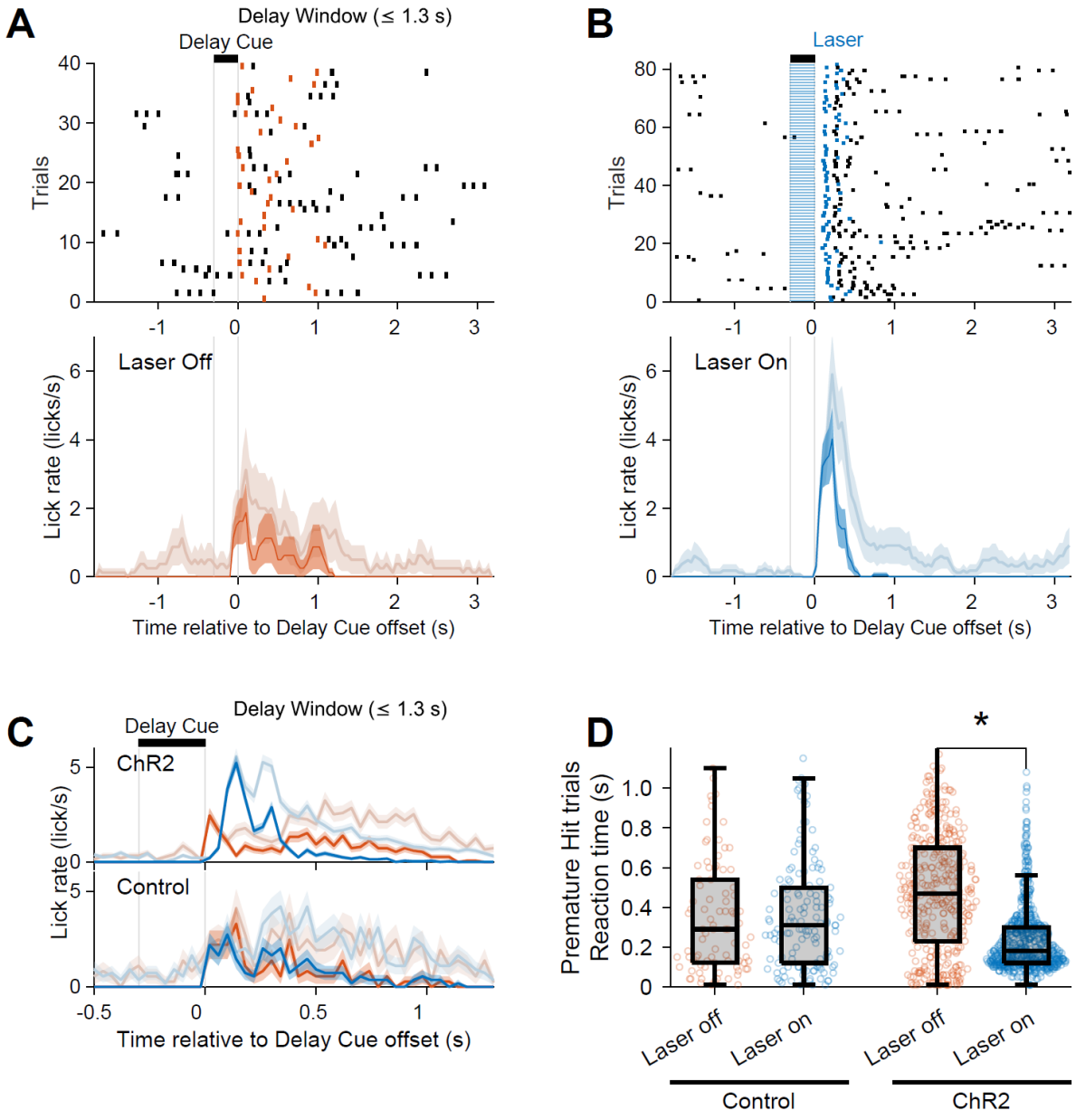


Figure 4.8 Reaction time in Premature Hit trials is accelerated when SNr neurons are optogenetically driven during the Delay Cue. A, B: Raster plots (top) and PETH curves (bottom) of licks in Premature Hit trials of a single session of a mouse (gms064) with ChR2 expression in SNr. The first licks are color-coded in red for laser-off trials (A) and blue for laser-on trials (B). All licks are color-coded in pale red for laser off-trials (A) and pale blue for laser on-trials (B). **C:** Group average PETH curves of the first licks (blue and red) and all the licks (pale blue and pale red) in laser-on (blue, pale blue) and laser-off (red, pale red) Premature Hit trials. **D:** The group average comparison of reaction time in Premature Hit trials in laser-on (blue) and laser-off (red) trials. Box plots denote the minimum and maximum values that are not outliers (whiskers), interquartile range, and medians (see Materials and methods section 2.9). * $p < 0.05$, MWUT.

Having observed that first licks were tightly aligned shortly after the laser offset in Delay Cue and Delay Window conditions, I computed the mean average reaction time of first licks from the laser offset (mice n = 4, 17 sessions, 429 trials). Despite belonging to different categories, reaction time of first licks in Hit trials from Delay Window laser offset and reaction time of first licks in Premature Hit trials from Delay Cue laser offset are very similar (reaction time Hit trials 0.16 s, reaction time Premature Hit trials 0.14 s; mean) (Figure 4.9).

As I will further discuss at the end of the chapter, the alignment of reaction times could be due to the low threshold spike (LTS) mechanism common to T-type calcium channels (T-type Ca2+) that abound in thalamic neurons (Bosch-Bouju et al. 2014; Person and Perkel 2007; Bosch-Bouju, Hyland, and Parr-Brownlie 2013; Person and Perkel 2005).

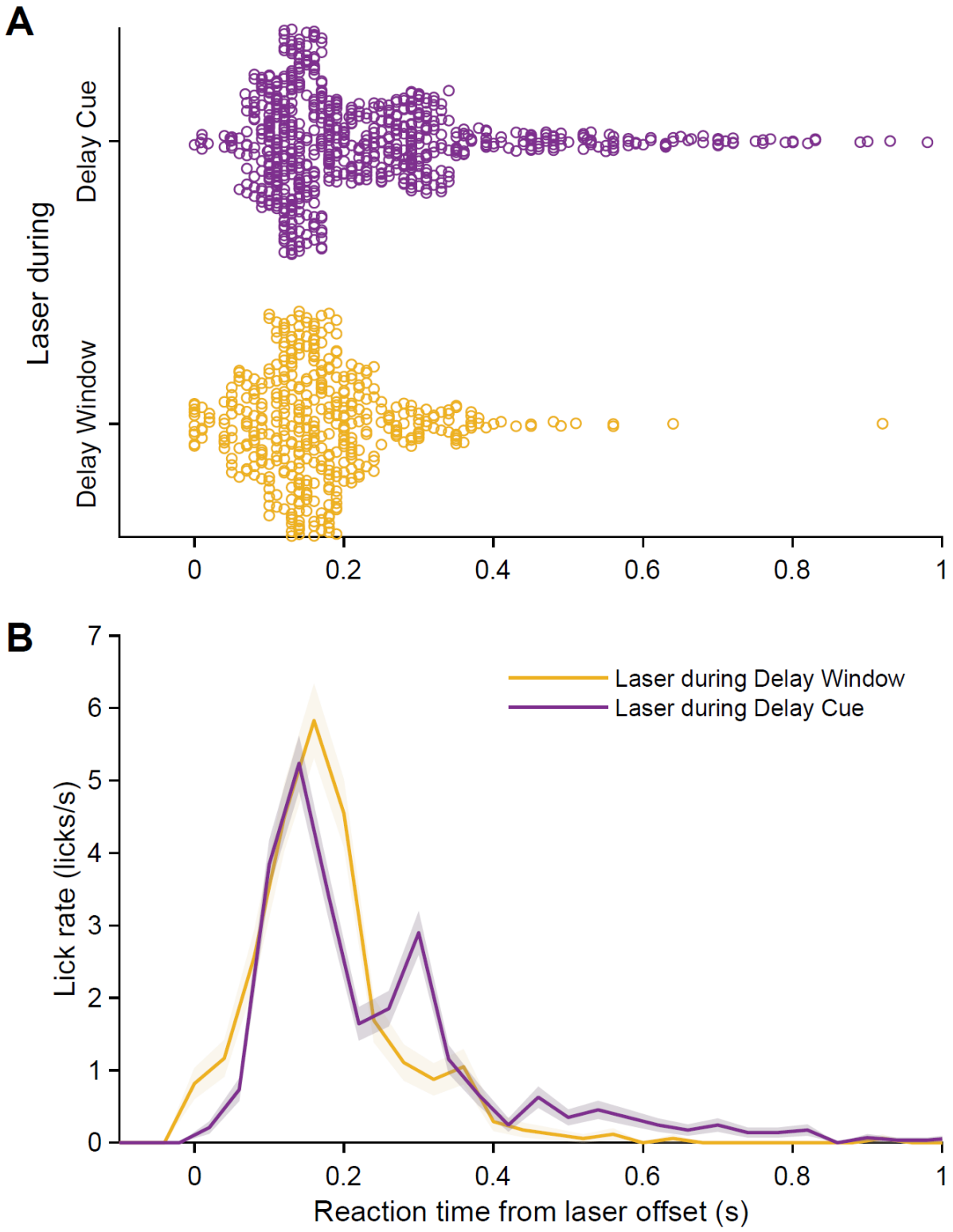


Figure 4.9 First licks of Hit trials and Premature Hit trials after laser offset. A: First licks of Premature Hit trials after laser-on during Delay Cue (purple) and Hit trials after laser-on in Delay Window (yellow). **B:**Group average PETH curves of first licks of Premature Hit trials after laser-on during Delay Cue (purple) and Hit trials after laser-on in Delay Window (yellow).

4.7 Optogenetic driving of SNr neurons altered the amount of Hit, Premature Hit, and Miss trials in ChR2 and control groups

Having assessed the impact of optogenetic driving of SNr neurons on reaction time (first licks), I computed the mean change in the amount of Hit, Premature Hit, and Miss trials when the laser light was delivered during different stages of the task. Hit rates significantly decreased in both ChR2 and control groups when laser was activated during Delay Cue (Figure 4.10A) (ChR2 group, 30.763 ± 0.83 laser on, 60.816 ± 3.47 laser off; control group, 56.989 ± 1.792 laser on, 69.373 ± 5.321 laser off; mean ± SEM; ChR2, p = 5.3124x10^{-04}; Control, p = 0.0020), and Delay Window (Figure 4.10B) (ChR2 group, 34.169 ± 4.10 laser on, 65.633 ± 0.95 laser off; control group, 52.046 ± 9.145 laser on, 71.524 ± 14.572 laser off; mean ± SEM; ChR2, p = 5.3124x10^{-04}; Control, p = 0.0020), but significantly increased when the laser was activated during Action Cue (ChR2 group, 92.02 ± 10.833 laser on, 56.981 ± 17.921 laser off; control group, 83.297 ± 14.732 laser on, 34.169 ± 15.288 laser off; mean ± SEM; ChR2, p = 5.3124x10^{-04}; Control, p = 0.00137). Premature Hit rates significantly increased in both ChR2 and control groups when laser was activated during Delay Cue (Figure 4.10D) (ChR2 group, 60.967 ± 17.804 laser on, 32.891 ± 17.171 laser off; control group, 31.442 ± 14.732 laser on, 18.199 ± 7.573 laser off; mean ± SEM; ChR2, p = 6.4304x10^{-04}; Control, p = 0.0020), and Delay Window (Figure 4.10E) (ChR2 group, 65.223 ± 17.106 laser on, 30.179 ± 17.905 laser off; control group, 45.564 ± 14.789 laser on, 25.0576 ± 14.678 laser off; mean ± SEM; ChR2, p = 6.4304x10^{-04}; Control, p = 0.0020). Miss rates significantly decreased in the ChR2 group only when the laser was

activated during the Delay Window (Figure 4.10H) (ChR2 group, 11.57 ± 17.773 laser on, 12.428 ± 16.152 laser off; mean ± SEM; ChR2, $p = 5.3124x10^{-04}$).

As shown in recent studies (Catanese and Jaeger 2020; Morrissette et al. 2019) optogenetic modulation on SNr neuronal population altered movement by affecting the amount of trials performed by the mice in the delayed-Go task. Despite this, rate changes in the control group represents a severe caveat and suggest that the effects of the optogentic modulation are likely due to an artifact.

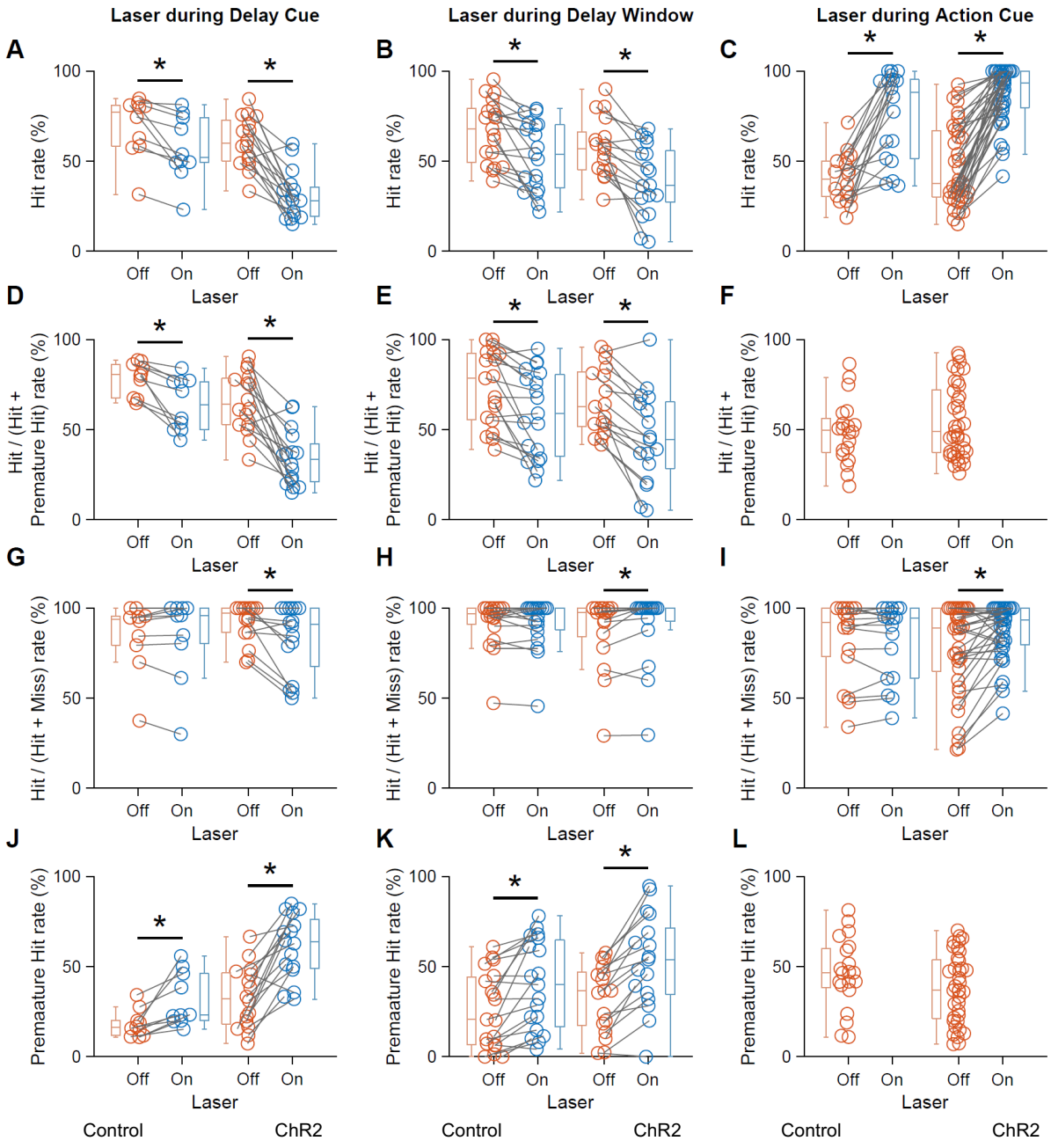


Figure 4.10 Rate changes in the delayed–Go task from optogenetic driving of SNr neurons in ChR2 mice (right column) and Control mice (left column). Mean Hit rate changes color-coded in red for laser-off trials and blue for laser-on trials when laser is activated during **A:** Delay Cue, **B:** Delay-Window, and **C:** Action Cue. Mean Premature Hit rate changes color-coded in red for laser-off trials and blue for laser-on trials when laser is acitvated during **D:** Delay Cue, **E:** Delay-Window, and **F:** Action Cue. Mean Miss rate changes color-coded in red for laser-off trials and blue for laser-on trials when laser is activated during **G:** Delay Cue, **H:** Delay-Window, and **I:** Action Cue. Box plots denote the minimum and maximum values that are not outliers (whiskers), interquartile range, and medians (see Materials and methods section 2.9). * $p < 0.05$, Wilcoxon sum rank test.

4.8 Discussion

One of my thesis aims was to test whether SNr activity has a causal impact on movement initiation or preparation. To answer that, I have optogenetically driven SNr neurons in different moments of the delayed–Go task when the mouse was preparing to move (Delay Window) or executing movement (Action Window).

My data show that driving GABAergic SNr neurons during Action Cue in Hit trials overall delayed the reaction time of first licks (Figure 4.3). A possible explanation for the delayed peak in licking is that optically driving the SNr neurons inhibited neurons in their target structures (e.g., motor thalamus), temporarily preventing them from reaching activity levels that support movement and therefore impairing the initiation of movement execution. This result is consistent with the disinhibition model proposed by Hikosaka and is in line with more recent findings in rodents (Freeze et al., 2013; Basso and Sommer, 2011).

My data also show that optogenetic manipulations of SNr neurons during movement preparation phases of the task affected licking behaviours. Delivery of light to SNr during Delay Cues in Premature Hit trials, and light delivery during Delay Windows in Hit trials, both accelerated first licks (Figures 4.5 and 4.8). These results are somewhat counterintuitive given the effect of light delivery during Action |Cue had an opposite effect on licking behaviour. If driving SNr neurons provides excessive inhibition to its downstream target structures, then why should this inhibition

accelerate movement execution? An interpretation might follow from observing that first licks were tightly aligned shortly after (~200 ms) the laser offset in Delay Cue and Delay Window conditions (Figure 4.9). This exact timing of response repeated itself in multiple non-consecutive trials. This could be explained by a model in which BG output may promote subsequent target cell activation through a low-threshold spike (LTS) mechanism common to neurons that express T-type calcium channels , such as thalamic neurons (Bosch-Bouju et al. 2014; Person and Perkel 2007; Bosch-Bouju, Hyland, and Parr-Brownlie 2013; Person and Perkel 2005). According to this model, driving BG output nuclei would evoke inhibitory postsynaptic potentials (IPSPs) that leave the thalamic cell at a hyperpolarized potential, allowing T-type Ca2+ channels to recover from inactivation. After the barrage of IPSPs ceases, depolarization of thalamic neurons is initially driven by HCN currents. However, T-type channels take over as the membrane potential enters their activation range until the threshold for Na+ spikes is reached. This is called the "rebound mode." Rebound spikes are thus facilitated by a preceding increase in SNr firing rate that increases hyperpolarization and decreases T-channel inactivation. This feature makes rebound responses depend on the recent history of SNr input. So, optogenetically driving and then abruptly ceasing inhibition from SNr could counterintuitively lead to thalamic activity that is mechanistically triggered but does not necessarily reflect the mouse ‘intending’ to lick. To my knowledge, the LTS mechanism has been proposed as a candidate model for basal ganglia-thalamic interaction in songbirds and rats (Goldberg, Farries, and Fee 2013). However, it has never been observed in behaving rodents.

LTS mechanism might explain why reaction times are shortened after optogenetic modulation in Delay Cue and Delay Window but does not explain why modulation in Action Cue does not accelerate licks. So how to explain? The answer might stem from differences in ongoing 'brain state' (wider circuit activity) during movement preparation vs movement execution. So, it could be that, during Action Cue, target neurons receive different sets of active inputs from other structures in the brain (as Nambu (2004) has shown, cortical neurons that constitute the hyperdirect pathway can drive BG output neurons via the subthalamic nucleus) that counteract the excessive inhibition arising from optogenetic manipulation of SNr (such that target neurons never recover sufficient T-channels for rebound spiking).

Several studies have shown how motor structures can regulate motor behaviour (e.g., hypothalamus, cerebellum, and brain stem reticular formations) through ascending-descending projections to higher motor areas and lower brainstem regions (Bentivoglio and Kuypers 1982; Risold, Thompson, and Swanson 1997). McElvain et al. (2021) noted that all SNr-thalamus projections comprise aggregate collaterals of SNr-brain stem projections suggesting that the brain stem could support locomotor without the mediation of higher thalamic or cortical areas in several behavioural contexts.

With one possible exception (Figure 4.6), delivery of light to the SNr of control mice did not alter their reaction times (first licks) in the different trial types of the delayed Go-task. However, I observed that light delivery affected other aspects the

behavioural performance of control mice; Figure 4.10 shows that optogenetic driving of SNr neurons altered the rates of Hit, Premature Hit, and Miss trials in the control group. A recent paper (Danskin et al. 2015) showed that light delivered into the forebrain via an optical fibre evoked a confounding behavioural effect in mice (not-injected with opsins) performing a visually-guided discrimination task. According to the study, red (640 nm) illumination evoked a greater behavioural effect and more activity in the retina as compared with blue (473 nm) or yellow (589 nm) illumination. In the mouse, the sensitivity of retinal opsins declines steeply with wavelength across the visible spectrum, but propagation of light through brain tissue increases with wavelength. Long-wavelength optogenetic stimuli are thus more likely to evoke confounding behavioural effects via propagation through tissue and activation of retinal opsins in the mouse. Although I used blue light (473 nm) for my optogenetic experiments, reducing the risks of confounding affects, I cannot rule out the possibility that mice could have confused the blue light of the laser with the Action Cue (300 ms green LED at 520 nm). This artifact might explain the higher number of Premature Hit trials when the laser was triggered through the Delay Window and the change in the amount of Premature Hit, Hit, and Miss trials in the control groups. Future experiments should implement a new version of the delay–Go task to address this problem. In the updated version, both Delay Cues and Action Cues should be auditory (but widely different tones). Mice are excellent in auditory discrimination, and several delayed response tasks have used auditory cues (Guo, Hires, et al., 2014).

The behavioural effect of optogenetic manipulations varied across ChR2 animals and sessions. I used the same protocol and stereotactic coordinates for intracranial viral vector injections for all the ChR2 mice (see Materials and Methods section 2.3.3). Despite this, variability in effects of light delivery could be due to different levels of viral transduction and opsin expression in SNr neurons (Guru et al. 2015), as well as and variable placement of the optic fibers with respect to the transduced neurons. Suboptimal placement of the optic fibres and low levels of viral transduction could also explain the small effect sizes that I have observed in some experiments in the ChR2 mice (e.g., Figure 4.3). Another possibility is that the light intensity delivered to the SNr was too weak to drive SNr neurons. Light intensity was adjusted pre-implantation with an integrating-sphere optical power meter to reach ~10 mW at the end of the implanted optic fibre (see Materials and Methods section 2.6). Light intensity was adjusted to the levels used in similar studies (Catanese and Jaeger 2020; Morrissette et al. 2019). Nevertheless, the optimal light intensity level for *in vivo* stimulation of neurons expressing ChR2 is still debated (Herman et al. 2014). I have used unilateral optogentic stimulation of SNr in the right hemisphere for my study. It has been shown that unilateral optogenetic excitation of basal ganglia output nuclei is powerful enough to affect directional lick choices and movement initiation in mice (Morrissette et al. 2019). Nevertheless, bilateral stimulation of the SNr might have increased the observed effect sizes in the ChR2 mice. It should also be remembered that the expected optical driving of the SNr neuron activity can be demonstrated only by combining light

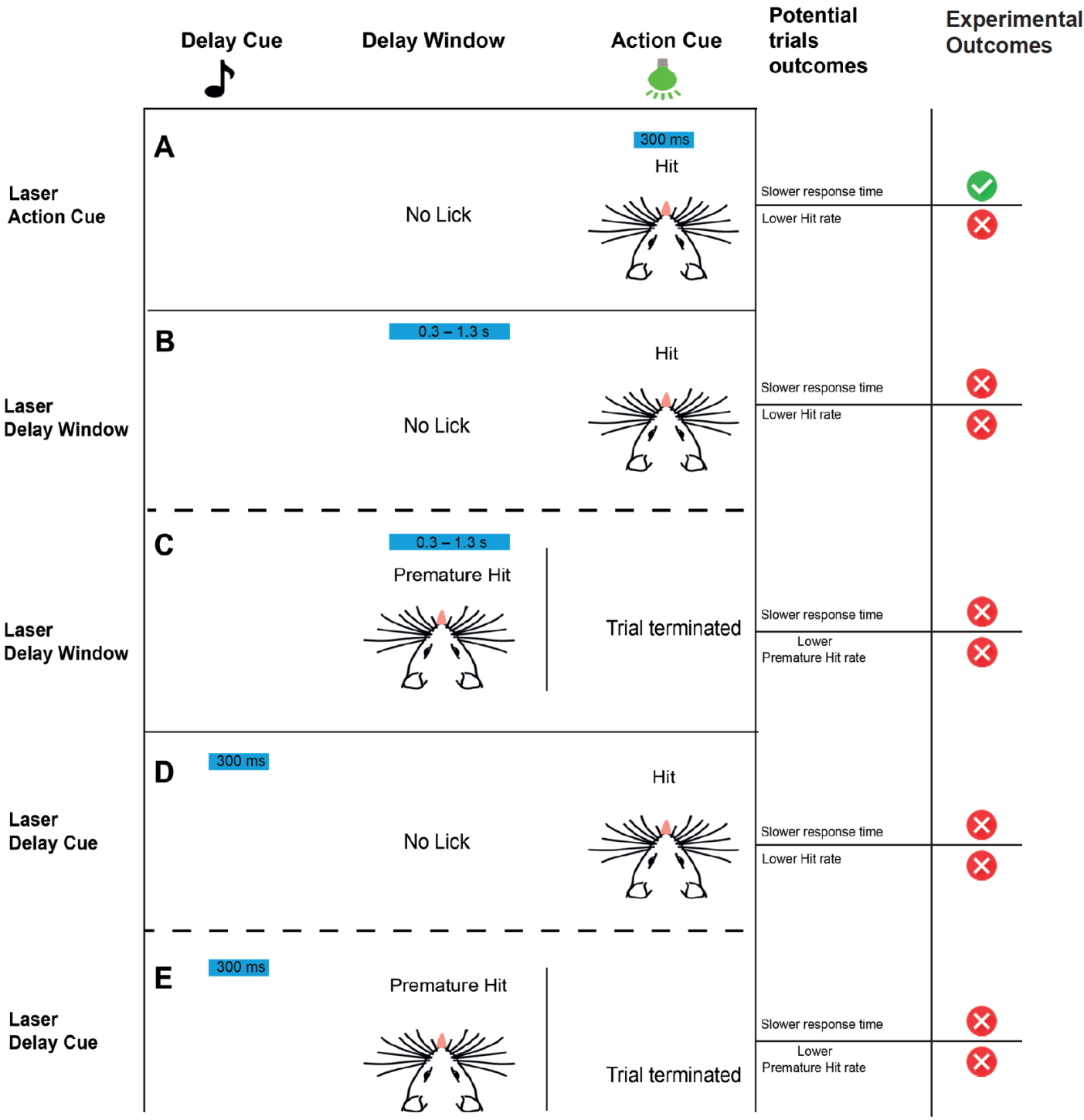
delivery and electrophysiological recordings of the opsin–expressing cells (Deubner, Coulon, and Diester 2019), an issue I address with work detailed in Chapter 5.

Figure 4.10 shows large variability in the amount of Hit, Premature Hit, and Miss laser–off trials, both in the ChR2 and control groups. This variability has also been observed in the results of the previous Chapter. It could be due to the mice not reaching a satisfactory performance level or to individual changes in performance from session to session. A way to solve this problem is to reach a more homogeneous level of learning across mice by introducing forms of negative reinforcement (see discussion in Chapter 3).

Results from analysing trials across animals do not consider individual performances that might vary between individual mice as shown in Figure 4.3D. One way to tackle this problem could be to compute group average comparisons of trials within a session for individual mice as shown in Figure 4.4C.

Like observed in Chapter 3, some reaction times after the Action Cue onset are very fast (<100 ms in some Hit trials). These reactions seem too brief considering the amount of time needed for visual information to travel from the retina to the visual areas and then propagate on to motor areas in the mouse brain (Laramée and Boire 2015). This suggests that, although I used a jittered Delay Window in the task design, mice might have occasionally still used a ‘counting strategy’ to solve some task trials (i.e., estimating the time between Delay Cue to Action Cue and get a reward). Possible solutions on how to correct this strategy are discussed in Chapter 3.

Overall, the results in this chapter indicate that SNr has a causal impact on movement preparation and execution in a more diverse way than predicted by (Hikosaka 2007) in the classical disinhibition model. A summary of experimental outcomes is presented in Box 1. The next chapter will investigate how SNr neurons encode movement preparation and execution through *in vivo* electrophysiological recordings.



Box 1 Schematic design of patterns and outcomes of laser stimulation during different moments of the delayed–Go task. Blue laser was delivered **A:** at the Action Cue onset (300 ms); **B-C:** during the Delay Window (0.3 – 1.3 s); **D-E**: at the Delay Cue onset (300 ms). Outcomes predictions (slower response time) were confirmed by experiments only in (A), when the laser was delivered during the Action Cue.

5. Encoding of the delayed-Go task by SNr neurons

5.1 Introduction

The delayed-Go task that I developed for head-fixed mice (Chapter 3) and the optogenetic modulation of SNr (Chapter 4) allowed me to assess the impact of SNr neurons on governing movement preparation and execution. Results in the previous chapter only partially confirmed the disinhibition model proposed by (Hikosaka 2007) and suggested that SNr might have a different impact on movement depending on whether the mouse is executing the movement or preparing for it. To further examine how SNr encodes movement preparation and movement execution, I recorded single-unit activities of SNr neurons in mice engaged in the delayed-Go task and assessed the response of the SNr neuronal population to the optogenetic modulation.

5.2 Materials and Methods

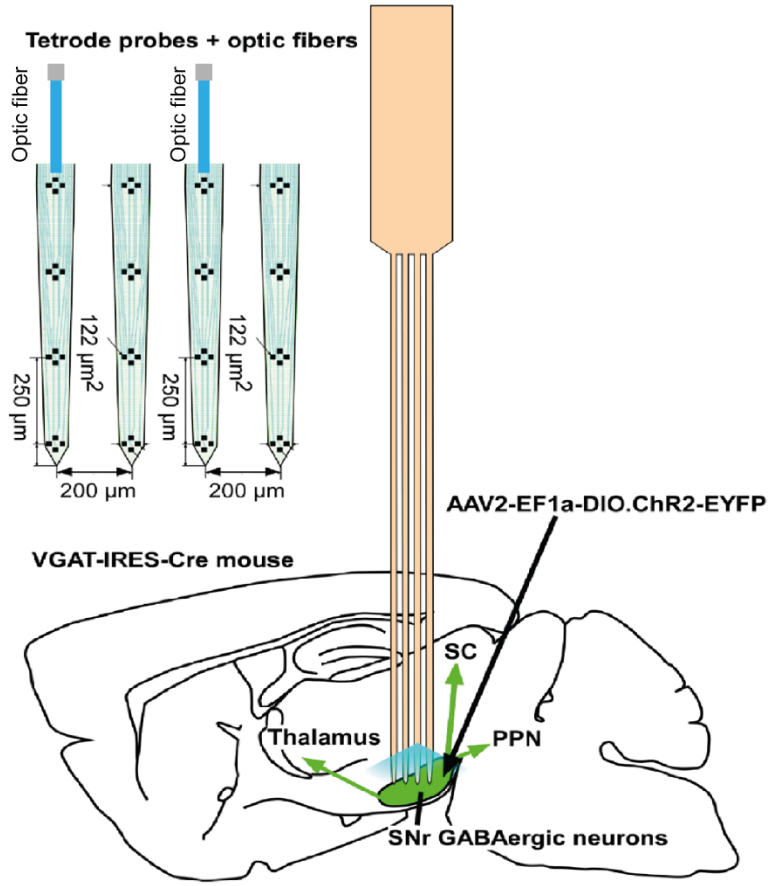
I trained 4 VGAT-IRES-Cre mice to perform the delayed-Go task (see section 2.4 and Chapter 3). The mice received unilateral SNr injections of Cre-dependent viral vectors harbouring ChR2-EYFP before training (see section 2.3.3). The mice were head-fixed, and an "optrode" (i.e., a multi-channel electrode with integrated optic fibres) was inserted unilaterally into the SNr (Figure 5.1A). The probe had four shanks

separated by 200 μm, each of which had sixteen recording contacts arranged in four tetrodes and with the tetrodes separated by 250 μm on each shank. Two 50-μm diameter optic fibers were mounted 200 μm above the most dorsal recording contact on the 1st and 3rd shanks (Figure 5.1A). Using a customized probe allowed me to sample activity across large parts of SNr in dorsoventral (D-V) and antero-posterior (A-P) axes, with and tetrode arrangement of contacts facilitating spike sorting (Chelaru and Jog 2005). As the mice performed the delayed–Go task, a train of blue laser light pulses (10 ms pulses at 50 Hz, 50% duty cycle, see Materials and Methods section 2.6) was delivered to the SNr via the optrode on some trials ("laser-on" trials), with the duration and timing of the train of pulses set according to occurrences of the Delay Window or Action Cue for a session. The laser-on trials (50%) were intermixed with trials without light delivery ("laser-off" trials, 50%). Only one variant of laser timing was tested within a single daily session of task performance. To mark the recording sites on the last day of electrophysiological recordings, the back of the silicon probe was evenly coated before use with a far-red fluorescent dye (DiD). The transduction of SNr neurons and placement of the optrode were assessed with posthoc histology (Figure 5.1B); for further details, see Materials and methods sections 2.7 and 2.8.

I focused my analyses on SNr neuron activity during the Delay Cue and Delay Window (movement preparation) and the Action Window (movement execution), taking into account distinct trial outcomes (i.e., Hit, Premature Hit or Miss). For analyses of neuronal activity, single units were isolated through spike sorting of wide-band recordings (see Methods section 2.9). Classification of significant changes in

single-unit activity patterns during a particular part of the task, was done after detecting activity changes in z-scored firing rate being > 2 for increase or < −2 for decrease (for one bin, 40 ms) within the time window of 0 < t <= 1 s from Action Cue or within the time window of −0.5 < t <= 0.5 s from the first licks. A neuron can be classified into: Cluster 1, increase; Cluster 2, both increase and decrease (in either order); Cluster 3, decrease; Cluster 4, no change. For the purposes of plotting activity patterns in figures, neurons were sorted by the timing of their peak activity within the window −0.3 < t < 1 s relative to Action Cue or within the window −1.6 < t < 1 s from to the first licks. When neurons did not have a peak above the threshold, the trough in activity below threshold was used instead. Data at in one bin around the onset of Delay Cue (−0.02 to +0.02 s, with t = 0 being onset) were ignored, because I found the contamination of electrophysiological recordings with brief mechanical artifacts. Firing rates were plotted as z-score with the means and standard deviations (SDs) of the baseline firing rates. The baseline firing rates were determined using the baseline time windows (1 s), ranging −1.1 to −0.1 s before Delay Cue onset (trial onset). For each neuron, the SD of the mean firing rates per window were computed across all the windows (i.e., all the trials). However, because I noticed that the mean firing rates of subset of trials can vary from the global average across a session, I computed the mean of the mean firing rates per window for a specific trial outcome (i.e., Hit, Premature Hit, or Miss). The combination of the means and SDs allowed z scored PETH with the baseline around 0 and the scaling comparable across outcomes.

A


Tetrode probes + optic fibers
Optic fiber
Optic fiber
122 µm2
122 µm2
250 µm
250 µm
200 µm
200 µm
AAV2-EF1a-DIO.ChR2-EYFP
VGAT-IRES-Cre mouse
SC
Thalamus
PPN
SNr GABAergic neurons

B

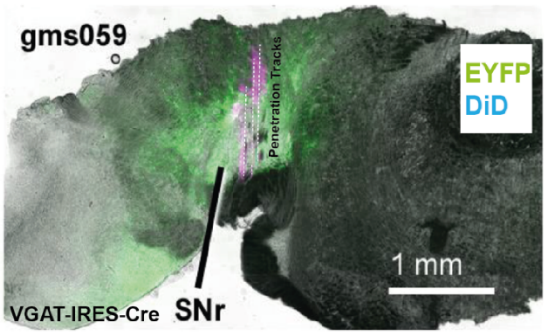

gms059
Penetration Tracks
EYFP
DiD
1 mm
VGAT-IRES-Cre
SNr

Figure 5.1 Experimental design for the electrophysiological recording and optical manipulation of SNr neuronal population in mice. A: Schematic of the experimental paradigm. VGAT-IRES-Cre transgenic mice were injected with a Cre-dependent viral vector (AAV2-EF1a-DIO-ChR2-EYFP) in the SNr to express ChR2. The activities of SNr neurons were recorded through an optrode with 4 shanks. During some task trials, SNr neurons were optogenetically activated by illumination with blue light. **B**: Parasagittal view of the expression of the opsin-reporter fusion proteins (ChR2-EYFP; endogenous EYFP fluorescence) after AAV injections into the SNr of a VGAT-Cre mouse. Histology was performed to locate the optrode and injections sites, and far-red fluorescent dye DiD was used.

5.3 Most SNr neurons increase their firing rate at movement onset in Hit trials

I quantified the activity of SNr neurons during the delayed-Go task to test for evidence of a decrease in their firing rate at movement onset, as the disinhibition model predicts. To do so, I analysed the activity of 360 single units (baseline firing rates; 14.8 ± 0.8 spikes/s; mean ± SEM) recorded in SNr during Hit trials from 4 trained animals (24 sessions in total).

When aligning spike firing data to the start of the Action Cue (0.3 s) in Hit trails, it was evident that just over half of all SNr neurons (Cluster 1, n = 189/360) rapidly increased their firing rates around the Cue onset (Figure 5.2C, D, E). Because the precise timing of movement can vary in relation to the Action Cue onset from trial to trial, I also aligned spike firing to first licks. I observed that Cluster 1 neurons significantly increased activity before or at the time of first licks (Figure 5.2G, H, I). The timings of these activity changes suggest that Cluster 1 neurons could play a role in sculpting movement. Importantly, the increases in activity often lasted beyond first

licks i.e., 1-2 s after the Action Cue onset when mice were often engaged in repetitive licking in response to the delivery of single water drops (see Figures 3.3 and 4.3). When aligned to Action Cue onset (Figure 5.2D, E) or first licks (Figure 5.2G, H) the activity of about one third of recorded neurons was not significantly modulated during these epochs of the delayed-Go task (Cluster 4, n = 118/360). Only a small proportion of recorded neurons (Cluster 3, n = 13/360) significantly decreased their firing rate (Figure 5.2D, E, F). Another small proportion of neurons (Cluster 2, n = 40/360) exhibited both and an increase and decrease in activity in the analysed epoch; on average, these neurons increased their firing rate around Action Cue onset (Figure 5.2 D, E) and first licks (Figure 5.2G, H). However, and in contrast to Cluster 1 neurons, the activity of Cluster 2 neurons was not sustained and rapidly decreased to baseline (< 1 s) from Action Cue onset or first lick. Importantly, alignment of spike firing to Action Cues did not reveal any clear and consistent changes in the activity of neurons of any Cluster during the 0.3 s immediately before Action Cue, i.e., the final epoch of the variable Delay Window common to all Hit trials (Figure 5.2D, E). These results suggest Cluster 1 neurons are encoding licks and not just Action Cue and/or reward.

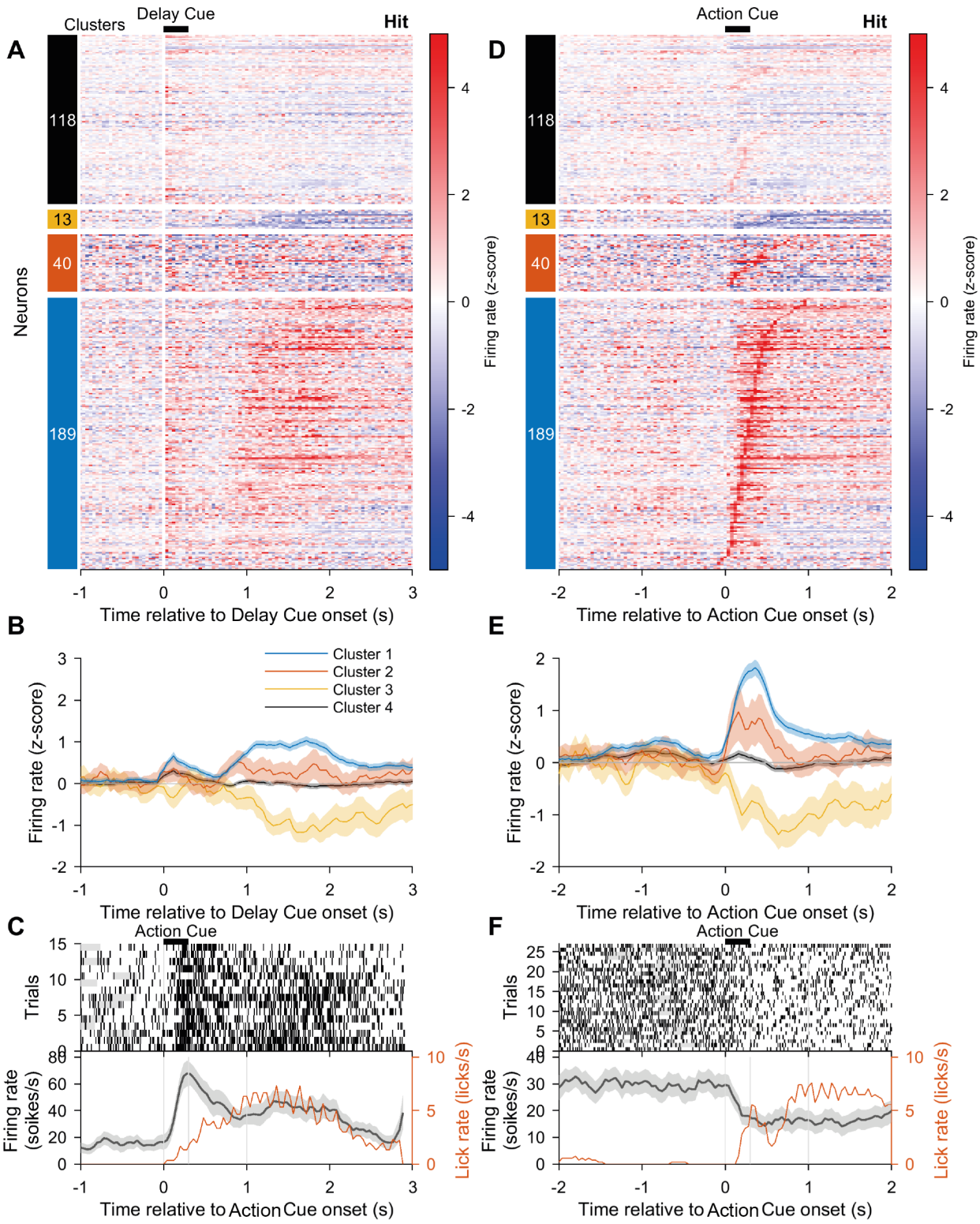
Examples of the typical activity of individual neurons assigned to Cluster 1 or Cluster 3 are shown in Figure 5.2C, F, I. The Cluster 1 neuron displays an increase in firing rate that began at the Action Cue onset (before licking commenced), peaked around Action Cue offset, and then exhibited a sustained activity lasting by ~2 s after Cue onset (Figure 5.2C). Another Cluster 1 neuron displayed an increase in firing rate that began before licking commenced, peaked before just first lick, and then exhibited

a sustained activity lasting for ~2 s after first lick (Figure 5.2 I). Note the sustained increase in neuron activity overlapped in time with bouts of multiple licks (Figures 5.2C, I). The Cluster 3 neuron (Figure 5.2F) showed an inverse activity profile around Action Cue, initially decreasing firing rate around Cue onset and then displaying a sustained decrease in firing rate lasting for at least 2 s after Cue onset, again overlapping in time with prolonged bouts of licking.

The diverse changes in SNr neuron activity and the prevalence of firing rate increases around the onset of Action Cues or licking are not in line with the key prediction of the disinhibition model that a uniform decrease in BG output neuron activity accompanies and supports movement execution

When the spike firing of SNr neurons, aligned to Delay Cue onset (Figure 5.2 A, B), those in Clusters 1, 2 and 4 weakly encoded (z-scores <1) the Delay Cue by increasing their firing rates. Their activity rapidly returned to baseline after Delay Cue onset (within 1 s). Neurons in Cluster 3 also weakly encoded (z-scores <1) the Delay Cue by decreasing their firing rate. Again, their activity rapidly returned to baseline after Delay Cue onset. Importantly, alignment of spike firing to Delay Cues did not reveal any clear and consistent changes in the activity of neurons of any Cluster during the 0.3-0.6 s after Cue onset, i.e., the initial epoch of the variable Delay Window common to all Hit trials (Figure 5.2A, B; note the change in activity from ~ 1 s after Cue onset are likely those accompanying Action Cues).

Taken together, these results indicate that the most SNr neurons increase their firing rate around Action Cue onset and first licks in Hit trials. Notably, I did not observe clear and consistent activity changes during the Delay Window. Cue encoding by subsets of SNr neurons was not surprising since it is well-known that, at least in non-human primates, SNr neurons encodes reward and visual cues (Hikosaka and Wurtz 1983b; Joseph and Boussaoud 1985; Handel and Glimcher 2000; Sato and Hikosaka 2002).


A
Clusters
Delay Cue
Hit
Neurons
118
13
40
189
Firing rate (z-score)
Time relative to Delay Cue onset (s)
D
Action Cue
Hit
Time relative to Action Cue onset (s)
B
Cluster 1
Cluster 2
Cluster 3
Cluster 4
Firing rate (z-score)
Time relative to Delay Cue onset (s)
E
Time relative to Action Cue onset (s)
C
Action Cue
Trials
Firing rate (soikes/s)
Lick rate (licks/s)
Time relative to Action Cue onset (s)
F

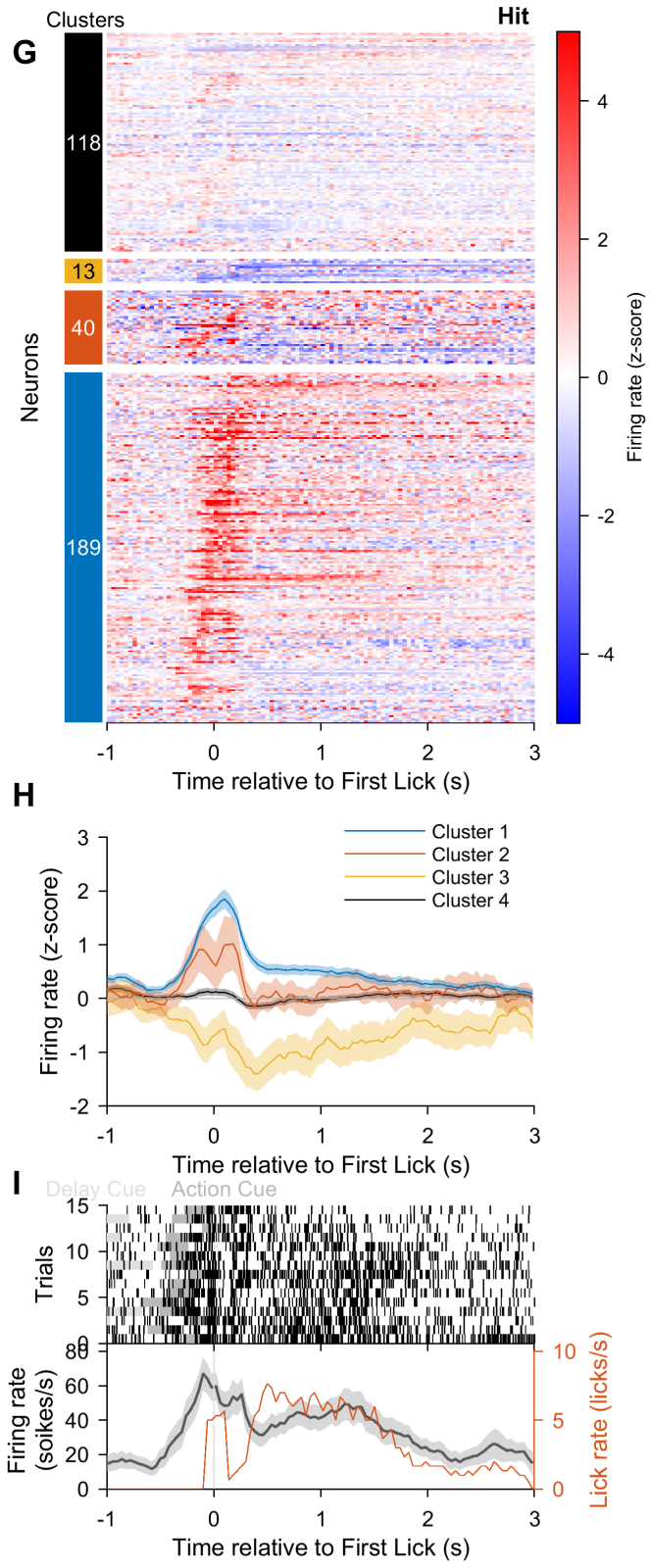

G
Clusters
Hit
118
13
40
189
Neurons
Firing rate (z-score)
4
2
0
-2
-4
-1
0
1
2
3
Time relative to First Lick (s)
H
Cluster 1
Cluster 2
Cluster 3
Cluster 4
Firing rate (z-score)
3
2
1
0
-1
-2
-1
0
1
2
3
Time relative to First Lick (s)
I
Delay Cue
Action Cue
Trials
15
10
5
0
Firing rate (soikes/s)
80
60
40
20
0
Lick rate (licks/s)
10
5
0
-1
0
1
2
3
Time relative to First Lick (s)

Figure 5.2 Distribution of the peak normalized firing rate of neurons in Hit trials sorted by the peak activity. A, D: Peri-event time histograms of all SNr neurons (n = 360) from all mice (n = 4) recorded during Hit trials are shown as heat maps and sorted by timing of peak activity after Delay Cue onset (A) and Action Cue onset (D) (time zero). **B, E:** Mean (solid line) ± SEM (shadow) of firing rates of the Clusters of neurons are plotted as peri-event time histograms and aligned (at time zero) to Delay Cue onset (B) or Action Cue onset (E). Blue, dark orange, dark yellow and black bars represent Clusters of neurons. Smoothing is applied using moving average of 5 data points. **C, F:** Mean (solid line) ± SEM (shadow) of the activity of two exemplar units for Cluster 1 (C) and Cluster 4 (F). Rasters (top) and peri–movement spike–density functions (bottom) show changes in discharge rates at the time of Action Cue onset (time zero). **G, H, I:** same as D, E, C, but aligned to first licks. Gray bars correspond to the Delay Cue (0.3 s).

5.4 Some SNr neurons increase their firing rates in Premature Hit trials

To test whether and how SNr neurons encoded movement in the absence of the Action Cue, I analysed the activity of 297 single units recorded in SNr during Premature Hit trials from 4 trained animals (15 sessions).

When aligned to first licks Cluster 1 neurons (n = 115/297) increased their firing before, during and after the time relative to first licks (Figure 5.3D, F), suggesting that these neurons where encoding movement in addition to Delay Cue. Compared to encoding of licks in Hit trials (Figure 5.2G, H) movement-encoding activity in Premature Hits might not be as vigorous because in Premature Hits mice are not rewarded and they usually do not exhibit repetitive licking (see Figures 3.3 and 4.6). Other neurons (Cluster 2, n = 16/297; Cluster 3, n = 8/297) weakly encoded (1 < z-score), or not encoded (Cluster 4, n = 158/297) first licks.

When aligned to Delay Cue onset (Figure 5.3A, B), the majority of SNr neurons weakly encoded the Cue by increasing their firing rates (1 < z-score) (Cluster 1, n = 115/297; Cluster 2, n = 16/297; Cluster 4, n = 158/297). The activity of Cluster 2 and 4 rapidly decreased to baseline (<1 s from Delay Cue onset). The activity of Cluster 1 took longer to return baseline (~1.5 s by Delay Cue onset), the reason for sustained activity is that as shown in (Figure 5.3D, E). A small number of neurons (Cluster 3, n = 8/297) also weakly encoded the Delay Cue and possibly movement, given their negative peak anticipated first licks, by decreasing their firing rate (z-score < -1). The activity rapidly returned to baseline (1 s < from Delay Cue onset) (Figure 5.3A-E).

Examples of the typical activity of individual neurons assigned to Cluster 1 are shown in Figure 5.3C, F. The first neuron displays an increase in firing rate that began at the Delay Cue onset (before licking commenced), peaked around Delay Cue offset, and was then sustained for ~1.5 s after Cue onset (Figure 5.2C). The second neuron that displays an increase in firing rate that began before licking commenced, peaked around the time first lick, and then returned to baseline (Figure 5.3F).

Taken together, these results from Premature Hit trials indicate that, in the absence of overt sensory cues, many SNr neurons encode movement execution by increasing their firing ratess .Some neurons also weakly encode the Delay Cue by briefly increasing their firing rate around the Cue onset. Both of these observations are consistent with results obtained from analyses of SNr activity during Hit trials.

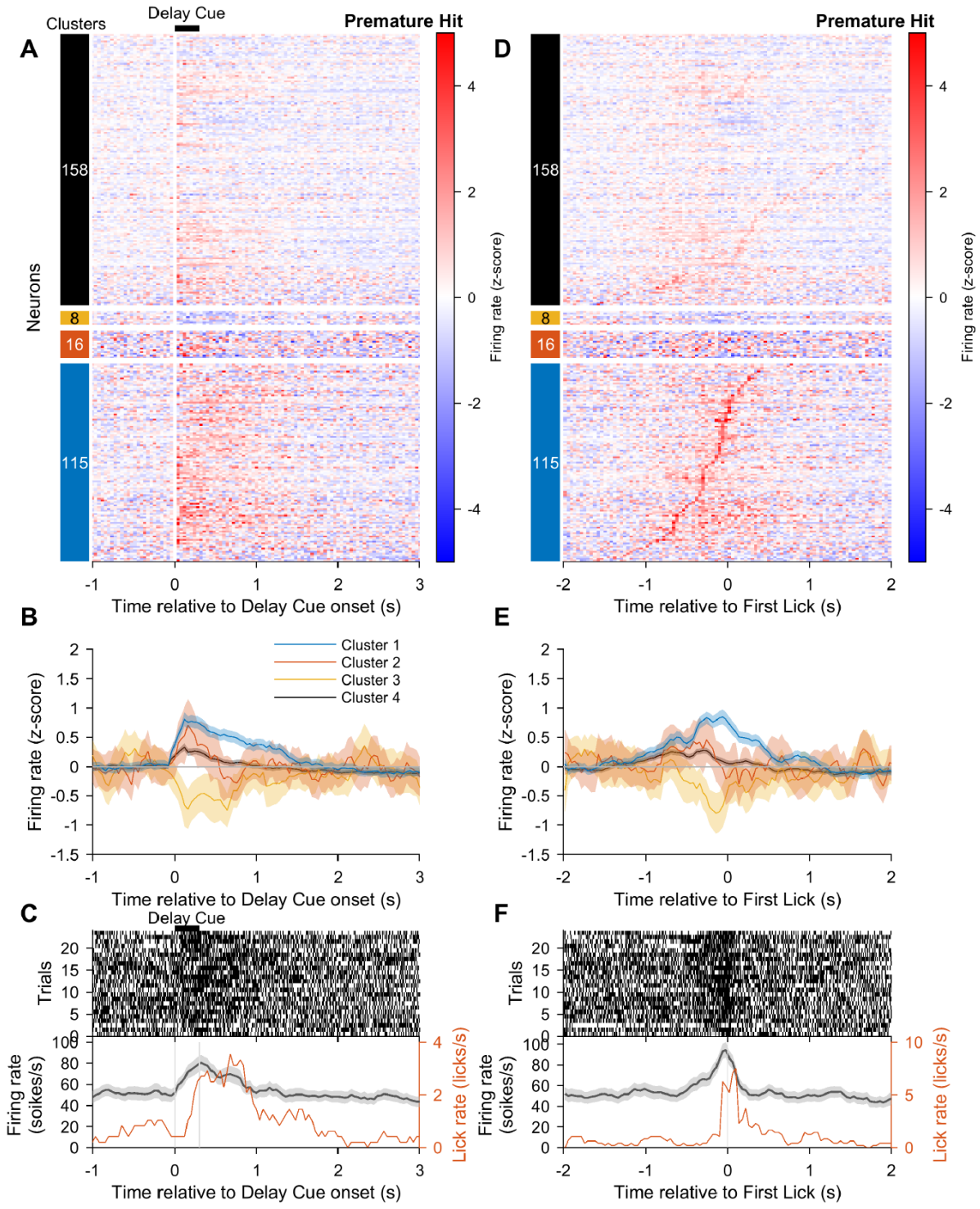

A
Clusters
Delay Cue
Premature Hit
Neurons
158
8
16
115
Firing rate (z-score)
Time relative to Delay Cue onset (s)
D
Premature Hit
Time relative to First Lick (s)
B
Cluster 1
Cluster 2
Cluster 3
Cluster 4
Firing rate (z-score)
Time relative to Delay Cue onset (s)
E
Time relative to First Lick (s)
C
Delay Cue
Trials
Firing rate (soikes/s)
Lick rate (licks/s)
Time relative to Delay Cue onset (s)
F
Time relative to First Lick (s)

Figure 5.3 Distribution of the peak normalized firing rate of neurons in Premature Hit trials sorted by the peak activity. A, D: Peri-event time histograms of all SNr neurons (n = 297) from all mice (n = 4) recorded during Premature Hit trials are shown as heat maps and sorted by timing of peak activity after Delay Cue onset (A) and first licks (D) (time zero). **B, E:** Mean (solid line) ± SEM (shadow) of firing rates of the Clusters of neurons are plotted as peri-event time histograms and aligned after Delay Cue onset (B) and first licks (E) (time zero). Blue, dark orange, dark yellow and black bars represent Clusters of neurons. Smoothing is applied using moving average of 5 data points. **C, F:** Mean (solid line) ± SEM (shadow) of the activity of two exemplar units for Cluster 1. Rasters (top) and peri–movement spike–density functions (bottom) show changes in discharge rates at the time of (C) Delay Cue onset (time zero) and (F) first licks (time zero).

5.5 SNr neurons can encode Cues but not movement in Miss trials

To test whether and SNr neurons encode sensory cues in the absence of licks and rewards, I analysed the activity of 104 single units (baseline firing rates; 14.83 ± 0.84; ± SEM) recorded in SNr during Miss trials from 3 trained animals (7 sessions).

When spiking was aligned to onset of the Action Cue two Clusters of neurons (Cluster 1 and Cluster 2, n = 2/104 and n = 19/104) weakly increased their firing rates for short periods that rarely exceeded the duration of the Action Cue. Since licks or reward where absent, and the firing rate did not precede Action Cue, it is likely that these neurons are encoding only the Action Cue (Figure 5.4D, E). Also, the rapid decrease to baseline (~1 s by first licks), shows that these neurons did not have sustained activity of neurons encoding movement (see Figure 5.2 G, H).

When aligned to Delay Cue onset (Figure 5.4A, B), a large number of SNr neurons did not encode Cue or movement (Cluster 4, n = 47/104). The rest of the neurons weakly (Cluster 1, n = 36/104) (1 < z-score), or very weakly (Cluster 2 and 3, n = 2 and n = 19) (0.5 < z-score) encoded the Delay Cue by increasing their firing rate and very rapidly decreasing to baseline (~0.5 s by Delay Cue onset).

Examples of the typical activity of individual neurons assigned to Cluster 1 are how in Figure 5.4C, F. The first neuron displays a brief increase in firing rate that peaked just after Delay Cue onset and rapidly returned to baseline by the time of Cue offset. The second neuron displays shows a similarly brief increase in firing rate that was well timed with the duration of the Action Cue (Figure 5.4 F).

Taken together, these results indicate that some SNr neurons encode sensory cues with brief firing-rate increases in the absence of licks and rewards.

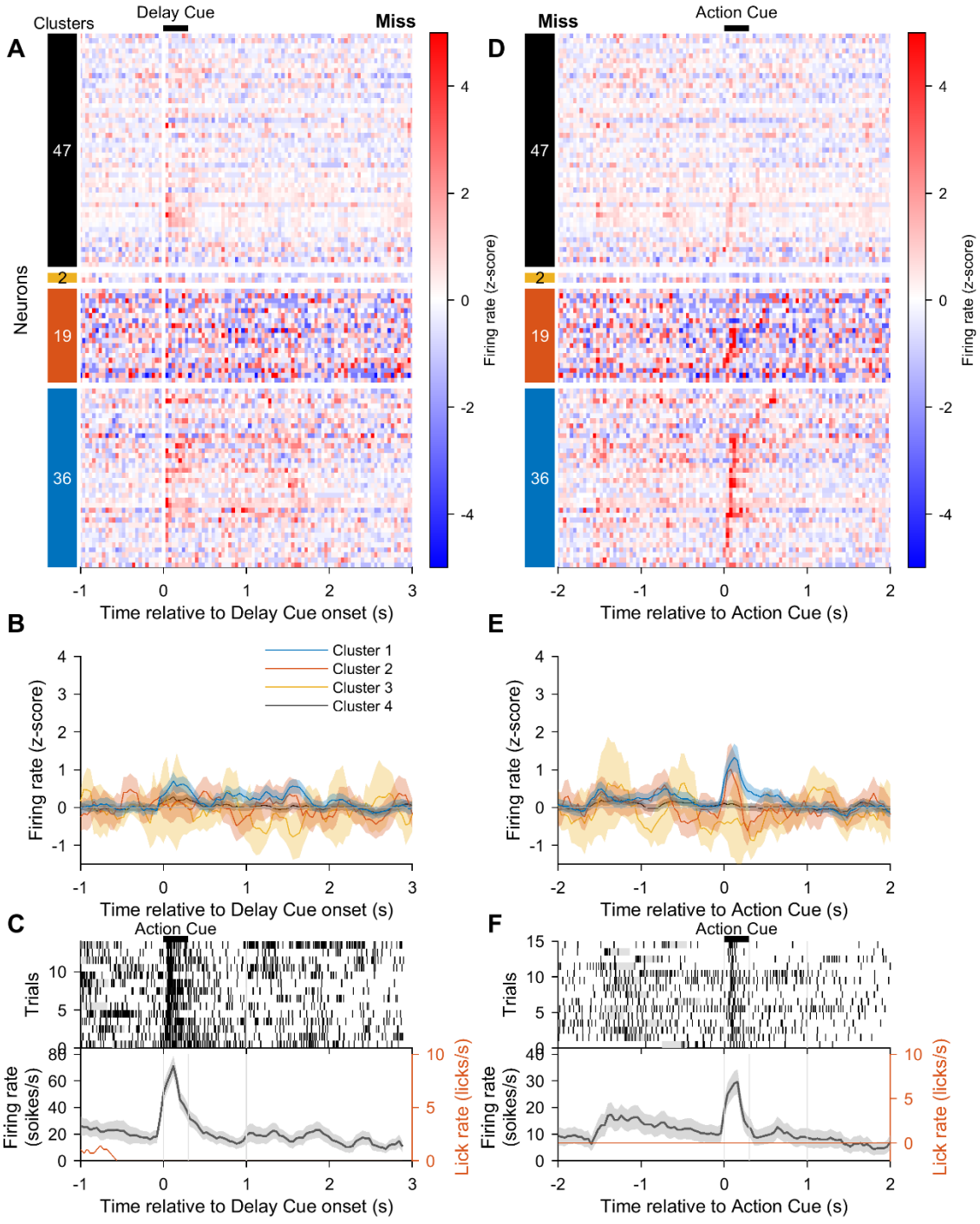


Figure 5.4 Distribution of the peak normalized firing rate of neurons in Miss trials sorted by the peak activity. A, D: Peri-event time histograms of all the significantly modulated SNr neurons (n = 104) from all mice (n = 3) recorded during Premature Hit trials are shown as heat maps and sorted by timing of peak activity after Delay Cue onset (A) and Action Cue onset (D) (time zero). **B, E:** Mean (solid line) ± SEM (shadow) of firing rates of the Clusters of neurons are plotted as peri-

event time histograms and aligned after Delay Cue onset (B) and Action Cue onset (E) (time zero). Blue, dark orange, dark yellow and black bars represent Clusters of neurons. Smoothing is applied using moving average of 5 data points. **C, F:** Mean (solid line) ± SEM (shadow) of the activity of two exemplar units for Cluster 1. Rasters (top) and peri–movement spike–density functions (bottom) show changes in discharge rates at the time of (C) Delay Cue onset (time zero) and (F) Action Cue onset (time zero). Gray bars correspond to the Delay Cue (0.3 s).

5.6 Summary of SNr neurons activity patterns during the delayed-Go task

In Figure 5.5 I superimpose the PETH curves from Figures 5.2–5.4 for direct comparison. When the spiking of SNr neurons is aligned to the Delay Cue (Figure 5.5 A), it is evident that Clusters of neurons increasing their firing rates during the Delay Cue showed either sustained firing rates throughout the Delay Window (Premature Hit increase), suggesting they were encoding subsequent (incorrect) movement, or a rapid decrease to baseline (Hit increase and Miss increase), suggesting they were only encoding the Cue. Interestingly, some neurons encoding the Action Cue and first licks (Hit increase) (Figure 5.5B, C) also encoded the Delay Cue (Figure 5.5A).

When spiking is aligned to the Action Cue (Figure 5.5B), it is evident that the firing-rate increases of neurons in Miss trials neurons peaked within the Cue and rapidly decreased to baseline within the Cue duration, suggesting these brief increases reflect the encoding of Action Cue only. On the other hand, neurons in Hit trials started to increase (or, less often, decrease) their activity at the Action Cue onset (before first lick, see Figure 5.5C), with peaks/troughs after Cue offset, and then showed sustained

activity changes that lasted for ~2 s from the Action Cue offset. These sustained activity changes are almost certainly related to movement because the Action Cue has terminated after 0.3 s, reward is provided at the first lick only, and mice are often engaged in repetitive licking in response to the delivery of single water drops (see Figures 3.3 and 4.3).

When spiking is aligned to the first licks (Figure 5.5C), it is evident that neurons in Hit trials increased (or, less often, decreased) their firing rate before movement initiation, with changes peaking after first licks, and then showed a sustained activity lasting for ~2 s from the first lick, suggesting they are positioned in time to play a fundamental role in encoding and controlling movement.

Firing rates histograms in Hit trials are shown in Figure 5.6A (Cluster1, 10.98 ± 0.92; Cluster 2, 22.30 ± 3.20; Cluster 3, 27.05 ± 5.20; Cluster 4. 16.80 ± 1.50; mean ± SEM). Firing rates histograms in Premature Hit trials are shown in Figure 5.6B (Cluster1, 9.75 ± 0.94; Cluster 2, 10.34 ± 1.81; Cluster 3, 18.64 ± 3.89; Cluster 4. 17.12 ± 1.20; mean ± SEM). Firing rates histograms in Miss trials are shown in Figure 5.6C (Cluster1, 15.35 ± 1.69; Cluster 2, 26.28 ± 9.16; Cluster 3, 11.59 ± 6.57; Cluster 4. 11.33 ± 2.18; mean ± SEM).

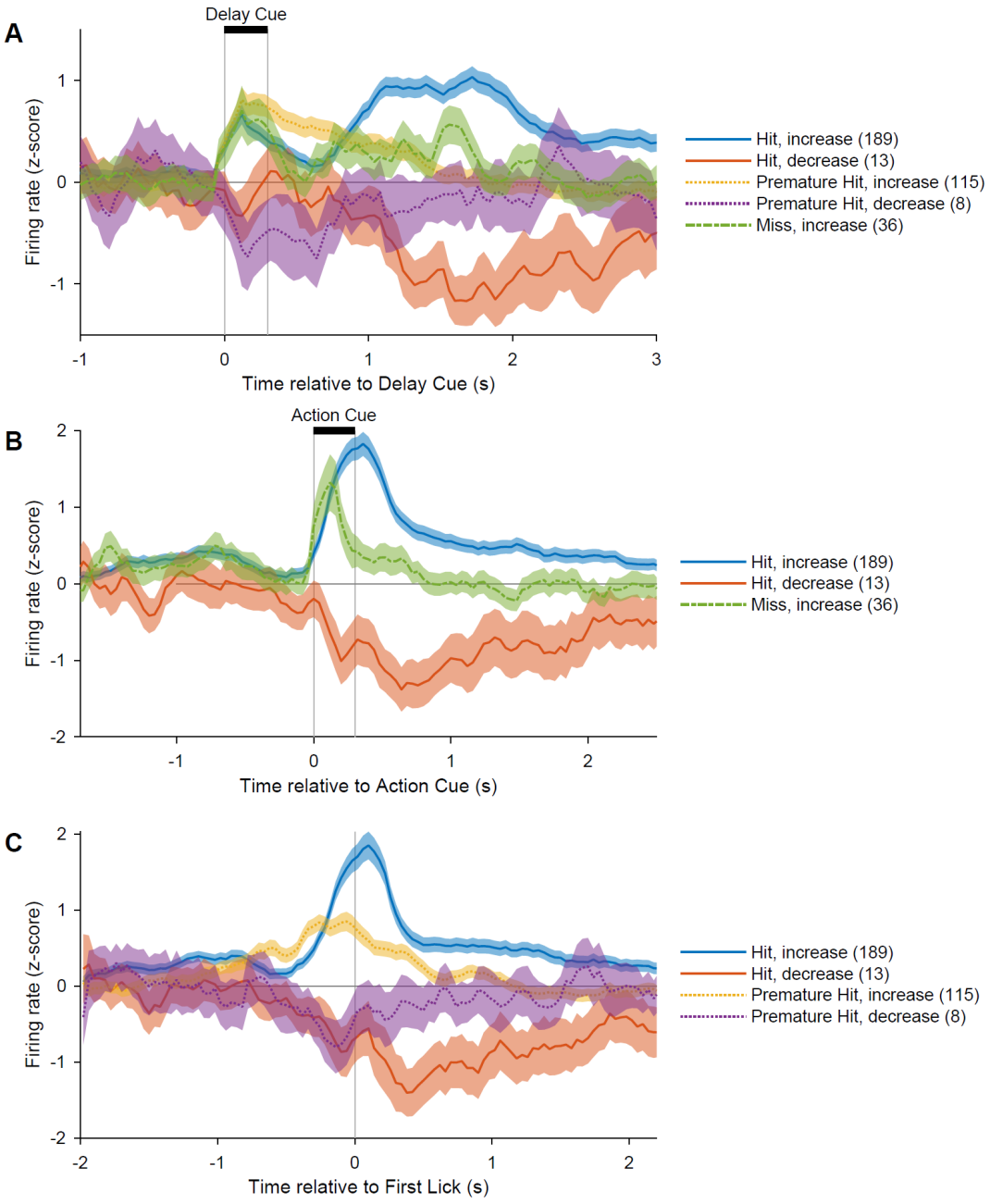


Figure 5.5 Comparison of spike PETH curves of SNr Clusters during the delayed-Go task. A–C: Peri-event time histogram curves in Figure 5.2–4 are superimposed for comparison: Hit increase (blue), Hit decrease (red), Premature Hit increase (yellow, dotted), Premature Hit decrease (purple, dotted), and Miss increase (green, lined). The peri-event time histograms are presented against three different X axes; time is relative to Delay Cue onset (A), Action Cue onset (B) and the first licks or the first premature hit licks (C).

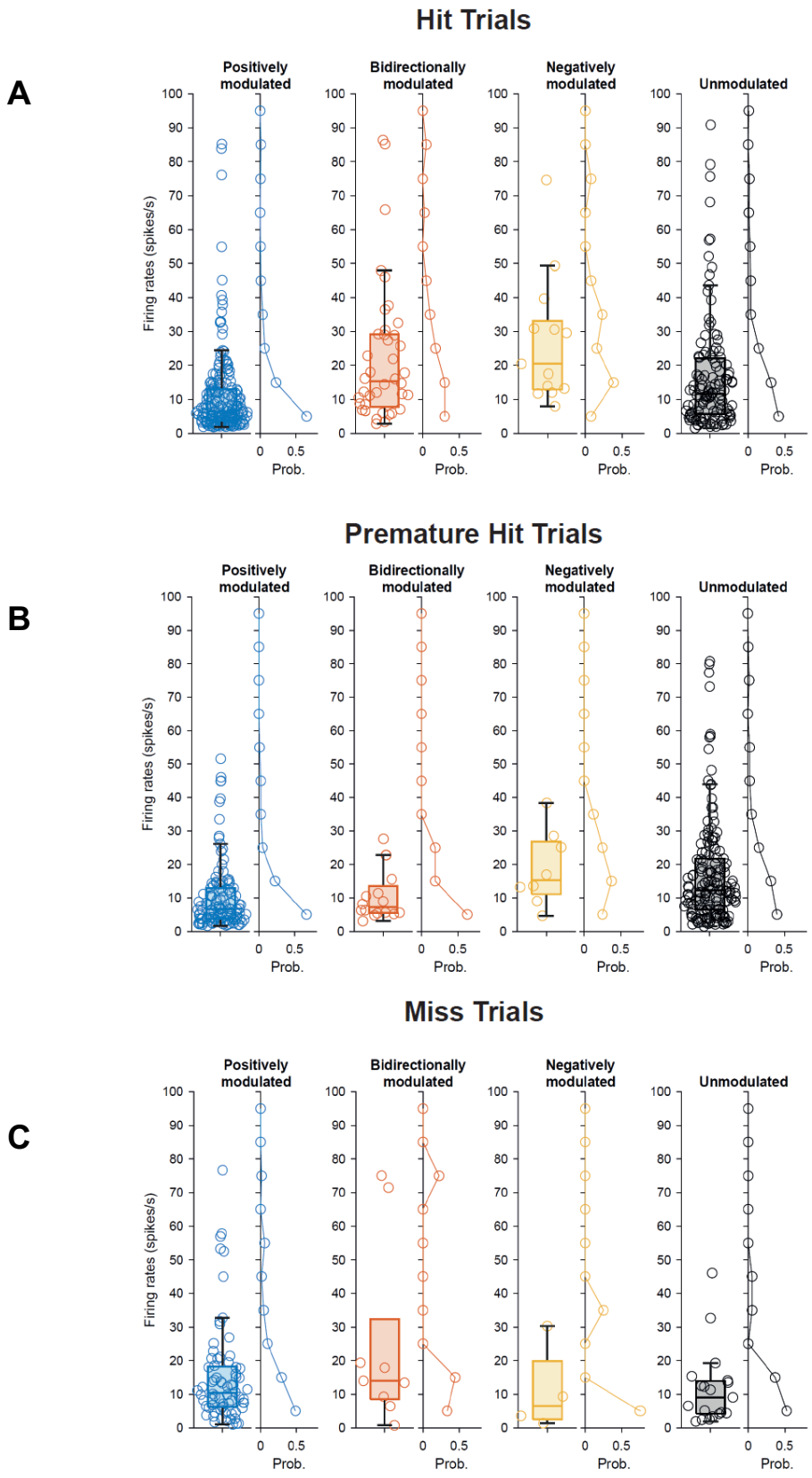


Figure 5.6 Firing rates histograms of SNr neurons during the delayed-Go task. Positively modulated neurons (blue, Cluster 1); bidirectionally modulated neurons (red, Cluster 2); negatively modulated neurons (yellow, Cluster 3); unmodulated neurons (black, Cluster 4) in A: Hit trials, **B**: Premature Hit trials, and **C**: Miss trials. Box plots denote the minimum and maximum values that are not outliers (whiskers), interquartile range, and medians (see Materials and methods section 2.9).

5.7 Optogenetic activation of SNr neurons during Action Cue and Delay Window

In Chapter 4, I detail the behavioural effects of optogenetic manipulations of the SNr. To give insight into the neuronal substrates underlying these behavioural effects and verify that SNr neurons were optogenetically activated as expected, I used the optoprobe to record the activity of SNr neurons while locally delivering blue light during the Action Cue or Delay Window of the delayed-Go task.

A train of blue laser pulses (10 ms, 50 Hz, 50% duty cycle) was delivered to SNr at the onset of Action Cue while recording 282 SNr neurons from 4 trained VGAT-IRES-Cre mice during the task. Light was not delivered in every trial of the task; trials during which light was delivered were designated 'laser-on' whereas other trials were designated 'laser-off'. I analysed data from 15 sessions of Hit trials (n = 110 laser-on trials, n = 111 laser-off trials), and 3 sessions for Miss trials (n = 20 laser-on trials; n =21 laser off trials); 241 and 41 SNr neurons were recorded during Hit trials and Miss trials, respectively. To examine how the delivery of light influenced SNr neuron activity around the time of Action Cue, I aligned spike firing data to the start of the Action Cue and separated out data recorded in laser-on and laser-off trials. The difference between the z-scored mean firing rages of laser-on trials and those of laser-off trials in Hit trials and Miss trials are plotted as heat maps (Figure 5.7A, E) and peri-event time histograms (Figure 5.7B, F).

When aligning spike firing data to the start of the Action Cue, it was evident that many SNr neurons rapidly increased their firing rates in response to delivery of blue light pulses. This was evident in both Hit trials (Figure 5.7A–C) and Miss trials (Figure 5.7E-G). This augmented activity was partly sustained for the duration of the laser pulse train; note that, by design, Action Cues and laser stimuli were aborted when first licks occurred, such that laser pulses were not delivered for the full 300 ms of Action Cue duration in some Hit trials. SNr neuron firing rates rapidly returned to baseline levels at the cessation of light delivery (Figure 5.6A–G). In general, SNr neurons did not respond to the light pulses with decreases in firing rate.

In Hit Trials, laser-on neurons show significantly higher activity ($p = 1.79\times10^{-87}$) than laser-off neurons (laser-on neurons, 3.57 ± 0.13; laser-off neurons, 0.710± 0.001; mean ± SEM) (Figure 5.6C). Likewise, in Miss trials, laser-on neurons show significantly higher activity ($p = 2.25\times10^{-81}$) than laser-off neurons (laser-on neurons, 4.26 ± 0.33; laser-off neurons 0.590 ± 0.008; mean ± SEM) (Figure 5.6G).

Figure 5.7G, H shows the effect of optogenetic manipulation on two single units during Hit trials and Miss trials. The laser lasting for the entire duration of the Action Cue (300 ms) drives the firing rate of the two units.

To evaluate the impact of the optogenetic stimulation delivered through the optrode on movement execution in Hit trials, I computed, as an illustrative example, the raster plots of the licks during laser-off (Figure 5.8A, top) and laser-on Hit trials (Figure 5.8B, top) of a single session for one mouse (gms068). The mouse frequently

licked more than once in a single Hit trial, and the overall number of licks across all trials appeared similar between laser-on and laser-off trials. Reaction times, defined as the first licks (coloured blue or red) occurring after the Action Cue onset, appeared to vary between laser-on and laser-off trials. This result was confirmed by the peri-event time histograms (PETH) of first licks (Figure 5.8A, B, bottom; blue and red traces). The times to first licks in laser-on trials appeared longer than the times to first licks in laser-off trials. In accordance with what I observed within a single session for this one mouse, in 4 ChR2 mice, PETH curve of mean reaction time in laser-on trials had broader, flatter distribution of lick times as compared to those in laser-off trials (Figure 5.8C). To compare the reaction times quantitatively, I Clustered the individual reaction times (n = 4 mice) across all the sessions (n = 15). The times to first licks in laser-on trials (110 trials; 0.38 s ± 0.31%; mean ± SEM) were on average significantly longer ($p = 3.0606\times10^{-17}$) than times to first licks in laser-off trials (111 trials; 0.35 s ± 0.004%; mean ± SEM) (Figure 5.8D).

Taken together, these data show that delivery of blue light to the SNr robustly increased the firing rates of many SNr neurons, irrespective of trial type. Moreover, optically-driven firing rates far exceeded the firing rates achieved during execution of the tasks when the laser was off. Light delivered via the optoprobe during the Action Cue of Hit trials delayed first licks in the same way as light delivered through chronically-implanted optic fibres as previously shown in Figure 4.3.

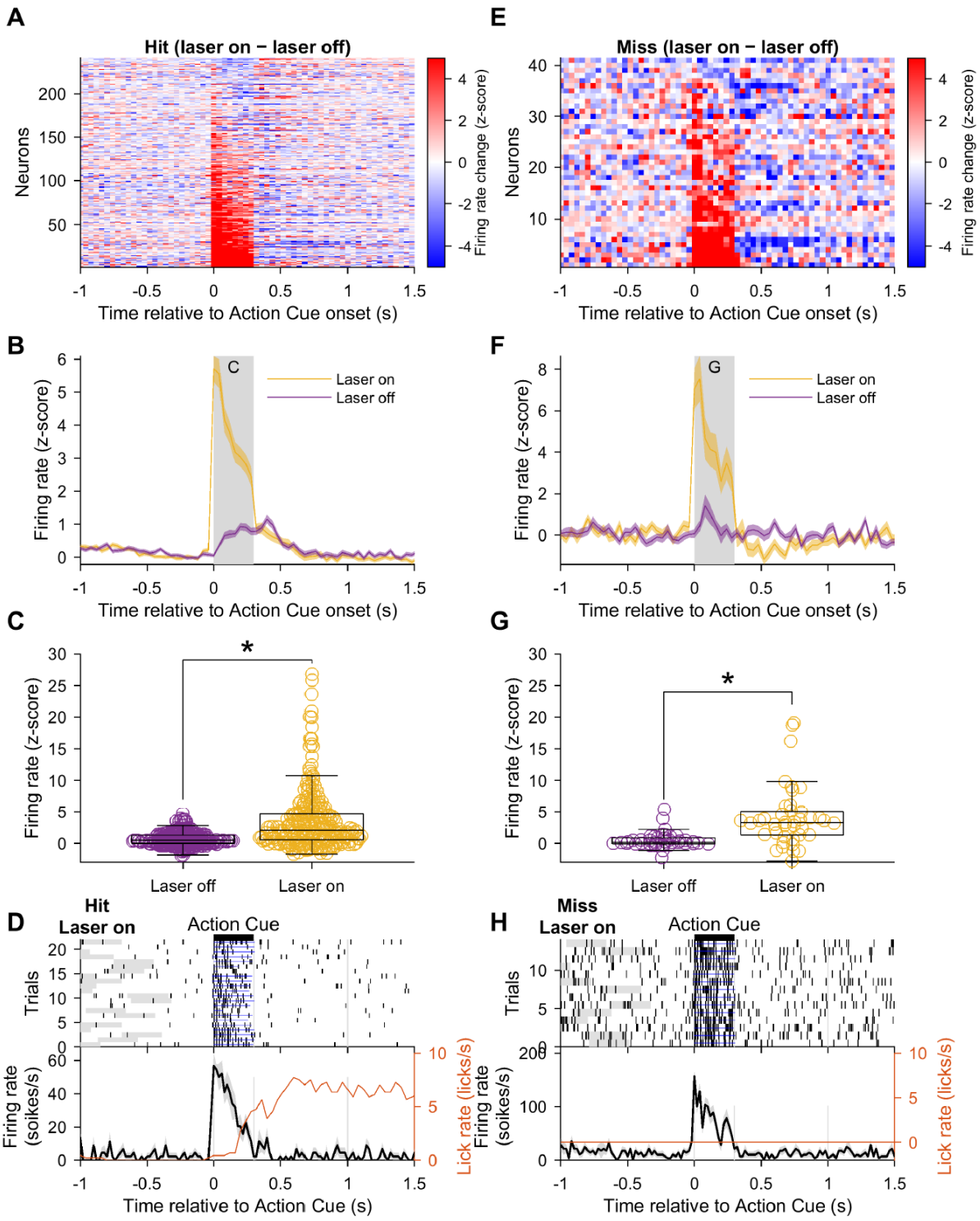


Figure 5.7 Optogenetic modulation of SNr neurons during Action Cue. A, E: The differences of z-scored firing rates of SNr neurons in laser-on trials from those in laser-off trials during Hit (A) and Miss (E) trials is plotted as heat maps. Activity is sorted by mean firing rate difference during Action Cue ($0 < t < 0.3$ s). Neurons were sorted according to the mean firing rate within the time window of 0 to 0.3 s from Action Cue onset. **B, F:** Mean firing rate of neurons in laser-on and laser-off trials. Bin = 40 ms, no smoothing. **C, G:** Firing rates were compared between laser-off and laser-on trials rate within the time window of 0 to 0.3 s from Action Cue onset. **D, H**: The activity of single exemplar

units. Rasters (top) and peri–event time histograms (bottom) show changes in discharge rate at the time of Action Cue onset (time zero). Gray bars denote Delay Cue (0.3 s). Blue lines denote laser stimulation. Bin = 20 ms, no smoothing. Box plots denote the minimum and maximum values that are not outliers (whiskers), interquartile range, and medians (see Materials and methods section 2.9). * $p < 0.05$, MWUT. Time zero is relative to Action Cue onset (A–D, G, H). Gray bars correspond to Delay Cue (0.3 s). Gray bars correspond to the Delay Cue (0.3 s).

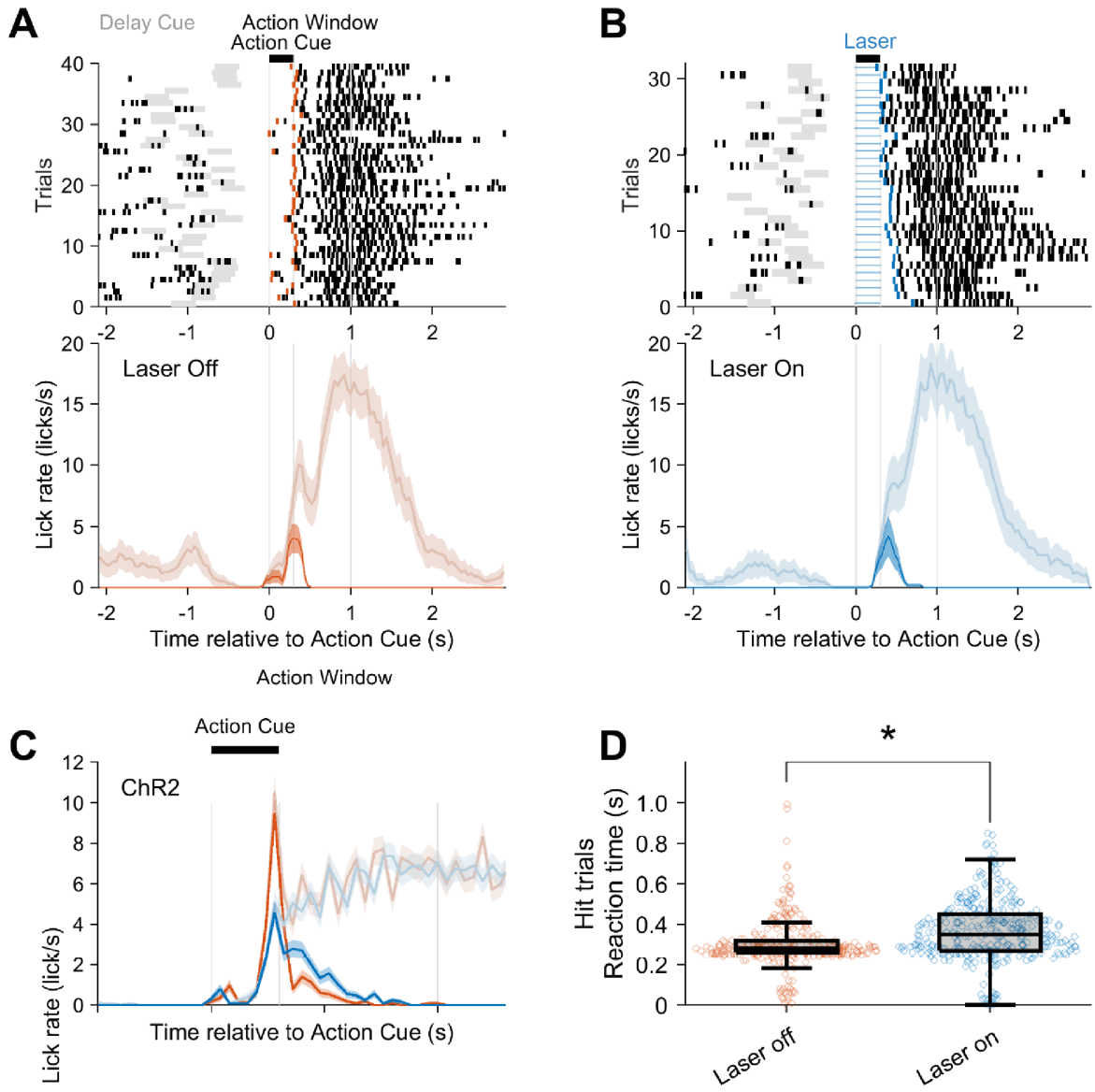


Figure 5.8 Reaction time in Hit trials is delayed when SNr neurons are optogenetically driven during the Action Cue. A, B: Raster plots (top) and PETH curves (bottom) of licks in Hit trials of a single session of a mouse (gms068) with ChR2 expression in SNr. The first licks in raster plots are color-coded in red for laser-off trials (A) and blue for laser-on trials (B). All licks are color-coded in pale red for laser off-trials (A) and pale blue for laser on-trials (B). The grey lines indicate timing of Delay Cues. The blue lines indicate timing of laser light delivered to SNr (i.e., during Action Cue). **C:** Cluster average PETH curves of the first licks (blue and red) and all the licks (pale blue and pale red) in laser-on (blue, pale blue) and laser-off (red, pale red) Hit trials. **D:** The Cluster average comparison of reaction time (first licks) in Hit trials in laser-on (blue) and laser-off (red) trials. Box plots denote the minimum and maximum values that are not outliers (whiskers), interquartile range, and medians (see Materials and methods section 2.9). * $p < 0.05$, MWUT.

I next investigated the effect of optogenetic activation of SNr neurons during Delay Window (0.3–1.3 s). I analysed data from 4 sessions of Premature Hit trials (n = 31 laser-on trials, n = 42 laser-off trials), and 9 sessions for Hit trials (n = 34 laser-on trials; n =26 laser off trials); 70 and 199 SNr neurons were recorded during Premature Hit trials and Hit trials, respectively. To examine how the delivery of light influenced SNr neuron activity around the time of Delay Cue ($0 < t < 0.3$ s), I aligned spike firing data to the start of the Delay Cue and separated out data recorded in laser-on and laser-off trials. The difference between the z-scored mean firing rages of laser-on trials and those of laser-off trials in Premature Hit trials and Hit trials are plotted as heat maps (Figure 5.9A, E) and peri-event time histograms (Figure 5.9B, F).

When spike firing data were aligned to the start of the Delay Cue, it was evident that many SNr neurons rapidly increased their firing rates in response to delivery of blue light pulses during the Delay Widow in both Premature Hit trials (Figure 5.8A–C) and Hit trials (Figure 5.9E–G). This augmented activity was partly sustained for most of the duration of the laser pulse train. SNr neuron firing rates rapidly returned to baseline levels at the cessation of light delivery (Figure 5.8A-G). In general, SNr neurons did not respond to the light pulses with decreases in firing rate.

In Premature Hit Trials laser-on neurons show significantly higher activity ($p = 1.79\times10^{-87}$) than laser-off neurons (laser-on neurons, 1.75 ± 0.16; laser-off neurons, 0.315 ± 0.002; mean ± SEM) (Figure 5.8C). Likewise, in Hit trials laser-on neurons show significantly higher activity ($p = 2.389\times10^{-5}$) than laser-off neurons (laser-on

neurons, 0.630 ± 0.0.070; laser-off neurons, 0.032 ± 0.000; mean ± SEM) (Figure 5.9 G).

Figure 5.9G, H shows the effect of optogenetic manipulation on two single units during Premature Hit trials and Hit trials. The laser lasting for the entire duration of the Delay Window (0.3–1.3s) drives the firing rate of the two units for no longer than ~0.8 s, after which the neurons become 'fatigued'.

To evaluate whether the impact of the optogenetic stimulation delivered through the optrode would interfere with motor preparation and therefore impair movement execution, I computed the raster plots of the licks during laser-off Hit trials (Figure 5.10A, top) and laser-on Hit trials (Figure 5.10B, top) of a single session for one mouse (gms068). The overall number of licks appeared similar between laser-on and laser-off trials. The first licks appeared to happen earlier in laser-on trials than laser-off trials when light was delivered during the Delay Window. This result was confirmed by the first licks' peri-event time histograms (Figure 5.10A, B, bottom; blue and red traces). First licks in laser-on trials peaked within the Action Cue, whereas those in laser-off trials peaked after the Action Cue. In the 4 ChR2 mice, the peak in the PETH curve of mean reaction time in laser-on trials preceded the peak in curves in laser-off trials (Figure 5.10C). To compare the reaction time quantitatively, I Clustered the individual reaction time of mice's first licks (n = 4) across all the sessions (n = 9). First licks in laser-on trials (34 trials; 0.28 s ± 0.33%; mean ± SEM) were significantly faster (p =

1.165×10^{-60}) than first licks in laser-off trials (26 trials; 0.30 s ± 0.58%; mean ± SEM) (Figure 5.10D).

Taken together, these data indicate that the delivery of blue laser light drove firing rates increases in a subset of SNr neurons both during the Delay Window, as expected. Optogenetic modulation delivered during the Delay window accelerated first licks in Hit trials in the same way as previously shown in Figure 4.5.

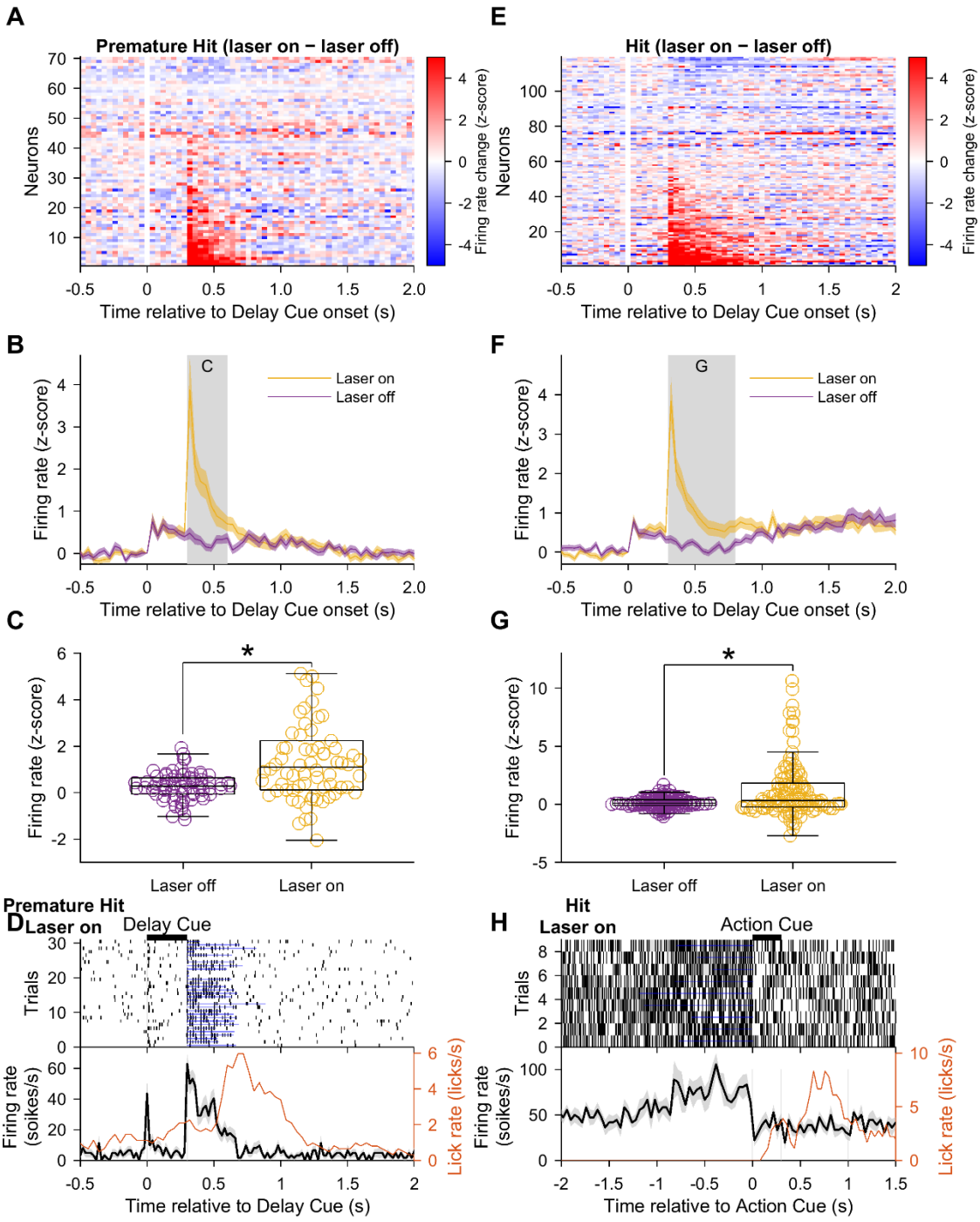


Figure 5.9 Optogenetic modulation of SNr neurons during Delay Window. A, E: The differences of z-scored firing rates of SNr neurons in laser-on trials from those in laser-off trials during Hit (A) and Miss (E) trials is plotted as heat maps. Activity is sorted by mean firing rate difference during Delay Cue and Action Cue ($0 < t < 0.3$ s). Neurons were sorted according to the mean firing rate within the time window of 0 to 0.3 s from Delay Cue and Action Cue onset. **B, F:** Mean firing rate

of neurons in laser-on and laser-off trials. Bin = 40 ms, no smoothing. **C, G:** Firing rates were compared between laser-off and laser-on trials rate within the time window of 0 to 0.3 s from Action Cue onset. **D, H**: The activity of single exemplar units. Rasters (top) and peri–event time histograms (bottom) show changes in discharge rate at the time of (D) Delay Cue onset (time zero) and (H) Action Cue onset (time zero). Blue lines denote laser stimulation. IN (D) bin = 20 ms, no smoothing; in (H) bin = 40 ms, no smoothing. Box plots denote the minimum and maximum values that are not outliers (whiskers), interquartile range, and medians (see Materials and methods section 2.9). * $p <$ 0.05, MWUT. Time zero is relative to Delay Cue onset (A, B, D, E, F) and Action Cue onset (H).

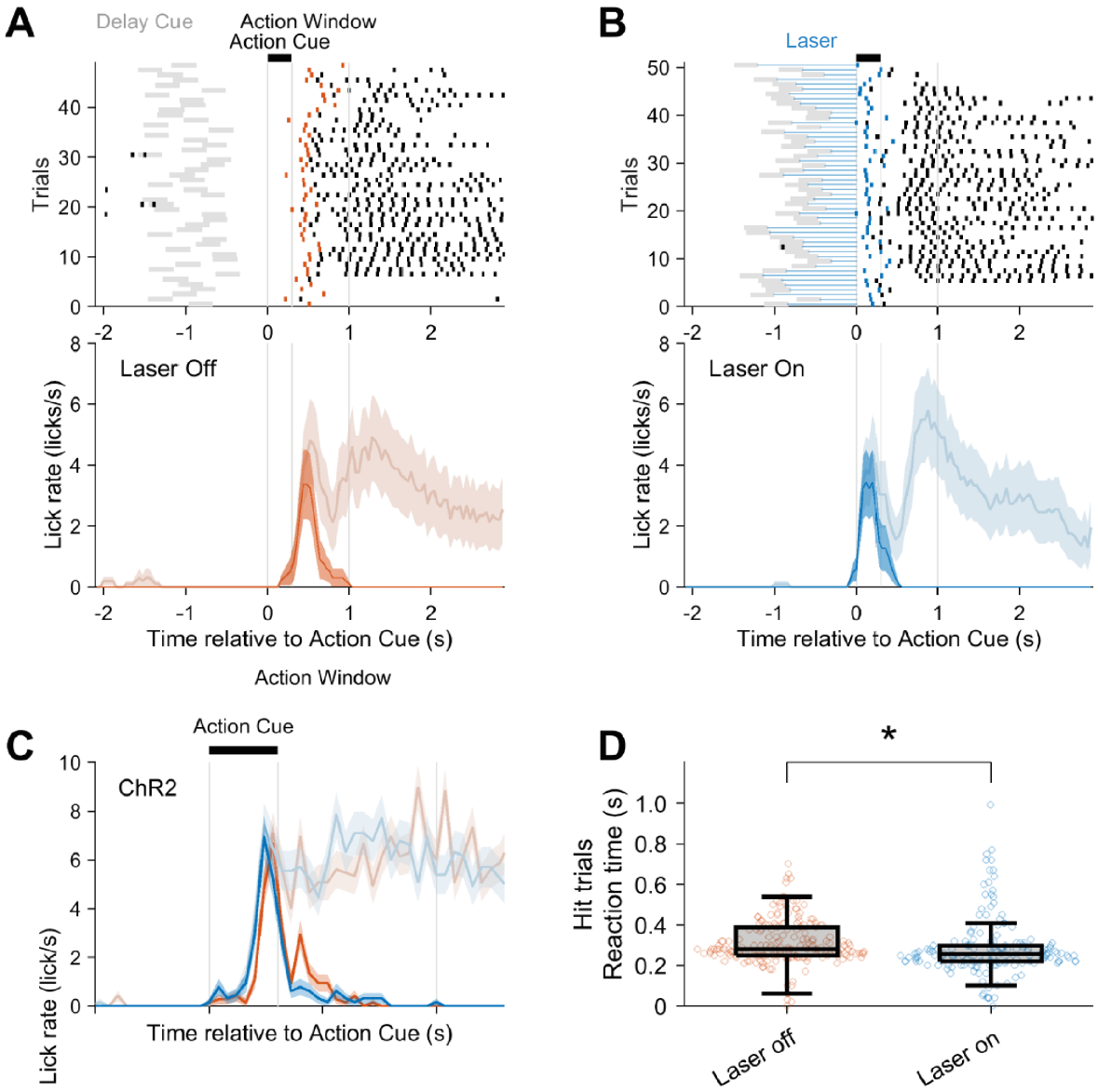


Figure 5.10 Reaction time in Hit trials is faster when SNr neurons are optogenetically driven during the Delay Window. A, B: Raster plots (top) and PETH curves (bottom) of licks in Hit trials of a single session of a mouse (gms068) with ChR2 expression in SNr. The first licks are color-coded in red for laser-off trials (A) and blue for laser-on trials (B). All licks are color-coded in pale red for laser off-trials (A) and pale blue for laser on-trials (B). Note that laser light delivery started at the end of the Delay Cue and was stopped at the end of the Delay Window (when the Action Cue then started). **C:** Cluster average PETH curves of the first licks (blue and red) and all the licks (pale blue and pale red) in laser-on (blue, pale blue) and laser-off (red, pale red) Hit trials. **D:** The Cluster average comparison of reaction time in Hit trials in laser-on (blue) and laser-off (red) trials. Box plots denote the minimum and maximum values that are not outliers (whiskers), interquartile range, and medians (see Materials and methods section 2.9). * $p < 0.05$, MWUT.

5.8 Discussion

In this chapter, I have recorded single-unit activity of SNr neurons in mice performing the delayed-Go task and searched for evidence consistent with the disinhibition model of BG output nuclei function. In Hit trials, recorded neurons displayed task-related firing rate modulation around movement onset (Action Cue and first licks). Critically though, most SNr neurons exhibited increased firing rates around movement onset and sustained higher activity for 1–2 s from the Action Cue onset. Overall, my data suggest that most neurons in the SNr encode movement onset and performance by increasing their firing rates.

Out of the 4 mice used for the electrophysiological recordings, I could histologically verify the position of the recording sites only in one mouse used. As such, I cannot exclude the possibility that some putative SNr neurons of my dataset were recorded from the neighbouring regions of SNr, such as the mesencephalic reticular formation (mRt) and the Zona incerta (ZI) (Paxinos and Watson 2006). Further electrophysiological experiments should ensure a correct histological verification of the recording sites to guarantee that only SNr neurons are analysed. All the neurons exhibited stereotypical firing rates of SNr neurons in rodents (~15-40 spikes/s) (Lobb and Jaeger 2015; McElvain et al. 2021; Willard et al. 2019). Given the homogeneity in electrophysiological properties in recorded neurons combined with the use of the same stereotaxic coordinates for all the mice recordings (see Materials and

Methods), I would argue that my data set is mainly, if not all, composed of SNr neurons.

A widely accepted model states that task-related changes in neuronal activity in BG-recipient structures are allowed or triggered by changes in firing rates in the BG output nuclei. The physiological mechanism most often referred to by this model is “disinhibition” (Hikosaka and Wurtz 1983b) or a "gated permission" to spike (Hikosaka 2007; Chevalier and Deniau 1990; Deniau and Chevalier 1984). My results seem to argue against the disinhibition model as popularized by Hikosaka (2007) and others. An alternative model of BG output has been described by Mink (1996). According to this model, focused selection of desired ‘motor programs and wider suppression of competing motor programs by the basal ganglia operate through near-simultaneous excitation and inhibition of neurons in the SNr and GPi and lead to opposing activity changes in the neuronal population therein. Experimental evidence collected in non–human primates have shown that task-related increases in firing of BG-output neurons are far more prevalent than decreases in firing (Mink 1991; Turner 1997). This is also the case for BG-recipient thalamus (Anderson 1991). According to Mink’s model, a substantial subset of neurons in the BG output nuclei should decrease their firing rates to allow the selection of motor programs. However, in my data only 14 neurons over the 360-recorded SNr neurons decreased the firing rate at movement onset (in Hit trials).

Although it's hard to state how many neurons should be inhibited to be consistent with Mink's hypothesis, studies have shown that a balanced activity of both direct and indirect pathway neurons is crucial for the correct selection of movement (Tecuapetla et al., 2014). It is hard to reconcile my results with Mink's models without considering an unknown physiological mechanism that would make decrease-type responses in SNr, which were the small minority, more effective at eliciting spikes in their target structures than increase-type responses are at inhibiting them. It is worth noting that the low number of neurons decreasing their firing rates could be affected by my experimental conditions, e.g., (topography of recordings). I cannot exclude that a consistent number of neurons could decrease their firing activity in different areas of the SNr. Also, the different amplitudes and distributions of the two PETH curves in Figure 4.3C could be consistent with studies that advance the hypothesis, consistent with Mink's model, that basal ganglia are not only regulating action selection and initiation but also movement vigour.

Several mechanisms could cause the increase in SNr activity, such as an excitation by the glutamatergic subthalamic nucleus (STN) and/or disinhibition resulting from the reduced activity of the GABAergic globus pallidus pars externa (Smith and Bolam 1990). Still, it is hard to bring into coherence my results that show an increased activation of SNr at movement onset and therefore an increase inhibition of motor structures, with models that indicate the removal of inhibition from SNr as a fundamental mechanism that allows movement execution to occur. Contradictory to the disinhibition model, increasing number of studies have shown that BG output

neurons exhibit firing rate increases at movement onset in the same behavioural tasks where thalamic neurons exhibit rate increases (Kunimatsu and Tanaka 2010; Goldberg and Fee 2012; Nambu 2004; Georgopoulos, DeLong, and Crutcher 1983; Anderson and Horak 1985; Yoshida and Tanaka 2009; Sheth et al. 2011). Stemming from work using songbirds, Goldberg et al. have defined this as "paradoxical coactivation" of the pallidus and the thalamus (Goldberg, Farries, and Fee 2013). As a possible explanation for these findings, they proposed that pallidal and thalamic neurons exhibiting rate increases could be in different motor "channels," i.e., the pallidal neurons displaying a rate increase could cause the firing-rate decrease in a small portion of thalamic neurons (Anderson and Horak 1985; Turner and Anderson 1997), while the minority of pallidal neurons exhibiting a firing-rate decrease could cause the firing-rate increase observed in most thalamic neurons (Chevalier and Deniau 1990; Mink 1996; Hikosaka 2007; Berns and Sejnowski 1998). It is noteworthy that the spatial extent, number, and strength of synaptic connections formed by BG output neurons that increase or decrease their firing rates with movement are not known.

A further possibility suggested by Goldberg et al. is that some (yet unknown) mechanism, which goes beyond the GABA-mediated synaptic inhibition, drives thalamic neurons to spike despite the increased pallidal activity at movement onset. Given the functional, cyto- and chemoarchitectural similarities between the SNr and the GPi (Lanciego, Luquin, and Obeso 2012), paradoxical coactivation could also occur between SNr and thalamus. Still, my observation that a very low number of SNr neurons decrease their firing rates does not seem to fit with this model either, which

predicts a high number of pallidal neurons decreasing their firing rates. Another possibility is that SNr-thalamus projections as described by (McElvain et al. 2021) support locomotor without the mediation of higher thalamic or cortical areas.

Projections of SNr neurons to the downstream targets such as VM, Pf, SC, and zona incerta display a mediolateral topographical arrangement distributed throughout the SNr (Lee, Wang, and Sabatini 2020; McElvain et al. 2021). Furthermore, the continuum found for each electrophysiological property (e.g., firing rates ranges, gain and rebound kinetics) can differentially tune the firing capabilities of individual neurons in the SNr (McElvain et al. 2021). Because of geometric arrangement of recording contacts on the optoprobe, my recordings at any one time covered a large portion of the SNr in the anterior-posterior axis (~ 600 um), and dorsal-ventral axis (~750 um) but did not robustly cover the mediolateral extent. There is a possibility that my recordings missed the clusters of neurons (e.g., 1.3mm mediolateral and 4mm dorsoventral) or individual neurons projecting to motor structures (e.g., thalamic or brain stem structures) that exhibit opposing activity changes (e.g., decrease in firing rates at movement onset). The possibility of missing Clusters of neurons decreasing their firing activity could fit both with Mink's model and Golberg's "coactivation" model suggesting different functional channels.

A possible mechanism that could shape SNr activity are neocortical regions that directly drive the thalamus and also indirectly inhibit it by activating a cascade of BG neurons that ultimately influence BG outputs. Cortical neurons that constitute the

hyperdirect pathway can drive BG output neurons via the subthalamic nucleus (STN) (Nambu 2004). It has also been shown that the cortical inputs to the hyperdirect pathway can also project directly to the BG-recipient thalamus (Kita and Kita 2012; Féger, Bevan, and Crossman 1994). Therefore, cortical stimulation simultaneously activates both the thalamic neurons and, through the hyperdirect pathway, their BG inputs (Wan et al. 1992). This indicates that modulation of BG output neurons and corticothalamic neurons could happen simultaneously and be a physiological consequence of the circuit connectivity. To elucidate how information propagates from the cortex through the BG output to the thalamus during behaviour would require combining multisite recordings approaches with optogenetic identification of thalamus-projecting neurons in the BG output nuclei and the cortex.

One aim of my thesis was to test whether SNr neurons encode motor preparation like the other cortico-basal ganglia thalamocortical loop structures, e.g., VM and ALM (Guo et al. 2017; Guo, Li, et al. 2014; Li et al. 2015). A recent paper by Wang et al. (2021) demonstrated that SNr encodes movement preparation, by showing that optical perturbation of SNr affected short-term memory and action selection, but not movement. In my experiment, SNr neurons displayed increased firing activity related to movement in Premature Hit trials that rapidly decreased to baseline. This suggests that SNr neurons do not robustly encode motor preparation by dynamically changing their firing rates, as opposed to the conclusions of Wang et al. Also, a subset of neurons increased their firing rates at the Delay Cue onset and Action Cue onset in Miss trials.

Optogenetic stimulation effectively drove many of the recorded cells in the Action Window and the Delay Window. The activation lasted for the entire duration of the laser illumination during the Action Cue (0.3 s) and for ~0.5 s of the laser illumination during the Delay Window (0.3–1.3 s). Unsurprisingly, the data show that the patterns of SNr activity evoked by light delivery were 'supraphysiological' and distinct from the activity present during the unperturbed encoding of behaviour. Nevertheless, these results support the effectiveness of the optogenetic modulation of SNr neurons and the related impact on licking behaviour presented in Chapter 4 and this chapter. In the General Discussion (Chapter 6), I synthesise behavioural results with insights from my electrophysiological/optogenetic experiments.

6. General discussion

6.1 Introduction

In rodents, the substantia nigra pars reticulata is the biggest output nucleus of the basal ganglia in terms of volume and cell count, and innervates the superior colliculus , motor and intralaminar thalamic nuclei, the pedunculopontine nucleus , and other targets in midbrain and brainstem (Mena-Segovia, Bolam, and Magill 2004; Alexander and Crutcher 1990a; Hikosaka 2007; McElvain et al. 2021). The SNr is widely considered to be important for the correct expression of purposeful movement.

SNr neuronal activity relationship to movement initiation was initially observed by Hikosaka and Wurtz (Hikosaka and Wurtz 1983c; Hikosaka and Wurtz 1983d; Hikosaka and Wurtz 1983b; Hikosaka and Wurtz 1983a). On the basis of recorded activity relationships and other data, the "disinhibition model" of the basal ganglia output function has been proposed. It posits that decreases or pauses in BG-output activity "gate" the task-related activation of its downstream motor targets via disinhibition and that this mechanism promotes movement.

A theoretical proposal by Mink (Mink 1996) further extended the disinhibition model, asserting that the output nuclei of the basal ganglia do not use disinhibition uniformly but in a distinct manner. According to Mink, when a voluntary movement is initiated, motor regions in the cerebral cortex send a corollary signal to the subthalamic nucleus (through the projections of the so-called "hyperdirect pathway" by Nambu et al. (2002), causing extensive activation of GPi and SNr and subsequent suppression of competing motor patterns. Simultaneously, signals from the cerebral cortex motor and other areas are sent to the striatum, which filters and alters them in a context-dependent manner and then focally inhibits GPi and SNr to remove tonic inhibition from motor pattern generators implicated in the desired movement. As a result, the output of the basal ganglia focally selects and activates preferred motor mechanisms while broadly inhibits competing motor programs, allowing movement to occur without interference. Many studies over the years have supported Mink's hypothesis (Jin and Costa 2010; da Silva et al. 2018; Jin, Tecuapetla, and Costa 2014).

Despite recent advancements (Freeze et al. 2013; Tecuapetla et al. 2014; Catanese and Jaeger 2021; Catanese and Jaeger 2020; Morrissette et al. 2019), relatively little information is available on SNr function in rodents during behaviour and is it unclear whether the disinhibition model holds true for rodent SNr neurons. Most evidence of SNr neurons decreasing their firing rate at movement onset has been collected in monkeys performing fixation tasks (Hikosaka and Wurtz 1983a) and supported by experiments in anesthetized rats (Chevalier and Deniau 1990) or songbirds (Goldberg and Fee 2012) or non-human primates (Schwab et al. 2020). It ultimately remains unclear how SNr contributes to the selection and initiation of movement in behaving mice.

Movement planning (also known as movement preparation) is considered in those regions of the brain where the initial correlations between neural activity and future actions arise. Movement planning has been widely studied using delayed response tasks, in which a sensory stimulus instructs a future action. During the delay, neurons in the frontal and parietal cortex and connected structures show persistent and ramping activity related to specific movements long before movement onset (Svoboda and Li 2018; Guo, Li et al. 2014). This neural activity is referred to as "preparatory activity" and is a crucial feature of movement planning and thus for future movement. Considering SNr relevant role in the cortico-basal ganglia thalamocortical loop, its collateral projections to the motor thalamus (McElvain et al. 2021), and the role of efference copies in movement planning (Fee 2012), it seems plausible to imagine its involvement in movement preparation.

This thesis aimed to answer the following questions:

1) Do SNr neurons encode movement preparation like the other structures of the cortico-basal ganglia thalamocortical loop, e.g., VM and ALM?

2) Does SNr activity have a causal impact on movement, and does this impact change with respect to movement preparation or movement initiation?

3) How do SNr neurons change their activity to movement? More specifically, I addressed whether SNr neurons show a uniform decrease in firing rates as Hikosaka's disinhibition model predicts or whether they show opposing activity changes, as predicted by Mink.

6.2 Summary of key findings

My thesis research started with the establishment of a novel behavioural task for mice. Inspired by studies of mouse behaviour and neuronal encoding in other delay response tasks (Guo et al. 2017; Guo, Li et al. 2014; Guo, Hires, et al. 2014), I designed and implemented a behavioural delayed-Go task that engaged mice in both movement preparation and movement execution. In each trial, mice were exposed first to an auditory Delay Cue, and after a variable delay period, they had to respond to a visual Action Cue by licking a spout to collect a water reward. Mice learned to perform the delayed–Go task to satisfactory levels of success in about two weeks of non-consecutive daily sessions. Furthermore, mice learned to associate both cues with an

appropriate response (i.e., withhold from licking after the Delay Cue and lick soon after the Action Cue). Overall, my behavioural data results aligned with the time and learning dynamics observed in mice learning similar tasks (Guo et al. 2017; Guo, Li et al. 2014; Li et al. 2015; Guo, Hires, et al. 2014; Catanese and Jaeger 2021; Guo, Hires, et al. 2014). Establishing a robust delayed–Go paradigm was crucial to maximise the likely engagement of SNr neurons during movement preparation and execution, thence allowing the functional roles of these neurons to be investigated through optogenetic manipulation and electrophysiological recordings.

To test whether SNr activity had a causal impact on movement initiation or preparation, I optogenetically drove GABAergic SNr neurons in different moments of the delayed–Go task, when the mouse was preparing to move (Delay Window) or executing movement (Action Window). Driving SNr neurons during the Action Cues that lead to movement (i.e., in Hit trials) caused an overall delay in the reaction time to move (first licks). My data also show that first licks were accelerated in Premature Hit and Hit trials when SNr neurons were optogenetically driven during movement preparation (Delay Cue and Delay Window). Overall, optogenetic manipulations showed SNr has a causal impact on movement preparation and execution.

To investigate whether and how SNr neurons encode movement preparation and execution, I performed in *vivo* electrophysiological recordings of single units in SNr as mice performed the delayed-Go task. In Hit trials, many of the recorded neurons displayed firing-rate modulations around the time movement onset (Action Cue). Critically, these modulations mainly consisted of increased firing rates at movement

onset and sustained activity for 1–2 s from the Action Cue onset. Overall, my data suggest that most neurons in the SNr encode movement onset by increasing their firing rates. Furthermore, despite occasional weak modulations of firing rates during the Delay Window, SNr neurons did not show the stereotypical "ramping up" activity that is typical of neurons encoding motor preparation (Wang et al., 2021; Guo et al. 2017).

6.3 Implications and further directions

In Hit trials, a large proportion of neurons increased their firing rate before or at the time of first licks and around Action Cue onset. Increases in activity before or at the time of first licks suggest that recorded neurons were ‘temporally positioned’ to play a role in sculpting the initiation of movement and/or the performance of ongoing movement. Furthermore, increased activity often lasted beyond first licks (1—2 s after the Action Cue offset), suggesting an encoding of subsequent licks and not just an encoding of Action Cue. A subset of neurons decreased firing rate in Hit trials. Subsets of neurons increased their activity around Delay Cue in different trial types, and subsets of neurons increased their activity around Action Cue in Miss trials. The magnitude of Delay Cue encoding was weak (< 1 z-score). A large number of neurons increased their activity in Premature Hit trials) before or at the time of first licks suggesting they encoded movement onset/performance that was not cued. Together, the data from Hit, Miss and Premature Hit trials suggest that SNr neurons can encode auditory and visual cues, but - critically - also that they encode movement that is not contemporaneous

with cues. SNr neurons did not show the stereotypical "ramping up" activity that is typical of neurons encoding motor preparation (Wang et al. 2021; Guo et al. 2017). One possibility is that ramping up activity is solely driven by a thalamic-cortico-cerebellar circuit that does not involve SNr (Gao et al. 2018). SNr GABAergic output might counteract cortical excitation of the thalamus and therefore not be part of the circuit. Another possibility is that I could not replicate the findings of Wang et al. (2021) because they used a different behavioural tasks (i.e., delayed-lick-left/lick-right object location discrimination task).Cue encoding by subsets of SNr neurons was not surprising since it is well-known that, at least in non-human primates, SNr encodes reward and visual cues (Hikosaka and Wurtz 1983b; Joseph and Boussaoud 1985; Handel and Glimcher 2000; Sato and Hikosaka 2002). Overall, and contrary to the predictions of the classical disinhibition model (Hikosaka 2007), my data indicate that the vast majority of task-responsive neurons in the SNr encoded movement onset and performance by increasing their firing rates.

Increases in SNr activity around movement onset could be explained by Mink's model of the basal ganglia; such increases would in theory serve to broadly suppress competing motor programs (Mink 1996). However, according to Mink's model, a substantial proportion of neurons in the BG output nuclei should still decrease their firing rates to allow the selection of motor programs. In my recordings, only a small subset of neurons decreased the firing rate at movement onset, thus is hard to reconcile my observation with Mink's model. It is possible that my recordings missed the clusters of neurons or individual neurons projecting to motor structures (e.g., thalamic

or brain stem structures) that exhibit opposing activity changes (e.g., decrease in firing rates at movement onset) from the targets neurons shown in my data set. Another possibility is that the proportions of neurons increasing, decreasing, or not changing their firing rates might dramatically change in different motor behaviours (e.g., limb movements). It remains to be determined whether my results, obtained in a specific behavioural context, will extend and generalise to other motor behaviours.

My data show that optogenetically driving SNr during movement preparation (Delay Cue and Delay Window) accelerated and synchronized premature licking, whereas driving SNr around movement onset (Action Cue) delayed the timing of first licks. During stimulation in the Delay Cue, the sharp alignment and the brief lag of first (premature) licks following the laser offset could suggest that laser modulation induces rebound-like increases in downstream structures i.e., thalamus. This result is in line with what was previously observed by Kim et al. (2017); however, the same mechanism does not explain the opposite effect observed when the laser was activated at the Action Cue. A possible mechanism for delayed first licks when the light was delivered during the Action Cue is that optically driving the SNr neurons inhibited their target structures (e.g., motor thalamus), temporarily preventing neurons in these effector circuits from reaching activity levels that support the initiation of movement. As such., this result is consistent with the disinhibition model proposed by Hikosaka and in line with more recent findings in rodents (Freeze et al., 2013; Basso and Sommer, 2011). However, it is hard to bring into coherence this result with my observation that most SNr neurons increased their firing rates at Action Cue onset,

which is assumed to already inhibit their downstream structures. One difference between the two stimulation conditions is that they are provided in two different contexts (whether provided during Delay Cue or Action Cue). Different behavioural effects of shining light during Delay Cue or Action Cue (accelerating or delaying licks, respectively) could be explained by the fact that optogentic modulation is altering different context-dependent ratios of SNr neurons.

It should be remembered that delivery of light to SNr was highly effective at driving the activity of many SNr neurons; it caused large firing-rate increases, which were tightly synchronized in time. The magnitude/timing of these light-evoked effects in activity were above and beyond the firing-rate changes and synchronization observed for SNr neurons when engaged in normative encoding of movement. Moreover, light delivery was not accompanied by neurons decreasing their firing rates, and light delivery likely changed the proportions of neurons that were responsive or non-responsive as compared to normative encoding. In short, optogenetic stimulation 'hijacked' or otherwise overwhelmed normative patterns of activity, which might explain the resulting impairment of movement. It follows that, to enable correctly-timed movement execution, there must optimal ratios of SNr neurons that increase, decrease or do not change their firing rates. In line with this notion, work in non-human primates suggests that the ratio of active/inhibited (A/I) neurons in GPi is crucial for the correct functioning of BG circuits and movement; in experimental Parkinsonism, impaired movement is accompanied by a shift of GPi neuron activity in favour of activated neurons (Boraud et al. 2000).

Further experiments that want to investigate the functional role of SNr on movement, and further test the disinhibition models of the basal ganglia, need to address several unresolved issues, such as the role of diverse activity patterns of SNr neurons and how this maps onto anatomical differences among SNr neurons, for example, their locations within SNr and their axonal projections to other brain areas (McElvain et al. 2021; Lee, Wang, and Sabatini 2020). The further development of behavioural tasks that functionally engage SNr will be important. New experiments could build on the delayed-Go task. Delayed-Go tasks with directional licking can engage the SNr in both movement preparation, execution and control for eventual ipsilateral or contra lateral activity in SNr (Li et al. 2015; Wang et al. 2021; Guo, Hires, et al. 2014). Head-fixed behaviours involving limbs movement (Harvey, Coen, and Tank 2012; Isomura et al. 2009) could test whether SNr activity would display a different ratio of neurons increasing or decreasing their firing rate during motor preparation or execution, thereby addressing whether my findings related to licking movements generalise to other types of movement. A combination of optogenetic and viral strategies for selectively accessing SNr cell types on the basis of their gene expression and and projection target(s) can be used to test the functions of anatomically segregated neurons in SNr. Opsins can be expressed in a specific SNr subset of neurons by injecting anterograde and/or retrograde viral vectors in projecting structures of SNr (e.g., superior colliculus and motor thalamus) (De La Crompe, Coulon, and Diester 2020). Different types of opsins can be used; specifically, archaerhodopsin-3 from *Halorubrum sodomense* (Arch) could be expressed in SNr neurons and used to

suppress/silence them in response to green light pulses (Han et al., 2011). These experiments could further investigate the impact of SNr increased activity on licking behaviour and potentially reverse the behavioural effects observed in my optical manipulation achieved using ChR2. Another thing to consider is whether SNr neurons are encoding rewards during Hit trials. In non-human primates it has been shown that SNr can encode reward and reward-cues (Hikosaka, Takikawa, and Kawagoe 2000). The delayed-Go task I have used for my experiments cannot rule out that possibility, but several adjustments can be made to resolve this issue e.g., (1) omission of water drops with some correct Hit trials, (2) require the mouse to perform multiple licks (over several hundred milliseconds) in order to gain a reward. In both of these cases, movement would be temporally separated out from reward consumption.

6.4 Concluding remarks

In conclusion, my data do not support the classical disinhibition model and, by extension, that appropriately timed decreases in the activity of many SNr neurons is a fundamental mechanism that allows movement execution to occur (Hikosaka 2007). However, my data do support the assertion that SNr neuron output has a causal impact on movement and that this impact might be context dependent according to whether an animal is preparing to move or is executing movement. Finally, my data do not provide evidence of SNr neurons encoding motor preparation with changes in their firing rates.

7. References

Abraham, Nixon M., Delphine Guerin, Khaleel Bhaukaurally, and Alan Carleton
2012 Similar Odor Discrimination Behavior in Head-Restrained and Freely Moving Mice. PloS One 7(12): e51789.

Albin, R. L., A. B. Young, and J. B. Penney
1989 The Functional Anatomy of Basal Ganglia Disorders. Trends in Neurosciences 12(10): 366–375.

Alexander, G. E., and M. D. Crutcher
1990a Functional Architecture of Basal Ganglia Circuits: Neural Substrates of Parallel Processing. Trends in Neurosciences 13(7): 266–271.
1990b Preparation for Movement: Neural Representations of Intended Direction in Three Motor Areas of the Monkey. Journal of Neurophysiology 64(1): 133–150.

Andermann, Mark L., A. M. Kerlin, and R. C. Reid
2010 Chronic Cellular Imaging of Mouse Visual Cortex during Operant Behavior and Passive Viewing. Frontiers in Cellular Neuroscience 4: 3.

Anderson, M. E., and F. B. Horak
1985 Influence of the Globus Pallidus on Arm Movements in Monkeys. III. Timing of Movement-Related Information. Journal of Neurophysiology 54(2): 433–448.

Anderson, M. E., and R. S. Turner
1991 A Quantitative Analysis of Pallidal Discharge during Targeted Reaching Movement in the Monkey. Experimental Brain Research 86(3): 623–632.

Anderson, M., and M. Yoshida
1977 Electrophysiological Evidence for Branching Nigral Projections to the Thalamus and the Superior Colliculus. Brain Research 137(2): 361–364.

Atherton, Jeremy F., and Mark D. Bevan
2005 Ionic Mechanisms Underlying Autonomous Action Potential Generation in the Somata and Dendrites of GABAergic Substantia Nigra Pars Reticulata Neurons in Vitro. The Journal of Neuroscience: The Official Journal of the Society for Neuroscience 25(36): 8272–8281.

Basso, Michele A., and Marc A. Sommer

2011 EXPLORING THE ROLE OF THE SUBSTANTIA NIGRA PARS RETICULATA IN EYE MOVEMENTS. Neuroscience 198: 205–212.

Beckstead, R. M., and A. Frankfurter
1982 The Distribution and Some Morphological Features of Substantia Nigra Neurons That Project to the Thalamus, Superior Colliculus and Pedunculopontine Nucleus in the Monkey. Neuroscience 7(10): 2377–2388.

Bentivoglio, M., and H. G. Kuypers
1982 Divergent Axon Collaterals from Rat Cerebellar Nuclei to Diencephalon, Mesencephalon, Medulla Oblongata and Cervical Cord. A Fluorescent Double Retrograde Labeling Study. Experimental Brain Research 46(3): 339–356.

Berns, G.S., and T.J. Sejnowski
1998 A Computational Model of How the Basal Ganglia Produce Sequences. Journal of Cognitive Neuroscience 10(1). Scopus: 108–121.

Boraud, T., E. Bezard, B. Bioulac, and C. E. Gross
2000 Ratio of Inhibited-to-Activated Pallidal Neurons Decreases Dramatically During Passive Limb Movement in the MPTP-Treated Monkey. Journal of Neurophysiology 83(3): 1760–1763.

Bosch-Bouju, Clémentine, Brian I. Hyland, and Louise C. Parr-Brownlie
2013 Motor Thalamus Integration of Cortical, Cerebellar and Basal Ganglia Information: Implications for Normal and Parkinsonian Conditions. Frontiers in Computational Neuroscience 7: 163.

Bosch-Bouju, Clémentine, Roseanna A. Smither, Brian I. Hyland, and Louise C. Parr-Brownlie
2014 Reduced Reach-Related Modulation of Motor Thalamus Neural Activity in a Rat Model of Parkinson's Disease. The Journal of Neuroscience: The Official Journal of the Society for Neuroscience 34(48): 15836–15850.

Bowen, Zac, Daniel E. Winkowski, and Patrick O. Kanold
2020 Functional Organization of Mouse Primary Auditory Cortex in Adult C57BL/6 and F1 (CBAxC57) Mice. Scientific Reports 10(1): 10905.

Brownstone, Robert M., and Jeremy W. Chopek
2018 Reticulospinal Systems for Tuning Motor Commands. Frontiers in Neural Circuits 12: 30.

Bruce, C. J., and M. E. Goldberg

1985 Primate Frontal Eye Fields. I. Single Neurons Discharging before Saccades. Journal of Neurophysiology 53(3): 603–635.

Buhusi, Catalin V., and Warren H. Meck
2005 What Makes Us Tick? Functional and Neural Mechanisms of Interval Timing. Nature Reviews. Neuroscience 6(10): 755–765.

Calabresi, Paolo, Barbara Picconi, Alessandro Tozzi, Veronica Ghiglieri, and Massimiliano Di Filippo
2014 Direct and Indirect Pathways of Basal Ganglia: A Critical Reappraisal. Nature Neuroscience 17(8): 1022–1030.

Cardozo Pinto, Daniel F., and Stephan Lammel
2019 Hot Topic in Optogenetics: New Implications of in Vivo Tissue Heating. Nature Neuroscience 22(7). Nature Publishing Group: 1039–1041.

Catanese, Julien, and Dieter Jaeger
2020 The Nigro-Thalamic Projection Contributes to the Control of Action Initiation Timing. Preprint. Neuroscience. http://biorxiv.org/lookup/doi/10.1101/2020.01.12.903500, accessed June 25, 2020.
2021 Premotor Ramping of Thalamic Neuronal Activity Is Modulated by Nigral Inputs and Contributes to Control the Timing of Action Release. The Journal of Neuroscience: The Official Journal of the Society for Neuroscience 41(9): 1878–1891.

Cebrián, Carolina, André Parent, and Lucía Prensa
2005 Patterns of Axonal Branching of Neurons of the Substantia Nigra Pars Reticulata and Pars Lateralis in the Rat. Journal of Comparative Neurology 492(3): 349–369.

Chelaru, Mircea I., and Mandar S. Jog
2005 Spike Source Localization with Tetrodes. Journal of Neuroscience Methods 142(2): 305–315.

Chen, Tsai-Wen, Nuo Li, Kayvon Daie, and Karel Svoboda
2017 A Map of Anticipatory Activity in Mouse Motor Cortex. Neuron 94(4): 866-879.e4.

Chevalier, G., and J. M. Deniau
1990 Disinhibition as a Basic Process in the Expression of Striatal Functions. Trends in Neurosciences 13(7): 277–280.

Cisek, Paul, and John F. Kalaska

2005 Neural Correlates of Reaching Decisions in Dorsal Premotor Cortex: Specification of Multiple Direction Choices and Final Selection of Action. Neuron 45(5): 801–814.

Crutcher, M. D., and G. E. Alexander
1990 Movement-Related Neuronal Activity Selectively Coding Either Direction or Muscle Pattern in Three Motor Areas of the Monkey. Journal of Neurophysiology 64(1): 151–163.

Cui, Guohong, Sang Beom Jun, Xin Jin, et al.
2013 Concurrent Activation of Striatal Direct and Indirect Pathways during Action Initiation. Nature 494(7436): 238–242.

Danskin, Bethanny, Daniel Denman, Matthew Valley, et al.
2015 Optogenetics in Mice Performing a Visual Discrimination Task: Measurement and Suppression of Retinal Activation and the Resulting Behavioral Artifact. PLOS ONE 10(12). Public Library of Science: e0144760.

De La Crompe, Brice, Philippe Coulon, and Ilka Diester
2020 Functional Interrogation of Neural Circuits with Virally Transmitted Optogenetic Tools. Journal of Neuroscience Methods 345: 108905.

Deisseroth, Karl
2011 Optogenetics. Nature Methods 8(1): 26–29.

DeLong, M. R.
1990 Primate Models of Movement Disorders of Basal Ganglia Origin. Trends in Neurosciences 13(7): 281–285.

Deniau, J. M., and G. Chevalier
1984 Synaptic Organization of the Basal Ganglia: An Electroanatomical Approach in the Rat. Ciba Foundation Symposium 107: 48–63.

Deniau, J. M., C. Hammond, A. Riszk, and J. Feger
1978 Electrophysiological Properties of Identified Output Neurons of the Rat Substantia Nigra (Pars Compacta and Pars Reticulata): Evidences for the Existence of Branched Neurons. Experimental Brain Research 32(3): 409–422.

Deniau, J. M., C. Hammond-Le Guyader, J. Feger, and J. S. McKenzie
1977 Bilateral Projection of Nigro-Collicular Neurons: An Electrophysiological Analysis in the Rat. Neuroscience Letters 5(1): 45–50.

Deniau, J. M., P. Mailly, N. Maurice, and S. Charpier

2007 The Pars Reticulata of the Substantia Nigra: A Window to Basal Ganglia Output. Progress in Brain Research 160: 151–172.

Deniau, J. M., A. Menetrey, and S. Charpier
1996 The Lamellar Organization of the Rat Substantia Nigra Pars Reticulata: Segregated Patterns of Striatal Afferents and Relationship to the Topography of Corticostriatal Projections. Neuroscience 73(3): 761–781.

Deniau, J. M., and A. M. Thierry
1997 Anatomical Segregation of Information Processing in the Rat Substantia Nigra Pars Reticulata. Advances in Neurology 74: 83–96.

Desban, M., C. Gauchy, J. Glowinski, and M. L. Kemel
1995 Heterogeneous Topographical Distribution of the Striatonigral and Striatopallidal Neurons in the Matrix Compartment of the Cat Caudate Nucleus. The Journal of Comparative Neurology 352(1): 117–133.

Deubner, Jan, Philippe Coulon, and Ilka Diester
2019 Optogenetic Approaches to Study the Mammalian Brain. Current Opinion in Structural Biology 57. Membranes ● Engineering & Design: Synthetic Signalling: 157–163.

Donahue, Christopher H., and Anatol C. Kreitzer
2015 A Direct Path to Action Initiation. Neuron 88(2): 240–241.

Dymecki, Susan M., and Jun Chul Kim
2007 Molecular Neuroanatomy's "Three Gs": A Primer. Neuron 54(1): 17–34.

Evarts, E. V.
1968 Relation of Pyramidal Tract Activity to Force Exerted during Voluntary Movement. Journal of Neurophysiology 31(1): 14–27.

Faull, R. L., and W. R. Mehler
1978 The Cells of Origin of Nigrotectal, Nigrothalamic and Nigrostriatal Projections in the Rat. Neuroscience 3(11): 989–1002.

Fee, Michale
2012 Oculomotor Learning Revisited: A Model of Reinforcement Learning in the Basal Ganglia Incorporating an Efference Copy of Motor Actions. Frontiers in Neural Circuits 6: 38.

Fee, Michale S., and Jesse H. Goldberg

2011 A Hypothesis for Basal Ganglia-Dependent Reinforcement Learning in the Songbird. Neuroscience 198: 152–170.

Féger, J., M. Bevan, and A. R. Crossman
1994 The Projections from the Parafascicular Thalamic Nucleus to the Subthalamic Nucleus and the Striatum Arise from Separate Neuronal Populations: A Comparison with the Corticostriatal and Corticosubthalamic Efferents in a Retrograde Fluorescent Double-Labelling Study. Neuroscience 60(1): 125–132.

Frank, Michael J.
2005 Dynamic Dopamine Modulation in the Basal Ganglia: A Neurocomputational Account of Cognitive Deficits in Medicated and Nonmedicated Parkinsonism. Journal of Cognitive Neuroscience 17(1): 51–72.

Freeze, Benjamin S., Alexxai V. Kravitz, Nora Hammack, Joshua D. Berke, and Anatol C. Kreitzer
2013 Control of Basal Ganglia Output by Direct and Indirect Pathway Projection Neurons. The Journal of Neuroscience 33(47): 18531–18539.

Fukushima, K.
1987 The Interstitial Nucleus of Cajal and Its Role in the Control of Movements of Head and Eyes. Progress in Neurobiology 29(2): 107–192.

Gao, Zhenyu, Courtney Davis, Alyse M. Thomas, et al.
2018 A Cortico-Cerebellar Loop for Motor Planning. Nature 563(7729): 113–116.

Georgopoulos, A. P., M. R. DeLong, and M. D. Crutcher
1983 Relations between Parameters of Step-Tracking Movements and Single Cell Discharge in the Globus Pallidus and Subthalamic Nucleus of the Behaving Monkey. The Journal of Neuroscience: The Official Journal of the Society for Neuroscience 3(8): 1586–1598.

Gerfen, C. R., T. M. Engber, L. C. Mahan, et al.
1990 D1 and D2 Dopamine Receptor-Regulated Gene Expression of Striatonigral and Striatopallidal Neurons. Science (New York, N.Y.) 250(4986): 1429–1432.

Gerfen, Charles R.
1992 The Neostriatal Mosaic: Multiple Levels of Compartmental Organization. Trends in Neurosciences 15(4): 133–139.

Gerfen, Charles R., and D. James Surmeier
2011 Modulation of Striatal Projection Systems by Dopamine. Annual Review of Neuroscience 34: 441–466.

Goldberg, Jesse H., Michael A. Farries, and Michale S. Fee
2013 Basal Ganglia Output to the Thalamus: Still a Paradox. Trends in Neurosciences 36(12): 10.1016/j.tins.2013.09.001.

Goldberg, Jesse H., and Michale S. Fee
2012 A Cortical Motor Nucleus Drives the Basal Ganglia-Recipient Thalamus in Singing Birds. Nature Neuroscience 15(4): 620–627.

González-Hernández, T., and M. Rodríguez
2000 Compartmental Organization and Chemical Profile of Dopaminergic and GABAergic Neurons in the Substantia Nigra of the Rat. The Journal of Comparative Neurology 421(1): 107–135.

Graybiel, A. M., and C. W. Ragsdale
1979 Fiber Connections of the Basal Ganglia. Progress in Brain Research 51: 237–283.

Graybiel, Ann M.
2008 Habits, Rituals, and the Evaluative Brain. Annual Review of Neuroscience 31: 359–387.

Grillner, Sten, and William Scott Thompson
2021 Basal Ganglia Reign through Downstream Control of Motor Centers in Midbrain and Brain Stem While Updating Cortex with Efference Copy Information. Neuron 109(10): 1587–1589.

Gulley, Joshua M, Masaaki Kuwajima, Emily Mayhill, and George V Rebec
1999 Behavior-Related Changes in the Activity of Substantia Nigra Pars Reticulata Neurons in Freely Moving Rats. Brain Research 845(1): 68–76.

Guo, Zengcai V., S. Andrew Hires, Nuo Li, et al.
2014 Procedures for Behavioral Experiments in Head-Fixed Mice. Sidney Arthur Simon, ed. PLoS ONE 9(2): e88678.

Guo, Zengcai V., Hidehiko K. Inagaki, Kayvon Daie, et al.
2017 Maintenance of Persistent Activity in a Frontal Thalamocortical Loop. Nature 545(7653): 181–186.

Guo, Zengcai V., Nuo Li, Daniel Huber, et al.
2014 Flow of Cortical Activity Underlying a Tactile Decision in Mice. Neuron 81(1): 179–194.

Guru, Akash, Ryan J Post, Yi-Yun Ho, and Melissa R Warden
2015 Making Sense of Optogenetics. International Journal of Neuropsychopharmacology 18(11): pyv079.

Guyenet, P. G., and G. K. Aghajanian
1978 Antidromic Identification of Dopaminergic and Other Output Neurons of the Rat Substantia Nigra. Brain Research 150(1): 69–84.

Han, Xue, Brian Y. Chow, Huihui Zhou, et al.
2011 A High-Light Sensitivity Optical Neural Silencer: Development and Application to Optogenetic Control of Non-Human Primate Cortex. Frontiers in Systems Neuroscience 5: 18.

Handel, A., and P. W. Glimcher
2000 Contextual Modulation of Substantia Nigra Pars Reticulata Neurons. Journal of Neurophysiology 83(5): 3042–3048.

Harvey, Christopher D., Philip Coen, and David W. Tank
2012 Choice-Specific Sequences in Parietal Cortex during a Virtual-Navigation Decision Task. Nature 484(7392): 62–68.

Herman, Alexander M, Longwen Huang, Dona K Murphey, Isabella Garcia, and Benjamin R Arenkiel
2014 Cell Type-Specific and Time-Dependent Light Exposure Contribute to Silencing in Neurons Expressing Channelrhodopsin-2. ELife 3: e01481.

Hikosaka, O.
2007 GABAergic Output of the Basal Ganglia. *In* Progress in Brain Research. James M. Tepper, Elizabeth D. Abercrombie, and J. Paul Bolam, eds. Pp. 209–226. Gaba and the Basal Ganglia. Elsevier. https://www.sciencedirect.com/science/article/pii/S0079612306600125, accessed September 22, 2021.

Hikosaka, O., Y. Takikawa, and R. Kawagoe
2000 Role of the Basal Ganglia in the Control of Purposive Saccadic Eye Movements. Physiological Reviews 80(3): 953–978.

Hikosaka, O., and R. H. Wurtz
1983a Visual and Oculomotor Functions of Monkey Substantia Nigra Pars Reticulata. IV. Relation of Substantia Nigra to Superior Colliculus. Journal of Neurophysiology 49(5): 1285–1301.

1983b Visual and Oculomotor Functions of Monkey Substantia Nigra Pars Reticulata. I. Relation of Visual and Auditory Responses to Saccades. Journal of Neurophysiology 49(5): 1230–1253.
1985 Modification of Saccadic Eye Movements by GABA-Related Substances. II. Effects of Muscimol in Monkey Substantia Nigra Pars Reticulata. Journal of Neurophysiology 53(1): 292–308.

Horak, F. B., and M. E. Anderson
1984 Influence of Globus Pallidus on Arm Movements in Monkeys. I. Effects of Kainic Acid-Induced Lesions. Journal of Neurophysiology 52(2): 290–304.

Huber, D., D. A. Gutnisky, S. Peron, et al.
2012 Multiple Dynamic Representations in the Motor Cortex during Sensorimotor Learning. Nature 484(7395): 473–478.

Huberman, Andrew D., and Cristopher M. Niell
2011 What Can Mice Tell Us about How Vision Works? Trends in Neurosciences 34(9): 464–473.

Inase, M., J. A. Buford, and M. E. Anderson
1996 Changes in the Control of Arm Position, Movement, and Thalamic Discharge during Local Inactivation in the Globus Pallidus of the Monkey. Journal of Neurophysiology 75(3): 1087–1104.

Isomura, Yoshikazu, Rie Harukuni, Takashi Takekawa, Hidenori Aizawa, and Tomoki Fukai
2009 Microcircuitry Coordination of Cortical Motor Information in Self-Initiation of Voluntary Movements. Nature Neuroscience 12(12): 1586–1593.

Isomura, Yoshikazu, Takashi Takekawa, Rie Harukuni, et al.
2013 Reward-Modulated Motor Information in Identified Striatum Neurons. Journal of Neuroscience 33(25): 10209–10220.

Jin, Xin, and Rui M. Costa
2010 Start/Stop Signals Emerge in Nigrostriatal Circuits during Sequence Learning. Nature 466(7305): 457–462.

Jin, Xin, Fatuel Tecuapetla, and Rui M. Costa
2014 Basal Ganglia Subcircuits Distinctively Encode the Parsing and Concatenation of Action Sequences. Nature Neuroscience 17(3): 423–430.

Joseph, J. P., and D. Boussaoud

1985 Role of the Cat Substantia Nigra Pars Reticulata in Eye and Head Movements. I. Neural Activity. Experimental Brain Research 57(2): 286–296.

Juraska, J. M., C. J. Wilson, and P. M. Groves
1977 The Substantia Nigra of the Rat: A Golgi Study. The Journal of Comparative Neurology 172(4): 585–600.

Karabelas, A. B., and A. K. Moschovakis
1985 Nigral Inhibitory Termination on Efferent Neurons of the Superior Colliculus: An Intracellular Horseradish Peroxidase Study in the Cat. The Journal of Comparative Neurology 239(3): 309–329.

Kaufman, Arnold, and Alan Baron
1968 Suppression of Behavior by Timeout Punishment When Suppression Results in Loss of Positive Reinforcement. Journal of the Experimental Analysis of Behavior 11(5): 595–607.

Kaufman, Matthew T., Jeffrey S. Seely, David Sussillo, et al.
2016 The Largest Response Component in the Motor Cortex Reflects Movement Timing but Not Movement Type. ENeuro 3(4): ENEURO.0085-16.2016.

Kim, Jeongjin, Youngsoo Kim, Ryuichi Nakajima, et al.
2017 Inhibitory Basal Ganglia Inputs Induce Excitatory Motor Signals in the Thalamus. Neuron 95(5): 1181-1196.e8.

Kita, T., and H. Kita
2012 The Subthalamic Nucleus Is One of Multiple Innervation Sites for Long-Range Corticofugal Axons: A Single-Axon Tracing Study in the Rat. Journal of Neuroscience 32(17). Scopus: 5990–5999.

Kolta, Arlette, Philippe Morquette, Raphaël Lavoie, Isabel Arsenault, and Dorly Verdier
2010 Modulation of Rhythmogenic Properties of Trigeminal Neurons Contributing to the Masticatory CPG. Progress in Brain Research 187: 137–148.

Komiyama, Takaki, Takashi R. Sato, Daniel H. O'Connor, et al.
2010 Learning-Related Fine-Scale Specificity Imaged in Motor Cortex Circuits of Behaving Mice. Nature 464(7292): 1182–1186.

Kunimatsu, J., and M. Tanaka
2010 Roles of the Primate Motor Thalamus in the Generation of Antisaccades. Journal of Neuroscience 30(14). Scopus: 5108–5117.

Lanciego, José L., Natasha Luquin, and José A. Obeso
2012 Functional Neuroanatomy of the Basal Ganglia. Cold Spring Harbor Perspectives in Medicine 2(12): a009621.

Laramée, Marie-Eve, and Denis Boire
2015 Visual Cortical Areas of the Mouse: Comparison of Parcellation and Network Structure with Primates. Frontiers in Neural Circuits 8: 149.

Lee, Jaeeon, Wengang Wang, and Bernardo L. Sabatini
2020 Anatomically Segregated Basal Ganglia Pathways Allow Parallel Behavioral Modulation. Nature Neuroscience 23(11): 1388–1398.

Li, Nuo, Tsai-Wen Chen, Zengcai V. Guo, Charles R. Gerfen, and Karel Svoboda
2015 A Motor Cortex Circuit for Motor Planning and Movement. Nature 519(7541): 51–56.

Li, Nuo, Kayvon Daie, Karel Svoboda, and Shaul Druckmann
2016 Robust Neuronal Dynamics in Premotor Cortex during Motor Planning. Nature 532(7600): 459–464.

Light, Kenneth R., Brian Cotten, Talia Malekan, et al.
2019 Evidence for a Mixed Timing and Counting Strategy in Mice Performing a Mechner Counting Task. Frontiers in Behavioral Neuroscience 13. https://www.frontiersin.org/article/10.3389/fnbeh.2019.00109, accessed February 12, 2022.

Lobb, C. J., and D. Jaeger
2015 Bursting Activity of Substantia Nigra Pars Reticulata Neurons in Mouse Parkinsonism in Awake and Anesthetized States. Neurobiology of Disease 75: 177–185.

Luo, Liqun, Edward M. Callaway, and Karel Svoboda
2008 Genetic Dissection of Neural Circuits. Neuron 57(5): 634–660.

Magill, Peter J., Alek Pogosyan, Andrew Sharott, et al.
2006 Changes in Functional Connectivity within the Rat Striatopallidal Axis during Global Brain Activation in Vivo. The Journal of Neuroscience: The Official Journal of the Society for Neuroscience 26(23): 6318–6329.

Maimon, Gaby, and John A. Assad
2006 A Cognitive Signal for the Proactive Timing of Action in Macaque LIP. Nature Neuroscience 9(7): 948–955.

Mar, Adam C., Alexa E. Horner, Simon R. O. Nilsson, et al.
2013 The Touchscreen Operant Platform for Assessing Executive Function in Rats and Mice. Nature Protocols 8(10): 1985–2005.

May, Paul J., Isabelle Billig, Paul D. Gamlin, and Julie Quinet
2019 Central Mesencephalic Reticular Formation Control of the near Response: Lens Accommodation Circuits. Journal of Neurophysiology 121(5): 1692–1703.

McElvain, Lauren E., Yuncong Chen, Jeffrey D. Moore, et al.
2021 Specific Populations of Basal Ganglia Output Neurons Target Distinct Brain Stem Areas While Collateralizing throughout the Diencephalon. Neuron 109(10): 1721-1738.e4.

Mena-Segovia, Juan, J. Paul Bolam, and Peter J. Magill
2004 Pedunculopontine Nucleus and Basal Ganglia: Distant Relatives or Part of the Same Family? Trends in Neurosciences 27(10): 585–588.

Mink, J. W.
1996 The Basal Ganglia: Focused Selection and Inhibition of Competing Motor Programs. Progress in Neurobiology 50(4): 381–425.

Mink, J. W., and W. T. Thach
1991 Basal Ganglia Motor Control. III. Pallidal Ablation: Normal Reaction Time, Muscle Cocontraction, and Slow Movement. Journal of Neurophysiology 65(2): 330–351.

Morrissette, Arthur E., Po-Han Chen, Conrad Bhamani, et al.
2019 Unilateral Optogenetic Inhibition and Excitation of Basal Ganglia Output Affect Directional Lick Choices and Movement Initiation in Mice. Neuroscience 423: 55–65.

Nakamura, Kouichi C., Andrew Sharott, and Peter J. Magill
2014 Temporal Coupling with Cortex Distinguishes Spontaneous Neuronal Activities in Identified Basal Ganglia-Recipient and Cerebellar-Recipient Zones of the Motor Thalamus. Cerebral Cortex (New York, N.Y.: 1991) 24(1): 81–97.

Nakanishi, H., H. Kita, and S. T. Kitai
1987 Intracellular Study of Rat Substantia Nigra Pars Reticulata Neurons in an in Vitro Slice Preparation: Electrical Membrane Properties and Response Characteristics to Subthalamic Stimulation. Brain Research 437(1): 45–55.

Nambu, Atsushi

2004 A New Dynamic Model of the Cortico-Basal Ganglia Loop. Progress in Brain Research 143: 461–466.

Nambu, Atsushi, Hironobu Tokuno, and Masahiko Takada
2002 Functional Significance of the Cortico-Subthalamo-Pallidal "hyperdirect" Pathway. Neuroscience Research 43(2): 111–117.

Neville, Vikki, Jessica King, Iain D. Gilchrist, et al.
2020 Reward and Punisher Experience Alter Rodent Decision-Making in a Judgement Bias Task. Scientific Reports 10(1): 11839.

O'Connor, Daniel H., S. Andrew Hires, Zengcai V. Guo, et al.
2013 Neural Coding during Active Somatosensation Revealed Using Illusory Touch. Nature Neuroscience 16(7): 958–965.

O'Connor, Daniel H., Daniel Huber, and Karel Svoboda
2009 Reverse Engineering the Mouse Brain. Nature 461(7266): 923–929.

O'Connor, Daniel H., Simon P. Peron, Daniel Huber, and Karel Svoboda
2010 Neural Activity in Barrel Cortex Underlying Vibrissa-Based Object Localization in Mice. Neuron 67(6): 1048–1061.

Ohmae, Shogo, Jun Kunimatsu, and Masaki Tanaka
2017 Cerebellar Roles in Self-Timing for Sub- and Supra-Second Intervals. The Journal of Neuroscience: The Official Journal of the Society for Neuroscience 37(13): 3511–3522.

Palmiter, Richard D.
2008 Dopamine Signaling in the Dorsal Striatum Is Essential for Motivated Behaviors: Lessons from Dopamine-Deficient Mice. Annals of the New York Academy of Sciences 1129: 35–46.

Pammer, Lorenz, Daniel H. O'Connor, S. Andrew Hires, et al.
2013 The Mechanical Variables Underlying Object Localization along the Axis of the Whisker. The Journal of Neuroscience: The Official Journal of the Society for Neuroscience 33(16): 6726–6741.

Panigrahi, Babita, Kathleen A. Martin, Yi Li, et al.
2015 Dopamine Is Required for the Neural Representation and Control of Movement Vigor. Cell 162(6): 1418–1430.

Parent, A., and L. De Bellefeuille

1983 The Pallidointralaminar and Pallidonigral Projections in Primate as Studied by Retrograde Double-Labeling Method. Brain Research 278(1–2): 11–27.

Paxinos, George, and Charles Watson
2006 The Rat Brain in Stereotaxic Coordinates: Hard Cover Edition. Elsevier.

Person, Abigail L., and David J. Perkel
2005 Unitary IPSPs Drive Precise Thalamic Spiking in a Circuit Required for Learning. Neuron 46(1): 129–140.
2007 Pallidal Neuron Activity Increases during Sensory Relay through Thalamus in a Songbird Circuit Essential for Learning. Journal of Neuroscience 27(32): 8687–8698.

Pienaar, Ilse S., Anthony Vernon, and Philip Winn
2017 The Cellular Diversity of the Pedunculopontine Nucleus: Relevance to Behavior in Health and Aspects of Parkinson's Disease. The Neuroscientist 23(4): 415–431.

Prensa, L., and A. Parent
2001 The Nigrostriatal Pathway in the Rat: A Single-Axon Study of the Relationship between Dorsal and Ventral Tier Nigral Neurons and the Striosome/Matrix Striatal Compartments. The Journal of Neuroscience: The Official Journal of the Society for Neuroscience 21(18): 7247–7260.

Redgrave, Peter, and Kevin Gurney
2006 The Short-Latency Dopamine Signal: A Role in Discovering Novel Actions? Nature Reviews. Neuroscience 7(12): 967–975.

Riehle, A., and J. Requin
1989 Monkey Primary Motor and Premotor Cortex: Single-Cell Activity Related to Prior Information about Direction and Extent of an Intended Movement. Journal of Neurophysiology 61(3): 534–549.

Riehle, Alexa, and Jean Requin
1993 The Predictive Value for Performance Speed of Preparatory Changes in Neuronal Activity of the Monkey Motor and Premotor Cortex. Behavioural Brain Research 53(1): 35–49.

Risold, P. Y., R. H. Thompson, and L. W. Swanson
1997 The Structural Organization of Connections between Hypothalamus and Cerebral Cortex. Brain Research. Brain Research Reviews 24(2–3): 197–254.

Roseberry, Thomas K., A. Moses Lee, Arnaud L. Lalive, et al.

2016 Cell-Type-Specific Control of Brainstem Locomotor Circuits by Basal Ganglia. Cell 164(3): 526–537.

Rossi, Mark A., Haofang E. Li, Dongye Lu, et al.
2016 A GABAergic Nigrotectal Pathway for Coordination of Drinking Behavior. Nature Neuroscience 19(5): 742–748.

Salamone, John D., and Mercè Correa
2012 The Mysterious Motivational Functions of Mesolimbic Dopamine. Neuron 76(3): 470–485.

Sanders, Joshua I., and Adam Kepecs
2012 Choice Ball: A Response Interface for Two-Choice Psychometric Discrimination in Head-Fixed Mice. Journal of Neurophysiology 108(12): 3416–3423.

Sato, Makoto, and Okihide Hikosaka
2002 Role of Primate Substantia Nigra Pars Reticulata in Reward-Oriented Saccadic Eye Movement. The Journal of Neuroscience 22(6): 2363–2373.

Schwab, Bettina C., Daisuke Kase, Andrew Zimnik, et al.
2020 Neural Activity during a Simple Reaching Task in Macaques Is Counter to Gating and Rebound in Basal Ganglia–Thalamic Communication. PLOS Biology 18(10). Public Library of Science: e3000829.

Schwarz, Cornelius, Harald Hentschke, Sergejus Butovas, et al.
2010 The Head-Fixed Behaving Rat--Procedures and Pitfalls. Somatosensory & Motor Research 27(4): 131–148.

Sheth, Sameer A., Tarek Abuelem, John T. Gale, and Emad N. Eskandar
2011 Basal Ganglia Neurons Dynamically Facilitate Exploration during Associative Learning. The Journal of Neuroscience: The Official Journal of the Society for Neuroscience 31(13): 4878–4885.

da Silva, Joaquim Alves, Fatuel Tecuapetla, Vitor Paixão, and Rui M. Costa
2018 Dopamine Neuron Activity before Action Initiation Gates and Invigorates Future Movements. Nature 554(7691): 244–248.

Smith, A. D., and J. P. Bolam
1990 The Neural Network of the Basal Ganglia as Revealed by the Study of Synaptic Connections of Identified Neurones. Trends in Neurosciences 13(7): 259–265.

Sommer, Marc A., and Robert H. Wurtz
1998 Frontal Eye Field Neurons Orthodromically Activated From the Superior Colliculus. Journal of Neurophysiology 80(6): 3331–3335.

Stamatakis, Alice M., and Garret D. Stuber
2012 Optogenetic Strategies to Dissect the Neural Circuits That Underlie Reward and Addiction. Cold Spring Harbor Perspectives in Medicine 2(11): a011924.

Svoboda, Karel, and Nuo Li
2018 Neural Mechanisms of Movement Planning: Motor Cortex and Beyond. Current Opinion in Neurobiology 49. Neurobiology of Behavior: 33–41.

Takakusaki, Kaoru
2013 Neurophysiology of Gait: From the Spinal Cord to the Frontal Lobe. Movement Disorders 28(11): 1483–1491.

Tanaka, Masaki
2006 Inactivation of the Central Thalamus Delays Self-Timed Saccades. Nature Neuroscience 9(1): 20–22.
2007 Cognitive Signals in the Primate Motor Thalamus Predict Saccade Timing. The Journal of Neuroscience: The Official Journal of the Society for Neuroscience 27(44): 12109–12118.

Tanji, J., and E. V. Evarts
1976 Anticipatory Activity of Motor Cortex Neurons in Relation to Direction of an Intended Movement. Journal of Neurophysiology 39(5): 1062–1068.

Tecuapetla, Fatuel, Sara Matias, Guillaume P. Dugue, Zachary F. Mainen, and Rui M. Costa
2014 Balanced Activity in Basal Ganglia Projection Pathways Is Critical for Contraversive Movements. Nature Communications 5(1): 4315.

Turner, R. S., and M. E. Anderson
1997 Pallidal Discharge Related to the Kinematics of Reaching Movements in Two Dimensions. Journal of Neurophysiology 77(3): 1051–1074.

Turner, Robert S., and Michel Desmurget
2010 Basal Ganglia Contributions to Motor Control: A Vigorous Tutor. Current Opinion in Neurobiology 20(6): 704–716.

Utter, Amy A., and Michele A. Basso

2008 The Basal Ganglia: An Overview of Circuits and Function. Neuroscience and Biobehavioral Reviews 32(3): 333–342.

Wan, X. S. T., F. Liang, V. Moret, M. Wieesendanger, and E. M. Rouiller
1992 Mapping of the Motor Pathways in Rats: C-Fos Induction by Intracortical Microstimulation of the Motor Cortex Correlated with Efferent Connectivity of the Site of Cortical Stimulation. Neuroscience 49(4): 749–761.

Wang, Yu, Xinxin Yin, Zhouzhou Zhang, et al.
2021 A Cortico-Basal Ganglia-Thalamo-Cortical Channel Underlying Short-Term Memory. Neuron 109(21): 3486-3499.e7.

Wiegert, J. Simon, Mathias Mahn, Matthias Prigge, Yoav Printz, and Ofer Yizhar
2017 Silencing Neurons: Tools, Applications, and Experimental Constraints. Neuron 95(3): 504–529.

Willard, Amanda M, Brian R Isett, Timothy C Whalen, et al.
2019 State Transitions in the Substantia Nigra Reticulata Predict the Onset of Motor Deficits in Models of Progressive Dopamine Depletion in Mice. Yukiko Goda and Eve Marder, eds. ELife 8: e42746.

Wright, A. K., and G. W. Arbuthnott
1981 The Pattern of Innervation of the Corpus Striatum by the Substantia Nigra. Neuroscience 6(10): 2063–2067.

Wurtz, R H, and M E Goldberg
1972 Activity of Superior Colliculus in Behaving Monkey. 3. Cells Discharging before Eye Movements. Journal of Neurophysiology 35(4): 575–586.

Yoshida, Atsushi, and Masaki Tanaka
2009 Enhanced Modulation of Neuronal Activity during Antisaccades in the Primate Globus Pallidus. Cerebral Cortex (New York, N.Y.: 1991) 19(1): 206–217.